Computing breakwater stability using SWASH

The effects of model choices, shallow foreshore and oblique waves on the stability of a rubble mound breakwater

Dirk-Jan Michels

TU Delft

Computing breakwater stability using SWASH

The effects of model choices, shallow foreshore and oblique waves on the stability of a rubble mound breakwater

by

Dirk-Jan Michels

in partial fulfilment of the requirements for the degree of

Master of Science
in Hydraulic Engineering

at the Delft University of Technology,
to be defended publicly on Wednesday September 7, 2022 at 11:00 AM.

Student number:	4319745	
Project duration:	October, 2021 – September, 2022	
Thesis committee:	Dr. ir. B. Hofland	TU Delft, Chair
	Dr. ir. M. Zijlema	TU Delft
	Ir. P. S. P. van Loon	Van Oord, Daily supervisor
	Ir. D. C. P. van Kester	TU Delft & Van Oord

TU Delft

Van Oord
Marine ingenuity

Acknowledgments

This report presents the results of my research, in partial achievement of my master's degree in Hydraulic Engineering, completed at the Delft University of Technology. It therefore marks the end of my time as a student in Delft. I am grateful for all those who have supported me during these past years and especially along the adventure of my research.

First, I would like to specially thank the members of my thesis committee, without whom this report would not have been realised. Even though your agendas were fully booked, I could always walk by your offices, text, call or email you and receive your full attention. Thanks for the many progress meetings, that were filled with constructive feedback and new ideas, which energized me every time. Philip, thank you for your close supervision, infinite patience and your help tackling the challenges together. Dennis, thank you for the opportunity to conduct my thesis at Van Oord and the numerous advice, both content-related as personal, that helped me during my thesis. Bas, thank you for unstoppable enthusiasm and helpful insights during the entire span of this research. Marcel, thank you for your help with SWASH, the clear explanations and your endless experience in numerical modelling. Lastly I would like to thank Ad Reniers, who was not part of my committee, but who was always available to brainstorm and troubleshoot while setting up my numerical model and interpreting the results.

Secondly, I would like to thank all the colleagues at Van Oord, whom I can now officially call my colleagues as I'm starting my professional career at this organisation. Thanks for the help with my thesis, the nice activities and the many coffee and lunch breaks sitting in the sun by 'de Maas'.

Lastly, I would like to thank my family and friends for your unconditional support throughout my time in Delft. Thanks for the many amusing, memorable and lovely moments. I can't wait to start a new chapter in my life with you involved.

Enjoy reading this report.

Dirk-Jan Michels
Amsterdam, September 2022

Abstract

On the east coast of Romania, at Eforie, coastal erosion manifests. To strengthen the coastal area a large coastal protection project was setup involving beach nourishment combined with the construction of breakwaters. The breakwaters are designed with the well known modified Van der Meer formulas. To ensure confidence in the breakwaters stability the designs were tested during a 3D physical model test. The designs were stable, however the measured damage to the breakwater was larger than was expected. Investigating the physical model test resulted in three important aspects, that need to be investigated. First, a broad list of configurations, that could responsible for the damage, could be identified. Secondly, excessive wave breaking on the foreshore during the model test resulted in a shift in wave energy from higher to lower frequency waves. These low frequency waves, or so-called infragravity waves became increasingly dominant near the coast. Their effect on the stability of the structure is however unknown. Thirdly, the incoming waves were very oblique and on a shallow foreshore, resulting in a different failure mechanism than is incorporated in the modified Van der Meer formulas. A new stability method has to be formulated to investigate breakwater stability for this physical model test. Due to the broad list of configurations and the possible influence of infragravity waves, real scale or physical model tests are not feasible and a numerical model needs to be used. A reliable and widely applicable method to link breakwater stability to a numerical model has however not yet been composed. Therefore, the goal of this thesis is to propose a method that can link breakwater stability to a numerical model and to assess whether the identified configurations resulted in the damage along the statically stable rubble mound breakwater, measured during the Eforie physical model test.

First, an investigation is performed on the physical model test set-up and observations, resulting in a final list of 5 configurations, that are investigated in this research: The applied offshore transitional slope (1), the assumption of uni-directional waves (2), the slope of the lower foreshore (3), the depth-contour lines inducing wave focusing (4) and the very oblique wave angle on a shallow foreshore (5). Secondly, a method is proposed linking breakwater stability to a velocity signal from the numerical model SWASH. An equation is formulated, based on the theory of Izbash (1935), with a slope factor included, and scaled with the theory of Shields (1936). It requires a velocity signal, that can be obtained from SWASH, to calculate a stone size required for stability. This formula is presented in equation 1.

$$\Delta d_{n,50} = 0.83 * \frac{u^2}{2g} \tag{1}$$

Thirdly, a numerical model is set up in SWASH, with grid dimensions 3m x 2m, resembling the physical model test. The breakwater is modelled as an impermeable core with a permeable porosity layer placed on top. The thickness of the porosity layer is based on the thickness of the outer armour layer of the original breakwater. The numerical model is validated by comparing the wave characteristics, at several locations along the breakwater, to wave data available from the physical model test. The numerical model shows accurate resemblance of the wave characteristics. Since the wave velocity is linked to the wave height, it is assumed that the wave velocity on the breakwater is also correctly modelled. The model is therefore found valid for the modelling study. In the numerical model along the still waterline measurement points are indicated that provide the velocity and waterlevel signal during a simulation. In the numerical model two layers in the vertical are assumed and tested to be sufficient. The velocity of the top layer resembles the velocity that flows just over the stones. Therefore from the velocity signal of the top layer the governing $u_{0.2\%}$ along the waterline at the breakwater is obtained and from the waterlevel signal the wave spectrum is derived. In the study simulations are performed in which the configurations are tested one by one, and all simulations are assessed on two parameters: the $u_{0.2\%}$ and the wave spectral transformation along the breakwater. The results from the different simulations are compared relatively to identify the relative effect the configurations have on the velocity and wave characteristics.

The results of this research show that breakwater stability can be predicted reasonably well from a velocity signal obtained from SWASH. The velocity signal, obtained from SWASH, results in reliable stone sizes. The configurations could be investigated with the proposed method and the results provide reliable and useful insights. In addition, the proposed method is able to identify the effect of infragravity wave energy on the stability of a breakwater. The method is also tested by calculating the relative obliqueness factors for different incoming wave angles, which shows promising results. It is important to reproduce the breakwater porosity well in the numerical model as it can significantly influence the velocity signal. A decrease/increase of the porosity thickness with 30% or 0.6m can result in an increase/reduction of 20-26% in velocity respectively.

The five discussed configurations provide partial explanations to (in)directly induce the higher breakwater damage in the physical model test. Both the applied offshore transitional slope (1) as the assumption of uni-directional waves (2) result in a slight underestimation of the breakwater stability and therefore a somewhat conservative design along the entire length of the breakwater. The combined effect resulted in a reduction of 0-6% around the head of the breakwater, h/Hs = 2.5-4.8, and a reduction of 16-24% near the shore, h/Hs = 1.1-1.8. Especially near the shore the breakwater is conservatively designed, due to the fact that both the transitional slope as the assumption of unidirectional waves increases the infragravity wave energy in the system. It is found that incoming waves break around h/Hs = 1.7 after which the infragravity waves induce a temporary increase in waterlevel, around h/Hs = 1.1-1.8. This allows the depth-limited short waves to become bigger resulting in higher velocities and more damage on the breakwater. This affects the breakwater stability closer to shore and needs to be taken into account when designing a breakwater in these conditions. The lower foreshore (3) induces the generation of infragravity waves, which affect the velocity closer to shore as described above. The depth-contour lines (4) result in a wave focusing effect increasing the velocity around h/Hs = 1.1-1.8 with 8-11%. Based on the results of this thesis the very oblique wave angle on a shallow foreshore (5) does not induce higher velocities and breakwater instability. It is however assumed that the effect of a breaking plunging wave, inducing acceleration and pressure difference effects on the stones on a slope, is not sufficiently into account, due to the grid dimensions used in the model. As other plausible causes of the increased damage are disproven, it seems likely that the different oblique wave breaking process that is not modelled in detail leads to the increased damage.

Contents

1

Introduction

1.1. Context and background

As over 40% of the world's population lives near the coast, all over the world breakwaters are constructed as part of coastal defence systems. By influencing the waves, the (wave driven) current and the sediment transport, they protect the area behind the breakwater from wave impact and erosion (Rietberg, 2017). There are numerous types of breakwaters that can, based on their structural characteristics, be divided in monolytical structures, statically stable breakwaters and dynamically stable breakwaters (van den Bos and Verhagen, 2018). A statically stable rubble mound breakwater is a structure made of loose elements such as quarry stones or concrete blocks. Displacement of these elements is not allowed and if displacement occurs its called damage (van der Meer, 1988). In this research a statically stable rubble mound breakwater is investigated, thus when furthermore spoken about a breakwater in this research a statically stable rubble mound breakwater is meant.

Breakwaters date back to ancient civilizations, with the oldest dating to the Egypt of 2000 BC (Takahashi, 2002). Back then breakwaters were mostly build with locally found rock and realised via trial and error. When after a storm a breakwater was damaged it was reshaped and repaired, which resulted in breakwaters with large and flat outer slopes of up to 1:12 (van den Bos and Verhagen, 2018). Since breakwater failure can lead to large economical damage and even loss of life, more reliable design methods were desired. In the past century much research has focused on sediment and stone stability under the influence of flow and waves. From Izbash (1935) and Iribarren (1938), who computed mathematical explanations for stone stability under the influence of flow. To Hudson (1960) and Van der Meer (1988), who performed model tests to empirically enhance the stability formula for stone stability during wave attack. In addition, many researchers have contributed and enhanced their work, such as Shields, Pilarczyk, Paintal, Battjes and Groenendijk, Bijker, Galland, van Gent, etc (Bijker, 1967). This eventually led to the modified Van der Meer equations and standard layout that are widely used today, basing breakwater stability on wave characteristics close to the breakwater (van der Meer, 1988). In figure 1.1a an example is shown presenting one of the oldest breakwaters that still exists today and in figure 1.1b a typical cross section of a present day rubble mound breakwater is shown. The differences in design and layout are clearly visible.

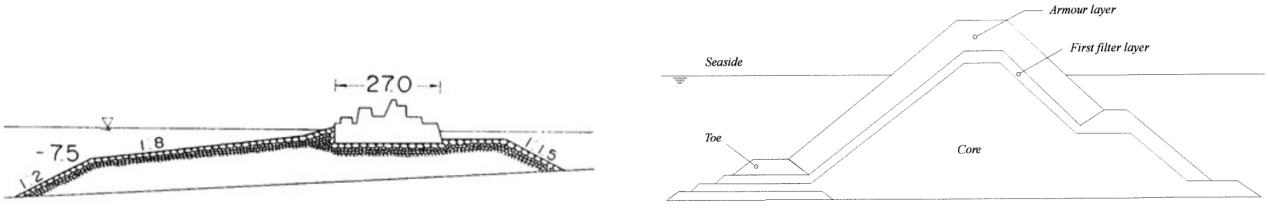

(a) Civitavecchia (van den Bos and Verhagen, 2018)

(b) Present day (De Heij, 2021)

Figure 1.1: Cross sections of rubble mound breakwaters

1.2. Eforie

On the east coast of Romania, at Eforie, breakwaters are designed to limit wave impact and longshore sand transport at the beach (de Bruin, 2019). Here in the Black Sea littoral area coastal erosion manifests and represents a real risk for the 240 km of shoreline. In the present conditions the degradation of the coastline continues and therefore a large coastal protection project was setup to strengthen the coastal area. These measures involve beach nourishment combined with the construction of breakwaters, which are designed with the modified Van der Meer equations.

The Eforie coastal area is a dynamic and challenging environment. It introduces multiple coastal and wave characteristics that can influence the stability and effectiveness of a breakwater. To increase confidence in the design the contractor executing the works performed a physical model test, in which the stability of the Northern side of one of the breakwaters was examined. The results from these tests concluded a stable design, however the measured damage to the breakwater was larger than was expected on beforehand.

1.3. Problem definition

Investigating the physical model test three important aspects, that needed to be investigated in this thesis, were identified:

1. The damage, measured along the breakwater was larger than expected based on the conventional design equations. In addition, it was fairly constant at the waterlevel line and observed along the full length of the breakwater. An extensive investigation of the characteristics of the Eforie coast, the modelling choices applied for the model test and the observations during the model test resulted in a list of configurations that could be responsible for this observed damage. These will be elaborated in chapter 2, but contain configurations regarding the Eforie modelling choices, the Eforie coast layout and the oblique wave angle on a shallow foreshore. The identified configurations are expected to influence breakwater stability, however their exact effect is not known.

2. Excessive wave breaking on the foreshore during the model test resulted in a shift in wave energy from higher to lower frequencies. These low frequency waves, or so-called infragravity waves, became increasingly dominant near the coast. Research regarding overtopping and dune erosion show that infragravity wave energy induces a set-up of the waterlevel near the coast (Roelvink et al., 2009). The short waves at these smaller water depths are depth-limited and therefore this increase of the water depth results in an increase in short wave height. This effect could also influence structural stability. In 2007 Bux already claimed the idea that longer period waves would induce more damage (Bux, 2007). The exact effect of the infragravity waves on the (short) wave development along the structure and the stability of the structure is however unknown.

3. The incoming waves were very oblique and on a shallow foreshore. This resulted in a faster propagating breaking wave along the breakwater length, further referred to as a siderush, instead of the more conventional up- and downrush along the breakwater slope. It was assumed that the faster propagating breaking wave along the breakwater was not represented in the conventional modified Van der Meer formulas. This explains why these design equations might not be applicable for the Eforie coast. To investigate the identified configuration a new stability method had to be formulated that does not base breakwater stability on wave characteristics, but on the observed velocity. Research into breakwater stability can be done via real scale tests, physical model tests and numerical model tests. A rough indication and comparison between these three methods is visualised in table 1.1.

Type of test	Accuracy	Applicability	Time	Space	Costs
Real scale test					
Physical model test					
Numerical model test					

Table 1.1: Comparison of different test methods. Green indicates that the model performs well on this aspect, orange means reasonably well and red indicated badly

As real scale tests are often not feasible, due to space and cost limitations, preferably physical model tests would be performed where the configurations are investigated to see their effects on breakwater stability. As Monteban (2016) described, physical model tests can be designed to exactly resemble the case and to include practically all the relevant physical processes. However, first step inventory research then can become costly and time consuming (Monteban, 2016). In addition, investigating the effect of long waves via physical model tests is hard, because of the scale effects. Performing physical model tests for the above mentioned case is thus impossible given the limited space, time and budget available. For several applications in coastal research numerical models are applied. Numerical models make assumptions and simplifications of certain physical processes. This limits their exactness, but when validated to be reliable, numerical models are cheap ways to correctly investigate aspects such as wave transformation, overtopping values and erosion volumes. The application of numerical models for breakwater stability is however scarce in the literature. In 1986 Kobayashi presented a paper in which he developed a computer program that could be used to evaluate an armor size (Kobayashi, 1986). Van Gent discussed in 1992 the use of a numerical model to calculate water movement near the surface of a berm (Van Gent, 1992). A reliable and widely applicable method to link breakwater stability to a numerical model has however not yet been composed. To be able to investigate the physical model test this method needs to be proposed.

1.4. Research objective

It is clear that there are still some important aspects of the observations and results from the Eforie model test which are not fully understood. This research serves as a first step to provide insight in the governing processes for the Eforie coast. The results of this research will improve the knowledge on breakwater stability and result in recommendations for further research such as field investigations and specific physical model tests. Therefore the (in)direct effects of the identified configurations, regarding the Eforie modelling choices, the Eforie coast layout and the oblique wave angle on a shallow foreshore, will have to be investigated. For such an application a numerical model should be used and therefore breakwater stability needs to be linked to a numerical model. In the problem definition it was stated that a faster propagating breaking wave was observed. Therefore, it is chosen to use the model SWASH in this thesis and propose a method that can link the numerical model SWASH to breakwater stability. SWASH will then be used to investigate the (in)direct effects of the multiple configurations on breakwater stability. Providing this link will improve confidence in breakwater design and reduce costs of physical model tests. Especially for cases with distinctive coastal or wave characteristics or where alterations from the conventional design formulas could be expected, such as the Eforie coast.

Concluding this, the main objective of this research is to propose a method that can link breakwater stability to SWASH and to assess whether the identified configurations resulted in the damage along the statically stable rubble mound breakwater, measured during the Eforie physical model test.

1.5. Research question

Based on the research objective, the following research question is formulated:

To what extent can SWASH determine breakwater stability using the Eforie physical model test as a case study?

To answer the above stated research question, some sub-questions have been formulated:

1. How can a velocity signal be obtained from SWASH and produce stable stone sizes?
2. What is the influence of the Eforie modelling choices on the stability of a breakwater?
3. What is the influence of the Eforie layout on the stability of a breakwater?
4. What is the influence of oblique incoming waves on a shallow foreshore on the stability of a breakwater?
5. What is the influence of infragravity wave energy on the stability of a breakwater?

To find out to what extent SWASH can determine breakwater stability the Eforie physical model test is taken as a case study. A new method will be proposed of which the applicability will be tested via several aspects of the Eforie physical model tests. For this first a method needs to be proposed. In the problem definition it was stated that a faster propagating breaking wave was observed. Therefore it is chosen to find a link to velocities calculated by SWASH to stone or breakwater stability. The first sub-question is therefore formulated to help set-up the method and propose a link between a velocity signal obtained from SWASH to a stable stone size. When the new method is formulated and a link is made from SWASH results to breakwater stability, the effectiveness of this theory is tested in the next sub-questions. Sub-question 2,3 and 4 investigate whether the modelling choices applied by Deltares, the Eforie layout and the wave angle have an effect on the breakwater stability and whether the proposed method is able to prove this. This strengthens the confidence in the proposed method and indicated possible aspects that need to be further investigated. Finally, sub-question 5 checks what effect some of the configurations have on the infragravity wave energy, that is present in the model, and whether this affects the breakwater stability. This provides more insight in the effect infragravity wave energy has on breakwater stability and whether this can be indicated by the proposed method. These sub-questions together provide an explanation to what extend SWASH can determine breakwater stability.

1.6. Research approach and thesis outline

Physical and numerical model data analysis
In chapter 2 the Eforie model case is investigated in depth. The model setup, the observations during the tests and the obtained data are discussed from which the above introduced list of relevant configurations results. In addition, the available data of the Eforie model test, that can be used for realisation and validation of the numerical model is listed.

Literature study
In chapter 3, the origin and formation of the current stability formulae is discussed. The status of research into the influence of wave angle, slope layout, wave characteristics and infragravity waves on these stability formula is listed. This way the gap between the used formulae and the Eforie case is further investigated. As discussed above, the basis of the breaking mechanisms on which these formulas are based might not hold for the Eforie coast. Therefore a step back from breakwater stability is taken and the basic theory of stone stability under flow is reviewed. This results in a stability formula that can be used in this research which is not based on the typical Van der Meer breaking mechanisms. In addition, the theory and consideration behind the used numerical model is stated. It's flavours, strengths and weaknesses are linked to the composed stability formula. This way the usability and limitations of the numerical model for this research is explained.

Modelling study
In chapters 4 and 5, the numerical model is set-up, validated and its robustness is checked via a sensitivity analysis. When the model is proven sufficient simulations are done, in which one of the configurations is changed to investigate its relative effect on the stone stability. The results from the different simulations are presented in chapter 6. In chapter 7 the assumptions and model settings are critically reflected on. This way the validity of the results is discussed and it is assessed whether they extend, contradict or dispute existing knowledge.

Conclusion and recommendations
The results of these different steps are summarized in chapter 8 to present the conclusions with respect to the research questions and the recommendations that have resulted from the study.

Figure 1.2: Methodology

2

Eforie case

The observations and results from the Eforie model tests form the basis of this thesis. A good understanding of the exact case specifics and results is therefore vital. The aim of this chapter is to analyse the Eforie physical modelling choices, discuss the relevant observations and results, and list the available data necessary to set up and validate a numerical model.

2.1. Context

The 3D physical model test was performed for a breakwater designed for the Eforie coast. The main objective was to verify the stability and the overtopping characteristics of the seaside (North-side) of the breakwater. At the Eforie coast the breakwater is orientated at 83.5°N as show in figure 2.1. The main part of the breakwater has a 2:3 slope, an approximate top width of 7m and it is 370m long.

Figure 2.1: Eforie coast

2.1.1. Layout

Figure 2.2 shows a cross-section of the Eforie coast. The bathymetry is schematised and divided in four parts. In the four sections multiple slopes are present of which the precise features are presented in table 2.1.

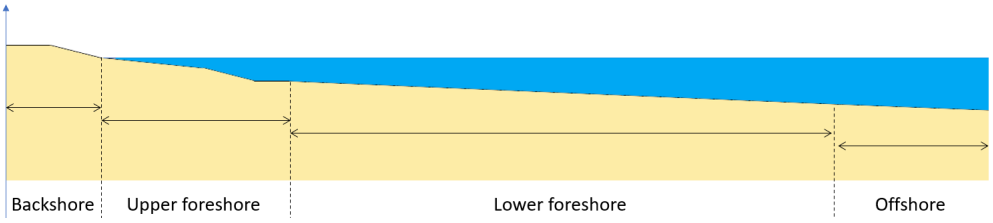

(a) Four sections of the coast

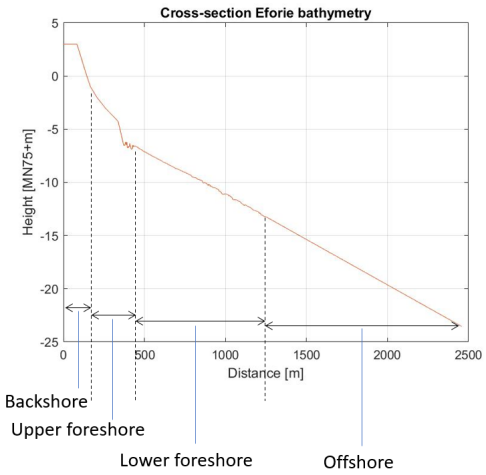

(b) Eforie slope

Figure 2.2: Bathymetry of the Eforie coast

	Backshore		Upper foreshore			Lower foreshore	Offshore slope
Distance	0-85	85-165	165-340	340-375	375-450	450-1250	1250-
Slope	-	1:20	1:50	1:15	-	1:120	1:120

Table 2.1: Eforie coast bathymetry schematization

The breakwater is constructed on the backshore and upper foreshore. The contour lines are almost perpendicular to the breakwater, which is visible in the top- and side-view shown in figure 2.3.

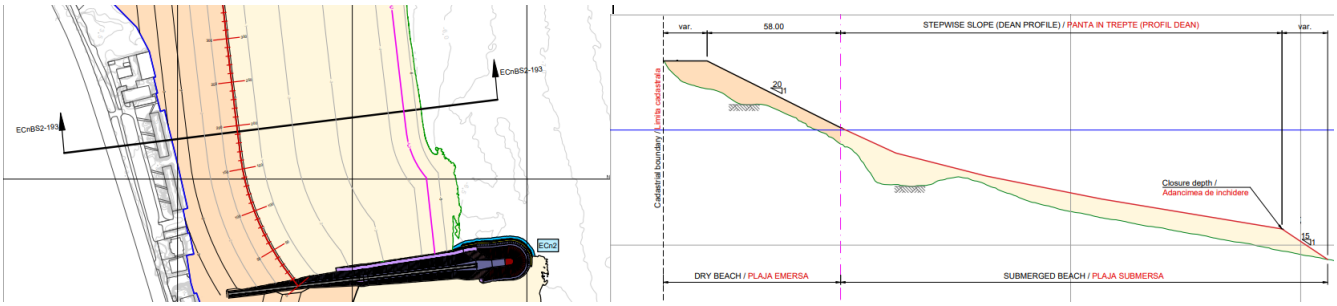

(a) Top view

(b) Side view

Figure 2.3: View beach (van Kester, 2021)

The backshore of the Eforie coast consists of a horizontal part and a 1:20 beach where the incoming waves break. The upper foreshore can be roughly schematised with three slope angles. The submerged profile follows a Dean equilibrium profile with a step-wise slope of approximately 1:50. Below the closure depth, the sand profile is connected to the existing bed via a 1:15 slope. The closure depth is the depth contour over which there is negligible cross-shore transport during normal conditions. It therefore determines the seaward extend of the Dean equilibrium profile used in the design. The last

part of the upper foreshore displays a horizontal part with a somewhat capricious gradient. This can be assumed as horizontal. Figure 2.3a shows that near the breakwater the beach is longshore non-uniform. The contour lines bend towards the breakwater in a parabolic bay shape but are cut-off and extended perpendicular to the breakwater. Around chainage 100-150 the parabolic bay shape is no longer cut-off, but extended to the breakwater. This cut-off parabolic bay shape is a typical feature which needs to be taken into account for the Eforie model test. The lower foreshore and the offshore part of the Eforie coast show a more or less constant 1:120 slope until a depth of MN75-23.5m.

Breakwater
Figure 2.4 shows four cross-sections of the breakwater schematization designed for Eforie. The breakwater has a slightly variable height and outer layer thickness. However over the main part the breakwater has a height of approximately MN75+3.00m and a outer layer thickness of 1.86m.

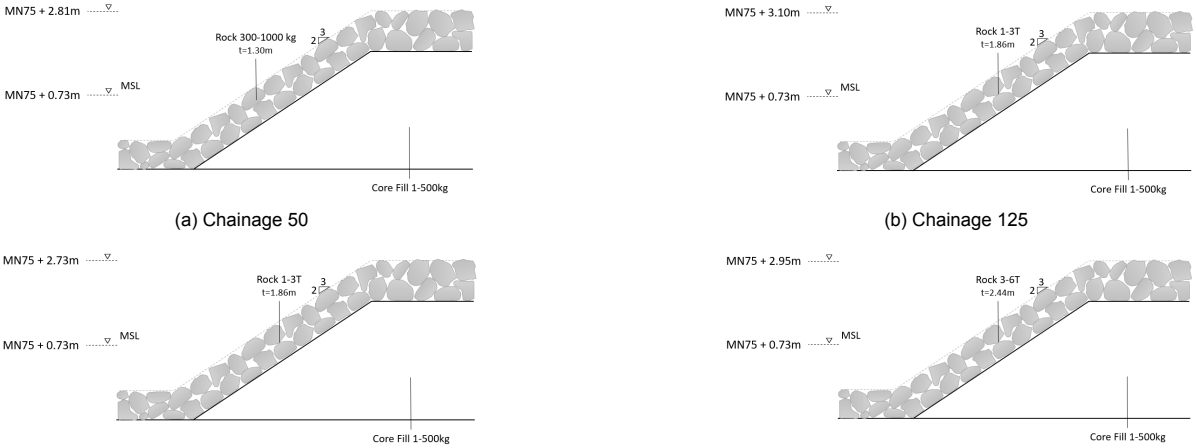

(a) Chainage 50 (b) Chainage 125

(c) Chainage 275 (d) Chainage 322

Figure 2.4: Cross-section breakwater for Eforie model test

2.1.2. Hydraulic boundary conditions
The hydraulic boundary conditions for the Eforie coast followed from a metocean study. The study presented various governing wave conditions for different storm conditions. For this research the governing design conditions at 10m water depth for a 1/100 year return period are used, presented in table 2.2. The incoming waves are very oblique compared to the breakwater, resulting in a relative angle of 13.4°at 10m water depth with the breakwater. The amount of directional spreading at the Eforie coast is 11°one-sided as standard deviation.

Design event	waterlevel (MN75+m)	$H_{m0,offshore}$ (m)	Tp (s)	β (°N)	ζ (°)
100 % SLS HWL	0.73	4.42	11.44	69.7	11

Table 2.2: Eforie model test program

2.2. Eforie model test
In this chapter the Eforie model test will be discussed. The modelling choices applied to the case compared to the prototype Eforie coast are presented. The relevant data that is collected during the test is elaborated.

2.2.1. Modelling choices
The Eforie model test was constructed in the Delta Basin of Deltares, with dimensions 50 m x 50 m. In order to translate the prototype characteristics to the basin dimensions some modelling choices where made, of which the most relevant for this thesis are listed below:

- Appropriate **scaling** relations where applied.
- The **layout** of the Eforie coast was simplified in three notable ways.
  - The foreshore was an immobile concrete foreshore, of which the guiding properties are assumed the same as the prototype situation.
  - Around the model, a conical shaped wave damping gravel beach was applied which prevented unwanted reflections.
  - From the bottom of the basin, located at MN75-23.5m, towards the first modelled depth contour a 1:10 transitional slope was used.
- For the **hydraulic boundary conditions**, directional spreading was not taken into account and only long-crested waves where applied during the test.

Scaling
In order to translate the model results to prototype values proper scaling relations were applied. The flow hydrodynamics were scaled by the Froude scaling law. In the case of the armour layer, the stability of the rock material was the most important, so the scaling was based on stability scaling. The density differences between the prototype and model materials were also accounted for in the scaling method. Permeability scaling was applied to small core material where the flow through the structure needed to be represented well. Due to the scaling the core of the breakwater was modelled as impermeable. It is assumed that this scaling is performed well and did not result in any deviations.

Layout
In figure 2.5 a top- and side-view of the Eforie model test setup are given. The same schematization is applied as was explained in chapter 2.1.1, with the division in four parts as shown in figure 2.5b and table 2.3.

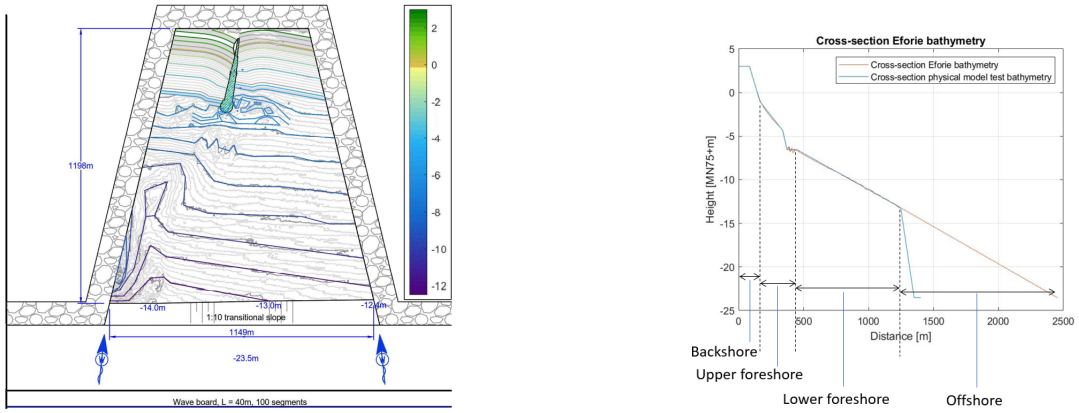

(a) Layout of Eforie model test setup

(b) Bathymetry of the Eforie model test

Figure 2.5: Overview of the foreshore schematisation (van der Werf, 2021)

	Backshore		Upper foreshore		Lower foreshore		Offshore slope	
Distance	0-85	85-165	165-340	340-375	375-450	450-1250	1250-1350	1350-
Slope	-	1:20	1:50	1:15	-	1:120	1:10	-

Table 2.3: Eforie model test bathymetry schematization

Closer to the structure the bathymetry was represented more accurate than further away from the structure as shown in figure 2.5a, which compares the prototype foreshore, indicated in gray, and the modelled foreshore, indicated by the coloured contour lines. In figure 2.5a it can be seen that the cut-off parabolic bay shape was taken into account in the Eforie model test. It is assumed that the important aspects of the Eforie coast were taken into account and the guiding properties of the Eforie model test were sufficient. Figure 2.5a shows the conical shaped wave damping gravel beach. It is assumed

that this prevented unwanted reflections and did not introduce other irregularities into the model. Figure 2.5b shows the applied transitional slope compared to the prototype bathymetry. This transitional slope of 1:10 was applied from a depth of MN75-13.5m till a depth of MN75-23.5m. The transitional slope will be further discussed during the literature research.

Hydraulic boundary conditions
For the hydraulic boundary conditions of the Eforie model test the governing storm conditions were used. Thus a design water level of MN75+0.73m, a significant wave height of 4.42m and a peak period of 11.44s. The wave spectrum was assumed as a JONSWAP spectrum, which means a Pierson-Moskowitch spectrum multiplied by a peak enhancement factor of γ=1.5. In the Eforie model directional spreading was not applied. This modelling choice will be further discussed in the literature research.

2.2.2. Data collection
At the deep (MN75-23.5m) and target (MN75-10m) contour lines GRSM wave height and direction meters where used. Along the structure WHM wave height measurement devices are positioned counting from the sea-side landward. Figure 2.6 show the location of the measurement devices used in the Eforie model test.

- GRSM01: Deep water at MN75-23.5m
- GRSM02: Target location at MN75-10m
- WHM01: Head of the structure at MN75-6.5m
- WHM02: Next to the structure at Chainage 370 at MN75-6.5m
- WHM03: Next to the structure at Chainage 270 at MN75-4.4m
- WHM04: Next to the structure at Chainage 190 at MN75-2.7m

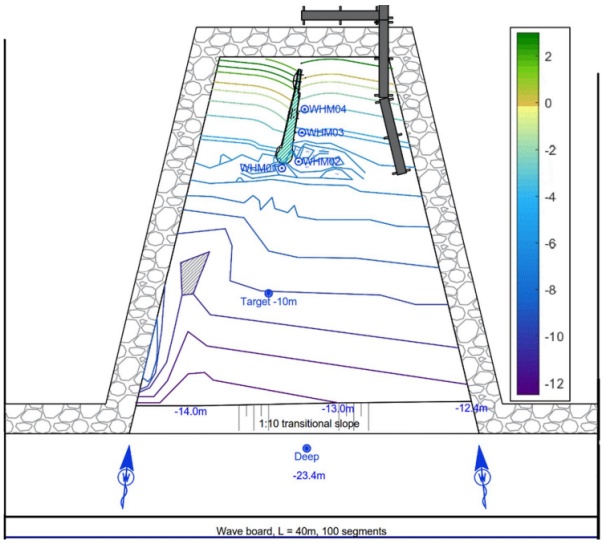

Figure 2.6: With wave measurement instruments

2.3. Observations from Eforie model test
During the Eforie model tests and after reviewing the results, multiple phenomena where observed. The four most important observations are listed and discussed in more detail below.

- The incoming waves were very oblique and on a shallow foreshore. This resulted in a faster propagating breaking wave, further referred to as a **siderush**. This siderush along the length of breakwater deviates from a more conventional run-up and run-down along the height of the breakwater.

- Layout influences of the Eforie model test seemed to induce a **wave focusing** refraction pattern.
- Excessive wave breaking on the foreshore resulted in a shift in a notable shift from swell wave energy to **infragravity wave energy** in the wave propagation along the breakwater.
- The **damage**, measured along the breakwater was larger than expected based on the conventional design equations and fairly constant at the waterlevel line along the breakwater.

Siderush

The conventional breaking mechanism for breakwater stability consists of waves breaking onto the structure, resulting in energy is dissipation into the structure, during up- and downrush of the wave over the breakwater slope (Van Gent and van der Werf, 2014). This up- and downrush results in significant impact on the toe part of the structure, where normally the highest impacts are expected (Baart et al., 2011). In the Eforie model test, the wave angle was very oblique. In addition, it was observed that due to the foreshore the incoming waves show heavy refraction and turn towards the coast to end in a 70 °N incoming wave, which means a 13.4 °relative angle with the breakwater. This seems to induce wave breaking along the breakwater instead of onto the structure and results in a siderush along the breakwater instead of the typical up- and downrush. The wave propagation along the breakwater does not show the same behavior for each wave. Some waves move along the breakwater in a straight line and break at the coast, as shown in figure 2.7a. Other waves show a faster propagating and continuously breaking behaviour along the breakwater, as shown in figure 2.7b. This could be described as a continuously breaking wave or a so-called bore. It is assumed that these faster propagating siderush waves along the breakwater are responsible for the occurred damage.

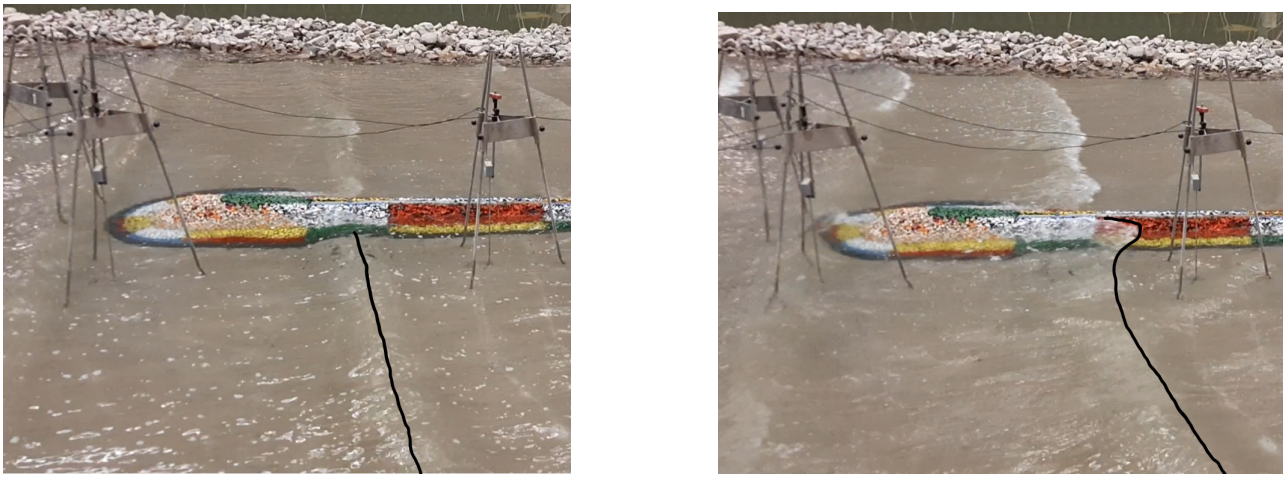

(a) straight wave line

(b) p line

Figure 2.7: Observations during physical model tests of the Eforie coast breakwater

After the test the effect and significance of this siderush became visible. Along the full length of the breakwater displacement of stones occurred, of which mostly at the waterline, while no significant damage at the toe armour was measured. Inspecting figure 2.8 clear damage around the waterline can be identified.

(a) Roundhead after design storm

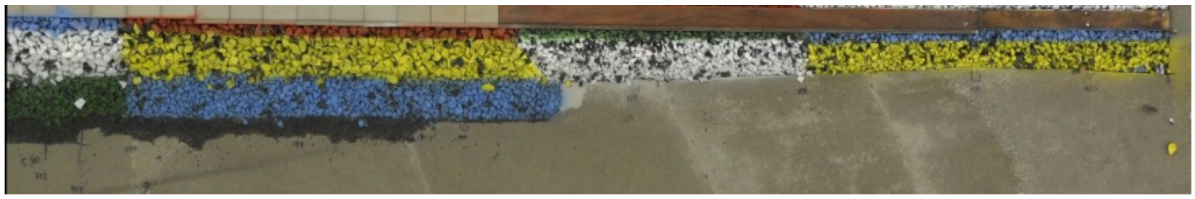

(b) Trunk after design storm

Figure 2.8: Overview of the Northern side of the breakwater after the design storm (van der Werf, 2021)

It is assumed that the very oblique wave angle and multiple slopes in front and along the breakwater cause the waves to show this siderush behaviour along the breakwater and therefore induce a different failure mechanism. In chapter 3 a different relation between flow action and stone stability will be set-up, to investigate breakwater stone stability for these very oblique wave angles.

Wave focusing

A phenomena is observed in some waves where part of the wave refract towards the breakwater and part of the wave stays parallel to the breakwater. These waves do not propagate as a straight line but are partially refracted. This phenomenon is shown in figure 2.9.

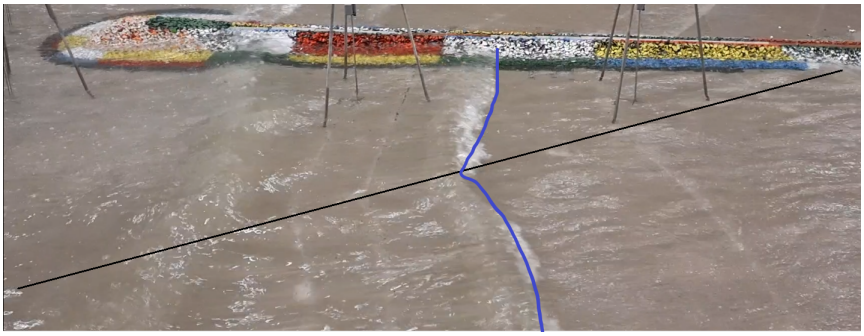

Figure 2.9: Refraction line

As stated before the upper foreshore is longshore non-uniform. The contour lines bend towards the breakwater in a parabolic bay shape but are cut-off and are extended perpendicular to the breakwater. This cut-off parabolic bay shape of the bathymetry seems to influence the wave propagation and refraction behaviour. At some point this refraction effect due to the bathymetry is no longer present which could lead to wave energy focusing to a certain part of the breakwater.

Shift from SS- to IG-wave energy

In the data from the Eforie model test a notable shift from swell wave energy to infragravity wave energy is visible in the wave propagation along the breakwater. Figure 2.12b shows different wave spectra along the breakwater, from WHM01 at the head of the breakwater to WHM04 at the shore.

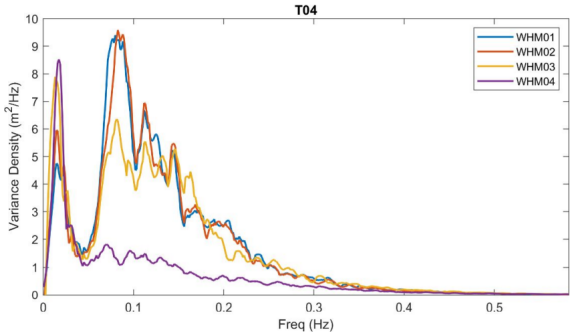

Figure 2.10: Wave spectra along breakwater (WHM01 at the head of the breakwater)

Damage

The damage values are only measured at the North side of the structure for chainages 0-310. Figure 2.11 presents the expected damage for the North side of the structure along chainages 0-310. There was no damage observed at the roundhead where X-blocs were placed and also not at the toe of the breakwater. The relevant area of the breakwater for this research is thus chainages 0-310 of the North side.

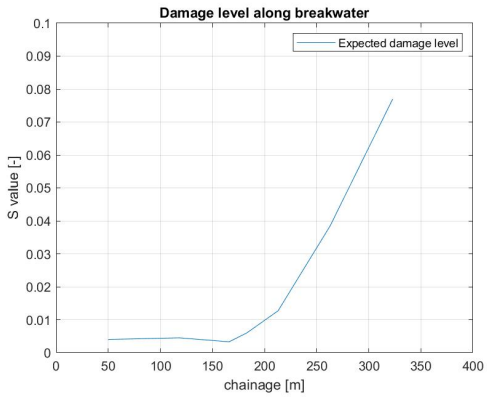

Figure 2.11: Calculated damage values front slope for design storm conditions

The expected damage was sufficiently low, with the largest expected damage at chainage 310 of around 0.08. The damage observed during the model test shows a different trajectory with larger measured damage values. Only a qualitative description of the damage figure is available. The measured damage during the model test shows two trajectories. Between chainages 0-125 the damage value increases from approximately 0 till just below 2. Around chainage 125 the stone size decreases, which could be an explanation for the increasing damage. Between chainages 125-310 the damage value increases again from approximately 0 till just below 2. This means the structure is stable, however the observed damage to the structure was larger than anticipated based on the available literature, shown in figure 2.11. Around chainage 100-150 is also where the before mentioned parabolic bay shape is no longer cut-off, but extended to the breakwater. This could be an explanation for the damage at that location.

2.4. Experimental data

For this research ideally one would have detailed information about flows and forces acting on the stones along the breakwater, as well as wave spectra of the wave moving along the breakwater, to validate the numerical model with data from the Eforie model test. That would allow for a better confidence in the eventual numerical model and chosen approach. As stated by Brown (2007), the performance of a numerical model depends most on the quality of the data that are put in the model and less on the incorporation of all the specific physics or the numerical method applied by the model (Brown and Kraus, 2007). Unfortunately these were not measured during the Eforie model tests. The relevant data that is available is listed first and then discussed in more detail below.

- The original Eforie bathymetry with breakwater implemented.
- The wave height, period and spectra at the different measurement locations.
- A qualitative description of the damage values along the breakwater.

Layout
From the contractor a file containing the original Eforie bathymetry with the breakwater implemented is available. It is assumed that the influences from the original bathymetry for the backshore slope and the upper foreshore slope where correctly taken into account in the Eforie model. For the numerical model the original bathymetry can be used, which will not result in deviations from the Eforie model data. Unfortunately, this does limit the options to make deviations to the upper foreshore slope and test the influence of this upper foreshore slope. The effect of the upper foreshore slope will not be investigated in this research.

Wave spectra
For output locations W01-W04 the wave spectra data are available. For output locations G01 and G02 the target -10m figure is available. During calibration of the numerical model at these locations the outcomes of the basecase model have to be compared with the target value. The gauges recorded the free surface elevation, which was translated to wave spectra. The wave spectra measured during the Eforie test are shown in figure 2.12.

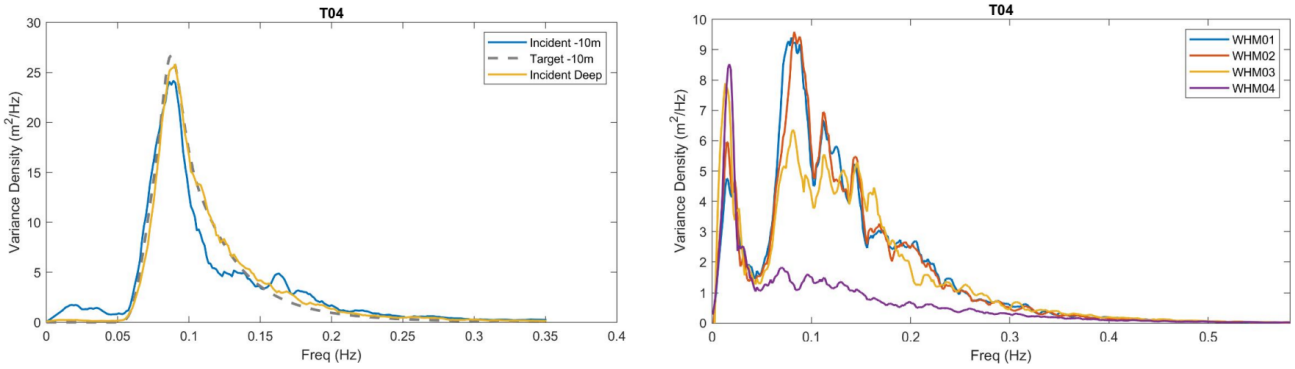

(a) SLS GRSM (b) SLS WHM

Figure 2.12: SLS (van der Werf, 2021)

	G01		G02	
	H_{m0} (m)	**T_p (s)**	**H_{m0} (m)**	**T_p (s)**
Eforie model test	4.40	11.3	4.40	11.3

Table 2.4: Eforie model test data of G01 and G02 - Full wave spectrum

	W01		W02		W03		W04	
	H_{m0} (m)	**T_p (s)**	**H_{m0} (m)**	**T_p (s)**	**H_{m0} (m)**	**T_p (s)**	**H_{m0} (m)**	**T_p (s)**
Eforie model test	4.05	13.0	4.01	10.7	3.86	76.1	2.54	62.8

Table 2.5: Eforie model test data of output locations W01-07 - Full wave spectrum

Damage values
A qualitative description of the damage values along chainages 0-310 of the North side of the structure is available. This is provided previously in this chapter.

2.5. Conclusion

The most important takeaways from this chapter are listed below.

1. From the Eforie case, the most important takeaways are that:
    - It contains multiple slopes in front and along the breakwater. The multiple slopes result in shallower water around the breakwater, which induces wave shoaling and breaking.
    - The incoming waves are very oblique.
    - Along the North side of the breakwater the contour lines are in a cut-off parabolic bay shape form near the breakwater.
2. From the Eforie model test, the most important takeaways are that:
    - In the Eforie model test a transitional slope was applied.
    - In the Eforie model test directional spreading was not applied at the offshore boundary.
3. From the Eforie model observations, the most important takeaways are that:
    - The damage, measured along chainages 0-310 of the breakwater, was more severe than expected based on the conventional design equations. The damage was fairly constant at the waterlevel line along the breakwater and therefore in this study this is the area of interest that is investigated.
    - Due to the oblique wave angle the wave impact on the breakwater showed a siderush instead of the more conventional up- and downrush. It is assumed that these faster propagating siderush waves along the breakwater are responsible for the occurred damage. This can explain why the conventional design equations are not sufficient for this case.
    - The cut-off parabolic bay shape seems to induce a refraction-pattern which could result in wave energy focusing.
    - Infragravity wave energy becomes increasingly dominant near the coast.
4. For the realisation of the numerical model several data files are available:
    - A bathymetry file, with the breakwater included. This implies that only the lower foreshore and offshore part of the bathymetry can be investigated in this thesis.
    - From the different measurement locations, wave spectra, wave heights and periods are available.
    - The measured damage-values along chainages 0-310 of the breakwater are available.

Concluding from these four points the relevant configurations to test in this thesis are the transitional slope, directional spreading, the wave angle, the foreshore slope and the cut-off parabolic bay shape. The precise interpretation of how these configurations are investigated is further explained in chapter 4. In addition to the effect these configurations have on stone stability, their effect on the presence of infragravity wave energy is interesting to investigate.

3

Theoretical background

In the previous chapter the Eforie case was investigated in detail. The measured damage along the breakwater was more than expected based on the conventional design equation. First the origin and applicability of this conventional design equation will be investigated. This results in a knowledge gap between the theory and the Eforie case. It was observed that due to the oblique wave angle a different failure mechanism occurred than is incorporated in the conventional design equation. If a different failure mechanism is responsible for the occurring damage, the conventional design equation can no longer be used for breakwater design and a different stability formula needs to be used. The knowledge gap will therefore be investigated with a different stability formula, that will be composed via the theory of stone stability under the influence of flow. The theory behind stone stability under the influence of flow is investigated and via this thread a stability formula is formulated, relating wave orbital velocity to a required stone size. The latest updates known in literature regarding the configurations, concluded from chapter 2, (transitional slope, directional spreading, wave angle, foreshore slope and cut-off parabolic bay shape) and their in(direct) on infragravity wave energy is stated. To test the usability and performance of the new stated formula and the effect of the stated configurations these will be investigated via a numerical model. The theory and consideration behind the used numerical model is elaborated in the final part of this chapter. It's flavours, strengths and weaknesses are linked to the composed stability formula. This way the usability and limitations of the numerical model for this research are explained.

3.1. Stability equations

The modified Van der Meer equation is a breakwater stability equation based on physical model test results. It is important to clearly state the test setup and the wave characteristics that governed during these physical model tests. This to understand the applicability and limitations of the formulated design equations and identify a knowledge gap between the design formula and the situation at the Eforie coast. To investigate this knowledge gap a more basic stability equation is setup, based on velocity as driving force.

3.1.1. Van der Meer

In 1938 Iribarren was among the first to link wave height to rock size via a stability formula. He developed a list of structure stability criteria that took into account an initial set of structural and hydraulic parameters De Heij (2021). In 1959 Hudson used the work done by Iribarren as the starting point for the development of his well known stability formula (Herrera et al., 2016). In 1988 Van der Meer adapted the Hudson formula and included the influence of permeability, allowed damage level, duration of the storm and the wave period. It was based on the work of Thompson and Shuttler from 1975 and resulted in a more robust formula that could be used in a large number of cases for statically stable structures (Vidal et al., 2006). These formulae are shown in equations 3.1 and 3.2, with 3.6 determining the critical Iribarren parameter. In these formulas the fit coefficients c_{pl} and c_s are 6.2 and 1.0 respectively. Besides table 3.1 shows the range of validity of the measurements taken into account by Van der Meer and thus the range of validity of his proposed formulas. It is important to note for this research that Van

der Meer based his formulas on data from tests with long crested waves, with deep water in front of the breakwater and normally incident incoming waves.

$$\frac{H_s}{\Delta * D_{n,50}} = c_{pl} * P^{0.18} * (\frac{S_d}{\sqrt{N}})^{0.2} * \xi_m^{-0.5} \quad (Plunging) \tag{3.1}$$

$$\frac{H_s}{\Delta * D_{n,50}} = c_s * P^{-0.13} * (\frac{S_d}{\sqrt{N}})^{0.2} * \sqrt{cot(\alpha)} * \xi_m^P \quad (Surging) \tag{3.2}$$

$$\xi_{cr} = [\frac{c_{pl}}{c_s} * P^{0.31} * \sqrt{tan(\alpha)}]^{\frac{1}{P+0.5}} \tag{3.3}$$

Parameter	Symbol	Range (1988)
Slope angle	tan(α)	1:1.5 - 1:6
Number of waves	N	<7500
Fictitious wave steepness based on T_m	s_{om}	0.01 - 0.06
Surf similarity parameter using T_m	ξm	0.7 - 7
Stability number	$H_s/\Delta * D_{n50}$	1-4
Damage level parameter	S_D	$1<S_d<20$
Armourstone gradation	D_{n85}/D_{n15}	<2.5
Relative buoyant density of armourstone	Δ	1 - 2.1
Relative waterdepth at toe	h/H_{s-toe}	> 3
Notional permeability paramter	P	0.1 - 0.6
Damage-storm duration ratio	$S_d/\sqrt{N}$	<0.9

Table 3.1: Range of validity of parameters in Van der Meer formulae (Ciria et al., 2006)

In the above formulas Van der Meer depends his stability on the significant wave height, H_s. It is however reasonable to assume that the larger wave heights are responsible for larger part of the damage. Further tests performed by Van der Meer concluded that $H_{2\%}$ was a better value to base breakwater stability on (van der Meer, 2017). Especially in shallow water where the distribution of wave heights deviates from a Rayleigh distribution. Offshore, in deep water, wave height statistics can be described via a Rayleigh distribution. This means H_s and $H_{2\%}$ have a fixed ratio of 1.4, which is incorporated into the formula via the fit coefficients c_{pl} and c_s. In shallow water however, due to processes such as wave breaking, the Rayleigh distribution no longer explains the wave height statistics. Therefore in 2000 Battjes and Groenendijk made a small adjustment to the equations to make it more valid for shallow water. They found that in shallow water, using the significant wave height to determine the breakwater stability results in a more conservative stone size than when the generally accepted $H_{2\%}$ is used (Ciria et al., 2006). Via laboratory experiments they concluded that a Weibull distribution, with its exponent depending on the wave height, can be used to more accurately describe the ratio between H_s and $H_{2\%}$ for shallow water conditions (Battjes and Groenendijk, 2000). By implementing the actual ratio between H_s and $H_{2\%}$, which can be calculated by means of the Battjes-Groenendijk method and excluding the implicit value of 1.4, the formula was better resilient for different water depths (Battjes and Groenendijk, 2000). Incorporating this into the formulae of Van der Meer results in the final Van der Meer equations, shown in equation 3.4 and 3.5. In these formulas the fit coefficients c_{pl} and c_s are now 8.7 and 1.4 respectively. Equation 3.4 must be applied for $\xi_m<\xi_{cr}$ and equation 3.5 must be applied for $\xi_m>\xi_{cr}$. However for gentle slopes, cot(α)>3, the transition from plunging to surging waves is only observed for long waves with a very low wave steepness. Therefore for situations where cot(α)>3, the same critical value as for cot(α)>3 should be used for determining the transition between plunging and surging (van der Meer, 2017). The Rock Manual recommends to use the above mentioned equations only if the local water depth at the toe of the structure is more then 3 times the significant wave height. A more accurate assessment can be made by calculating the actual $H_{2\%}/H_s$ ratio for the case at hand and check if this value deviates too far from 1.4 (van den Bos and Verhagen, 2018).

$$\frac{H_s}{\Delta * D_{n,50}} = \frac{H_s}{H_{2\%}} * c_{pl} * P^{0.18} * (\frac{S_d}{\sqrt{N}})^{0.2} * \xi_m^{-0.5} \quad (Plunging) \tag{3.4}$$

$$\frac{H_s}{\Delta * D_{n,50}} = \frac{H_s}{H_{2\%}} * c_s * P^{-0.13} * (\frac{S_d}{\sqrt{N}})^{0.2} * \sqrt{cot(\alpha)} * \xi_m^P \quad (Surging) \tag{3.5}$$

$$\xi_{cr} = [\frac{c_{pl}}{c_s} * P^{0.31} * \sqrt{tan(\alpha)}]^{\frac{1}{P+0.5}} \tag{3.6}$$

3.1.2. van Gent

In the past years van Gent made two adjustments to these final Van der Meer equations. Firstly, in 2003 van Gent expanded the physical model test research of Van der Meer and proposed to further modify the formula of Van der Meer for shallow water situations (Ciria et al., 2006). In these tests van Gent included two foreshore slopes in front of the structure, 1:100 and 1:30, applied shallow water depth at the breakwater and applied normally incident incoming waves (Van Gent et al., 2003). He concluded that for situations with shallow foreshores the equations give better results when using the spectral wave period, $T_{m-1,0}$, when determining the Iribarren parameter. Also he re-calibrated c_{pl} and c_s to 8.4 and 1.3 (Van Gent et al., 2003). These final formulas are shown in equations 3.7 and 3.8. Table 3.2 shows the range of validity of the measurements taken into account by van Gent and thus the range of validity of his proposed formulae. In 2008 Verhagen checked the above made adaptations to the Van der Meer formulas and concluded that these are valid in both deep and shallow water (Verhagen et al., 2008).

$$\frac{H_s}{\Delta * D_{n,50}} = \frac{H_s}{H_{2\%}} * c_{pl} * P^{0.18} * (\frac{S_d}{\sqrt{N}})^{0.2} * \xi_{m-1.0}^{-0.5} \quad (Plunging) \tag{3.7}$$

$$\frac{H_s}{\Delta * D_{n,50}} = \frac{H_s}{H_{2\%}} * c_s * P^{-0.13} * (\frac{S_d}{\sqrt{N}})^{0.2} * \sqrt{cot(\alpha)} * \xi_{m-1.0}^P \quad (Surging) \tag{3.8}$$

Parameter	Symbol	Range (shallow)
Slope angle	tan(α)	1:2 - 1:4
Number of waves	N	<3000
Fictitious wave steepness based on T_m	s_{om}	0.01 - 0.06
Surf similarity parameter using T_m	ξm	1 - 5
Stability number	$H_s/\Delta * D_{n50}$	0.5 - 4.5
Damage level parameter	S_D	<30
Armourstone gradation	D_{n85}/D_{n15}	1.4 - 2.0
Surf similarity parameter using $T_{m-1.0}$	$\xi s - 1.0$	1.3 - 6.5
Wave height ratio	$H_{2\%}/H_s$	1.2 - 1.4
Deep water wave height over water depth at toe	H_{so}/h	0.25 - 1.5
Core material - armour ratio	$D_{n50-core}/D_{n50}$	0 - 0.3

Table 3.2: Range of validity of parameters in the van Gent formulae (Ciria et al., 2006)

Secondly, van Gent continued the research on the influence of oblique wave attack on the stability of rubble mound breakwaters. In 1994 Galland already performed a series of model tests with long-crested waves and incident waves with angles between β = 0° and 75° on rock breakwater and concluded that armour stability increased (Galland, 1995). For crest walls this is the case since due to the wave obliquity the maximum loading does not occur over the full length of the crest wall at the same time. Instead of a rectangle-shaped force diagram acting on the wall a triangular-shaped force diagram should be used (Mares-Nasarre and van Gent, 2020). In 2011 Wolters performed tests for wave directions between perpendicular and 70°for a 1:1.5 slope. He confirmed the observations of Galland and even claimed the effects of obliquity were underestimated by Galland. He recommended to analyse the stability factor for more gentle slopes of 1:2 and 1:4 and for even larger wave angles such as 90 degree

(Wolters and Van Gent, 2011). In 2014 van Gent expanded the earlier research by Galland and Wolters. In the physical model tests he included the full range of obliquity for both and short- and long-crested waves, applied in relatively deep water, with a horizontal foreshore (Van Gent, 2014). He found that neglecting this influence results in conservative results for the required stone sizes and identified three wave angle groups with their own effect on stone stability (Van Gent, 2014). The influence of oblique waves is relatively small for small wave angles, between 0 and 15°. The influence of oblique waves is relatively large for wave angles between 15 and 30°. The influence of oblique waves does not increase much for the largest wave angles, above 70°. Besides he found that for rock slopes the influence of oblique waves depends on the type of wave, the influence is larger for long-crested waves than for short-crested waves (Van Gent, 2014). He proposed a reduction factor for the rock size that can be applied based on the angle of incidence of the incoming waves. The formula for this reduction factor is shown in equation 3.9 and results in the final design formula used to determine the required stone size for the tested breakwater. With c_β=0.35 for rock slopes with long-crested waves. It is expected that this expression provides reasonable estimates for wave angles between β = 0°(perpendicular waves) and β = 90°(parallel waves).

$$\gamma_\beta = (1 - c_\beta) * cos^2(\beta) + c_\beta \tag{3.9}$$

3.1.3. Knowledge gaps

To conclude the above, Van der Meer performed his tests in deep water with a horizontal foreshore and therefore did not include a foreshore slope in his research. Besides due to model limitations he only applied normally incident long crested waves. In the tests where van Gent tested the Van der Meer formulas for shallow water he included two foreshore slopes in front of the structure, 1:100 and 1:30 (Van Gent et al., 2003) and performed his tests in shallow water with normally incident long crested waves. In the tests where van Gent investigated the influence of wave obliquity he performed his tests in relatively deep water, with a horizontal foreshore and therefore no wave breaking occurring at the breakwater or on the horizontal foreshore (Van Gent, 2014). In these tests both long-crested (unidirectional) as short-crested multi-directional waves were tested. The short-crested waves were applied with a constant directional spreading of σ=25 °. This is summarized in table 3.3.

	Waterdepth	Foreshore	Angle
Van der Meer (1988)	Deep	Horizontal	Incident
van Gent (Shallow) (2003)	Shallow	Sloped	Incident
van Gent (oblique) (2014)	Deep	Horizontal	Oblique

Table 3.3: Comparing theories

The Eforie model test, contains a sloping foreshore, shallow water conditions at the breakwater and long-crested very oblique waves. Comparing this to table 3.3 indicates that the Eforie model test is a situation in which all three deviations, sloped shallow foreshore and oblique waves, from the classic Van der Meer tests are present. These have always been treated separately and not together. This presents a knowledge gap between the known literature and the Eforie case. The presence of a sloping foreshore, shallow water depth and oblique waves together could perhaps induce effects that are responsible for the observed damage. Investigating the effect of oblique incoming wave angle for a breakwater in shallow water has not been done before. In chapter 2 the observed siderush along the breakwater is discussed in depth. It is assumed that these faster propagating siderush waves along the breakwater are responsible for the occurred damage, which is a different failure mechanism than is incorporated in the modified Van der meer formula, which is based on $H_{2\%}$ and T_p. The modified Van der Meer formula is therefore not sufficient to use in this thesis. The original stone stability theory is explored to draw up a relation between stone stability and flow velocity along these stones.

3.1.4. Izbash and Shields

Izbash (1935) and Shields (1936) where among the first to study, via theoretical and experimental approaches, the stability of rocks under influence of flow. Around 1935 they derived stone stability formulae with stability parameters that both linked stone size to u^2. In 2013 Recking and Pitlick compared the approaches and results of the Shields and Izbash experiments. The two equations were derived via

different methods, but as shown in this study, in practice provide similar sediment transport volumes for flume and field experiments (Recking and Pitlick, 2013). Shields focuses on the average shear stress on the entire bed, based his theory on a uniform flow, with turbulence only generated by bed roughness and implicitly assumes that the Chezy formula is applicable to the situation. Shields resulted in a stability parameter of 0.05. Since then, this value has been continuously discussed and nowadays, the rock manual proposes a value of 0.03 for rubble mound structures. This is a very safe value in which no movement of rock is accepted (Recking and Pitlick, 2013). In situations with shallower water, induced turbulence and rough bed, the Izbash formula is recommended. Izbash focuses on the force action on a single grain and specifically looked at stone stability for a dam under influence of flow and wave action (van den Bos and Verhagen, 2018). Therefore for this research the Izbash theory and equation is taken as governing for the situation under investigation. He derived a mathematical formula from a balance of forces acting on one single grain and then scaled it with experimental data with K as the scaling coefficient and E the dimensionless stability parameter. The simplest form of this equation is shown in equation 3.10.

$$u^2 = K\Delta g d_{n,50} \rightarrow \Delta d_{n,50} = K * \frac{u^2}{2g} = \frac{1}{K} * \frac{1}{E^2} * \frac{u^2}{2g} \tag{3.10}$$

In this general formula Izbash requests the flow velocity near the stone (Izbash, 1935). As stated, the experiments where performed to provide criteria for dam stability, the findings are however also used for the design of rubble mound structures Izbash (1935). In the equation the velocity close to the rock should therefore be used. However in practice the depth-averaged velocity or the average maximum velocity is often used (Ciria et al., 2006).

There are several approaches for evaluating the stability of granular bed protectors. The threshold of motion and the stone transport notion used by Shields are the most well-known. As Hofland stated threshold of motion is described by Shields as the state of the bed in which some particles are displacing at each moment at each part of the bed Hofland (2005). Besides an extra safe critical value is identified, where rocks are observed to start rocking and occasionally displacement of rocks occur. Izbash performed his tests by dropping rocks into running water and resulted in two governing situations, as shown in figure 3.1. The stones placed on top of the triangular structure, left side of the figure, were more exposed and resembled a situation where nonuniform rocks are investigated. Therefore when the stone is exposed to the flow, the dimensionless stability parameter E is determined to be 0.86. The stones placed among the other stones in the triangular structure, right side of the figure, resemble when stones are sheltered by other stones. This results in a dimensionless parameter E of 1.2. Recking and Pitlick compared the applicability of the two different E-values (Recking and Pitlick, 2013). A breakwater is typically build to resemble a smooth and stable surface and therefore for this application the highly stable E-value of 1.2 is used. As Izbash was an engineer responsible for designing dams he probably took conservative assumptions to design resilient structures. This is confirmed by Recking and Pitlick, who found that the E-values of Izbash coincide with a critical Shields stress of around 0.03 and could therefore lead to oversizing (Recking and Pitlick, 2013).

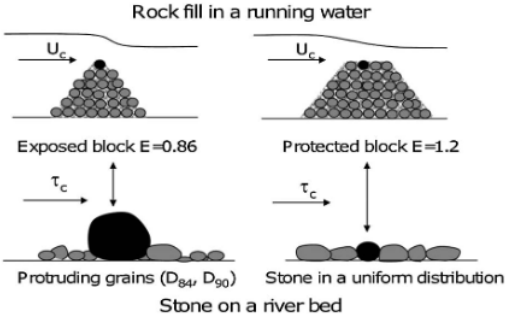

Figure 3.1: Izbash experiment setup (Recking and Pitlick, 2013)

In comparison to most published stone stability formulas, which focus on sand transport, rock transport

is characterized by low mobility. Therefore stability means that incidentally a stone may move over a limited distance. Furthermore, differences in physical phenomena such as bed roughness, grain shape (roundness), turbulence, and porous flow through the bed render existing sand transport formulas useless for rock transport analysis. Therefore Paintal conducted similar measurements where he focused on coarse-grained sand and low-mobility transport and created a probabilistic theoretical model of stone transport in which stones move in discrete steps, rolling and sliding a short distance along the bottom before being redeposited (Van den Bos et al., 2011). Paintal discovered that the dimensionless transfer rate is solely a function of the Shields parameter Paintal (1971). He linked the low-mobility transport formula for dimensionless shear stresses under the critical Shields value of Ψ = 0.05 Paintal (1971). The values of the critical shear stress parameter can be assumed to be 0.03 for rock for absolute stability. When some limited displacement of stones is accepted a value of 0.05 is accepted to be used. Therefore increasing the allowed critical Shields stress to 0.05 would coincide more with the damage values acquired in the physical model tests. Both the critical Shields stress and the stability parameter in Izbash-equation scale with u^2. Therefore in this research the scaling factor is scaled from 0.03 to 0.05. Applying this E-value and scaling it to an appropriate stability value for this research, results in formula 3.11.

$$\Delta d_{n,50} = \frac{1}{K} * \frac{1}{E^2} * \frac{u^2}{2g} = \frac{1}{K} * \frac{1}{1.2^2} * \frac{0.03}{0.05} * \frac{u^2}{2g} = \frac{1}{K} * 0.42 * \frac{u^2}{2g} \tag{3.11}$$

3.1.5. Pilarczyk

Later in 1985 Pilarczyk specified the scaling coefficient stated by Izbash and defined the most important relevant scaling factors. Via scaling coefficient the impact of turbulence, slope, acceleration, etc. can be included to the equation, such as described in Schiereck and Verhagen (Schiereck, 2017). These factors are often fitted empirical relations based on tests in specific settings. This results in a diverse set of influence factors, as shown in equation 3.12. It can be easily seen that this formula has the same form as the relation identified by Izbash, but now allows for more generic use in different situations (Steenstra et al., 2016). In our observed situation the effect seems not so much only due to the impact of the waves, but rather due to the flow velocity of the wave moving along the breakwater in combination with the turbulence due to the continuously breaking of the wave. As Ottemheim concluded the impact of the breaking wave does not inflict more damage to a stone layer than a uniform flow with the same velocity and turbulence (Ottenheim, 1997). Besides as stated by Iribarren higher wave means a higher wave celerity and the flow velocity of a bore is more or less equal to its wave celerity. Thus using the wave celerity as flow velocity to assess the influence on stone stability is legitimised. As this is a first step into this research field, for this research therefore only the influence of the perpendicular slope is taken into account via the slope factor. This means that influence from the water depth and turbulence are not taken into account.

$$\Delta d_{n,50} = 0.035 * \frac{\Phi}{\Psi} * \frac{K_t K_h}{K_s} * \frac{u^2}{2g} \tag{3.12}$$

Φ	Stability parameter
Ψ	Velocity parameter
K_t	Turbulence factor
K_h	Depth factor
K_s	Slope factor

Stability parameter
For two layer stone construction the stability parameter can be assumed 0.75.

Shields parameter
For rubble mound breakwater the velocity parameter can be assumed 0.035.

Turbulence factor
The turbulence factor varies between 0.67 for low turbulent flow and 4.0 for extreme high turbulent flow. This factor will be left out of the equation since a substantiated estimate can not be clearly made.

Depth factor
The depth factor can be calculated with equation 3.13 or equation 3.14 for a not fully developed velocity profile. For now this depth factor is also left out of the equation.

$$K_h = \frac{2}{log(\frac{12h}{N})^2} \tag{3.13}$$

$$K_h = (1 + \frac{h}{d})^{0.2} \tag{3.14}$$

Slope factor
In 1938 Iribarren was among the first to study the stability of rocks on a slope. He identified similar forces acting on a stone as Izbash, but included the effect of the slope. Iribarren could not measure the flow velocity of the waves rushing along the stones on the slope. He therefore assumed the velocity via the wave celerity in shallow water, where he took the wave height as the water depth (De Heij, 2021). The slope factor can be calculated with equation 3.15. Research performed by Beakawi Al-Hashemi and Baghabra Al-Amoudi, based on ealier research of Iribarren, suggests that the angle of repose is negatively correlated to the diameter of the material. As can be seen in figure 3.2c he derived a correction factor for the stone diameter in case of a slope along the flow and in situations with a slope perpendicular to the flow. As figure 3.2d shows a slope perpendicular to the flow leads to a reduction in stone stability. This means that the angle of repose decreases for a bigger used stone size diameter (Beakawi Al-Hashemi and Baghabra Al-Amoudi, 2018). The angle of repose influences the slope factor and via this factor influences the critical stone size quite significantly. In literature for angular rock an a angle of repose between 40-45°is suggested (Ciria et al., 2006) and (Froehlich, 2011). To be on the safe side an angle of repose of 40 °is used. However small deviations in this number can have significant effects on the calculated critical stone size. Therefore with an angle of repose of 40 a K_s is calculated. It shows that the chosen angle of repose influences the critical stone diameter as expected. This needs to be taken into account in the discussion. In this research a angle of repose of 40 is assumed, which for this research results in a K_s value of 0.505. The slope of the rubble mound rock part of the breakwater is 2:3. This results in a slope factor of 0.505.

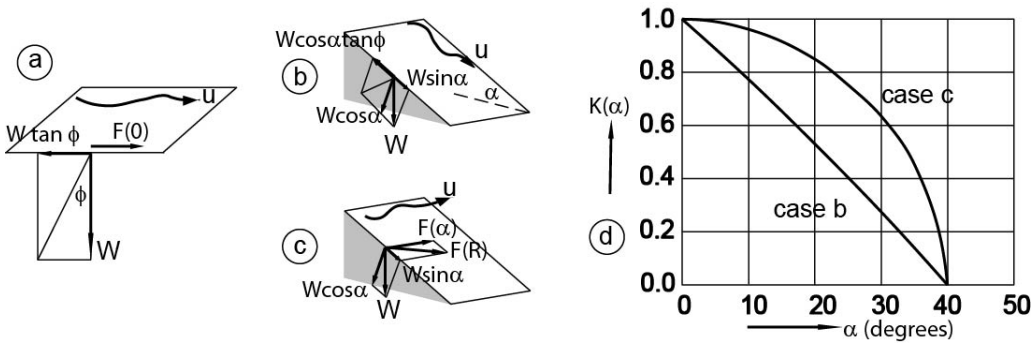

Figure 3.2: Damage on steep and gently sloping foreshore with similar wave conditions (Schiereck, 2017)

$$K_s = \sqrt{1 - \frac{sin^2(\alpha)}{sin^2(\phi)}} = \sqrt{1 - \frac{sin^2(33.7)}{sin^2(40)}} = 0.505 \tag{3.15}$$

The Pilarczyk formula can be reduced to formula equation 3.16. This formula is more conservative than the self established formula using the theory from Izbash, Shields, Paintal and Iribarren shown in equation 3.11. Since Pilarczyk resulted in a very generic formula that had to be safe for a large variety of structures, this is expected.

$$\Delta d_{n,50} = 0.75 * \frac{1}{K_s} * \frac{u^2}{2g} \tag{3.16}$$

3.1.6. Conclusion

The most important takeaways from this chapter are listed below.

1. A knowledge gap is identified for the Eforie case, with shallow water, a foreshore slope and oblique waves.
2. It is determined that for the Eforie case a different failure mechanism is governing for stone stability. The modified Van der Meer equation based on wave height and period are not sufficient, but stone stability will be based on velocity.
3. The influence of the slope, perpendicular to the flow direction is taken into account. Influence from water depth, turbulence or shear stresses are not taken into account.
4. The eventual stability formula governing in this research is presented in equation 3.17. In the equation the velocity close to the rock should be used. In practice it is sufficient to use the depth-averaged or average maximum velocity.

$$\Delta d_{n,50} = \frac{1}{K_s} * 0.42 * \frac{u^2}{2g} = \frac{1}{0.505} * 0.42 * \frac{u^2}{2g} = 0.83 * \frac{u^2}{2g} \tag{3.17}$$

3.2. Research related theory

The stability formula will be used to investigate the relative effect on stone stability of the different configurations presented in chapter 2. Namely, the transitional slope, directional spreading, wave angle, foreshore slope and cut-off parabolic bay shape. In addition, their effect on the presence of infragravity wave energy and the effect of infragravity wave energy on stone stability is discussed.

3.2.1. Infragravity wave energy

Infragravity waves are ocean waves, with typical period between 25-250 seconds. They are indirectly formed by the wind because they receive their energy from the short sea- and swell waves, from now on referred to as sea-swell (SS) waves (Longuet-Higgins and Stewart, 1964). During a storm waves with all kinds of frequencies and amplitudes are created/directed in all directions. After frequency and directional dispersion have influenced these waves, waves travel in groups of higher and smaller amplitude. Due to this wave height variation the radiation stresses also vary within the group, with the highest stress under the highest waves. This results in a time-varying set-down in the shoaling zone (outside the surf zone). With largest depressions under the highest waves. This results in a long wave motion on the wave group scale. The long wave is bound, it has the length, frequency and speed of the group (bound long wave). This is visualised in figure 3.3.

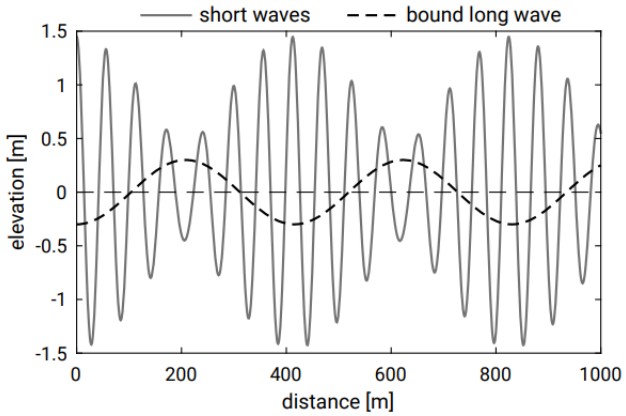

Figure 3.3: Bound long wave (Bosboom and Stive, 2021)

When SS-waves enter the surf zone and break this forcing mechanism becomes weaker. The bound long is released from the group and continuous as a free long wave. This released wave propagates

faster than the wave group. Infragravity waves tend to be significant and can even become dominant under shallow water conditions (Hofland et al., 2017).

The relevance of infragravity wave energy on dune erosion is a currently highly relevant topic (Diwedar et al., 2019). Research shows that low frequency wave energy induces a set-up of the waterlevel near the coast (Roelvink et al., 2009). Since the short waves at these smaller water depths are depth-limited, this increase of the water depth results in an increase in short wave height. These higher waves result in more dune erosion (van Thiel de Vries, 2009) and (Bertin et al., 2018)). This leads to the idea that infragravity waves could also be of influence for structural stability. Bux (2007) already claimed the idea that longer period waves would induce more damage (Bux, 2007). The direct effect of these low frequency waves on the short wave development along a structure and the stability of this structure is however unknown. Lashley (2021) investigated the influence of infragravity waves on overtopping. In this research he also investigated which configurations influence these infragravity waves. He draw two conclusions relevant for this research.

Firstly he concluded that certain foreshore slopes give rise to infragravity-wave dominance (Lashley, 2021). When waves enter shallower water over mildly-sloping foreshores and start shoaling the transfer of energy from the SS-waves to the IG-waves continues. This leads to IG-waves growing on mild slopes. This phenomena is stronger for mildly sloping foreshores, where the normalized bed slope parameter β_b, calculated via equation 3.18, is smaller than 0.3. However, on very steep slopes, where the normalized bed slope parameter β_b is equal to or bigger than 1, a phenomena may occur in which IG-waves may be generated on the very steep foreshore slopes (Lashley, 2021). Therefore IG-waves can be generated for β_b<0.3 and for β_b>1.

$$\beta_b = \frac{\beta}{\omega}\sqrt{\frac{g}{h_b}} \tag{3.18}$$

$$\omega = 2\pi f_{low} \tag{3.19}$$

Parameter	Unit	Description
β_b	[-]	Normalized bed slope
β	[-]	Bed slope
ω	[rad/s]	Angular frequency
f_{low}	[Hz]	mean frequency of IG-wave at breakpoint
g	[m/s^2]	Gravitational constant
h_b	[m]	mean breaker depth

Table 3.4: Parameters for calculating β_b

Secondly he concluded that directionally narrow-banded offshore waves give rise to infragravity-wave dominance (Lashley, 2021). IG-wave energy dissipation is significantly more present when directional spreading is taken into account. Directional spreading needs to be taken into account at the offshore boundary, since the assumption of uni-directionality leads to overestimation of $H_{m0,IG}$ (Van Dongeren et al., 2003). These conclusions are done for a case with shallow water conditions, where wave breaking results in an increase in directional spread of wave energy (Herbers et al., 1999). The effect of directional spreading is expected to be less for deeper conditions. In the Eforie case the waves are applied at deeper water depths, but propagate to shore to relative shallower water.

3.2.2. Configurations

The latest updates in the literature for the identified configurations are presented here.

Transitional slope

The transitional slope of 1:10 was applied from a depth of MN75-13.5m till a depth of MN75-23.5m. This transitional slope can affect both the SS-wave energy or the IG-wave energy part of the waves.

To make an assumption on the influence of the transitional slope on the SS-wave energy part, the Ursell number and the wave steepness are calculated. With the data from the physical model test at the offshore boundary, MN75-23.5m, and at the MN75-13.5m location. The Ursell number can be calculated with equation 3.20 and the steepness with 3.21 (Hedges, 1995). Table 3.5 shows the results.

$$U = \frac{H * L^2}{h^3} \tag{3.20}$$

$$s = H/L \tag{3.21}$$

	Deep	Transitional slope
H	4.40	4.40
T	11.30	11.30
d	24.23	14.23
L	152.0	123.50
s	0.029	0.036
U	7.15	23.29

Table 3.5: Ursell numbers and wave steepness

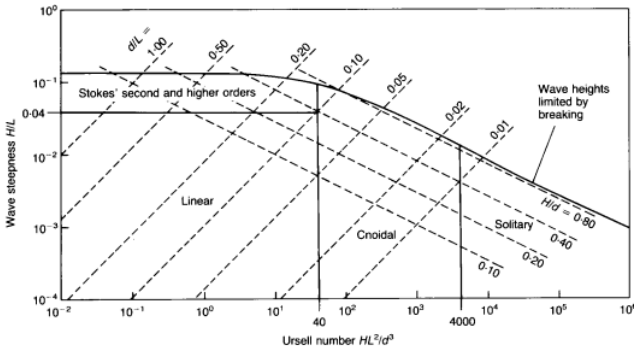

Figure 3.4: Approximate regions of validity wave theory (Hedges, 1995)

The main assumption on which the linear wave theory is based is that the second-order term is much smaller than first order term (Hedges, 1995). For waves with small Ursell numbers, this assumption holds and linear wave theory is valid. From table 3.5 and figure 3.4 it can be concluded that the Ursell number is small enough for this assumption to be valid. Therefore linear wave theory holds for both water depths, meaning the influence of the bottom is negligible. Therefore the assumption is that this transitional slope has no to limited direct influence on the SS-wave height. It lies deep enough, approximately 14m, relative to the waves, of around 4.4m.

By calculating the normalized bed slope ratio and discussing its relation to the critical values of 0.3 and 1, an expectation can be formulated for the expected effect of the transitional slope on the IG-wave energy. Stating again that IG-waves can be generated for β_b<0.3 and for β_b>1. Table 3.6 shows the calculated values for the 1:10 transitional slope.

Slope-part	β	f_{low}	ω	g	h_b	β_b
Transitional slope	1/10	1/60	0.105	9.81	7	1.2

Table 3.6: β_b for the lower foreshore and transitional slopes

Table 3.6 shows that the normalized bed slope ratio is bigger than 1, thus IG-waves may be generated on this steep foreshore slope (Lashley, 2021). This effect could be the cause of the observed IG-wave energy dominance near the coast in the Eforie model test.

Directional spreading
Long crested waves are defined as waves propagating from one direction, while the short crested waves are defined as the combination of different long crested waves propagating from different directions (Wang et al., 2006). The damages at the head of a breakwater under unidirectional waves are larger than those caused by multi-directional waves (Matsumi et al., 1995). In 2002 Yu et al performed stone stability tests for short- and long-crested oblique waves. They concluded that for oblique waves directional spreading did not significantly influence the stability of rocks (Yu et al., 2002). The unidirectional wave heights are expected to be larger than their corresponding multi-directional values (Briggs and Grace, 1988). Applying long crested waves will result in an overestimation of H and thus the required stone size. Besides as concluded by Lashley long crested waves lead to a better evolution of infragravity waves, which could increase the measured wave height even further. In the unidirectional case the period shifts more than in the directional cases due to wave transformation. So the influence of infragravity wave energy in the total wave energy distribution decreases for directionally wide-banded (short-crested) offshore waves (Lashley, 2021).

Wave angle
The influence of wave angle found by Galland and van Gent has already been discussed above. The Eforie case contains a combination of oblique wave angle with a shallow foreshore slope, which induces wave breaking. It is expected that this combination induces a different breaking wave propagation pattern that can be compared to a continuously breaking bore or a jet. Based on the clips from the model test it is expected that the oblique waves induce higher damage along the breakwater on the shallow foreshore. There is no literature available on this observed phenomena to substantiate this. In addition, another phenomena related to the wave angle is worth to be discussed here: The occurrence of a Mach-Stem wave. In an article of van Gent of 2021 he discussed the influence of oblique waves on wave overtopping at caisson breakwaters. In this research for oblique waves the conditions with long-crested waves approaching under the most oblique wave angle, over 70 °contribute the most to the scatter. An identified potential reason for this was the presence of stem waves for these very oblique long-crested waves. He states that the stem waves develop more easily and better for regular, one frequency, waves and require a number of wave lengths for irregular, a wave spectrum, waves. Besides the resonance is better for short-crested waves than for long-crested waves (van Gent, 2021). Mach stem waves originate when oblique waves reflect on the structure and create a second wave traveling behind the incident wave. This reflected wave travels faster than the incident wave, since it is traveling through water which is already moving due to the incident wave. At a certain point the reflected wave will merge with the incident wave and form a single Mach Stem wave. In 2002 Mase et al investigated stem wave effects near structures for oblique incoming waves and concluded that stem waves could increase the height of the occurring wave along the structure (Mase et al., 2002). In figure 3.5 a sketch of this phenomenon is shown compared to the observed effect in the Eforie model test.

(a) Sketch of stem waves along vertical wall (Mase et al., 2002)

(b) Picture of model tests

Figure 3.5: Comparing Stem wave sketch with model test picture

Comparing figure 3.5a with figure 3.5b it seems that an opposite effect is visible during the physical model test. In the occurrence of a mach stem wave the stem wave part of the wave increases in size along the breakwater. In the Eforie model test the opposite is observed. The straight part of the wave

decreases along the breakwater. Therefore it is assumed that mach stem waves are not responsible for the measured damage.

Lower foreshore

A foreshore slope in front of a structure leads to waves breaking, which induces energy loss and generates vorticity and thus induces turbulence (Gagarina et al., 2013). In the past decade many researchers have found that the foreshore slope does influence breakwater stability and that steep foreshores result in more damage than gentle foreshore slopes (Verhagen and Mertens, 2010). Research done by Bux in 2007 concluded that a steeper foreshore slope results higher wave impacts and therefore higher damage values (Bux, 2007). He stated that for structures realised on a steep slope, more consideration should be paid to the armour unit stability. Bux concluded that model studies should be performed to further investigate breakwater stability on steep foreshores. In 2017 Hofland et al. posted an article where they investigated the influence of mildly sloping shallow foreshores on the spectral wave period and its influences on the stability parameter. One of their conclusions was that the influence of the foreshore slope was not fully understood. Besides the tests where performed for a mildly sloping foreshore and the effect of a steep foreshore are not investigated. They discussed that it is interesting to extend the range of research to different foreshore slopes (Hofland et al., 2017).

Verhagen together with research from Muttray and Reedijk stated that the foreshore steepness affects the rock stability in two ways. Firstly the depth limited wave heights will be larger on a steep foreshore. Secondly the non-linear effects, such as wave asymmetry and peakedness result in a larger wave impact (Muttray and Reedijk, 2009). In 2010 Verhagen and Mertens published the conclusions of the research in this topic, where they looked at the influence of the foreshore slope on rock stability for shallow and deep water conditions. One-dimensional SWAN calculations where performed for various configurations that included shallow and deep water conditions and varying foreshore slopes. He concluded that for irregular waves on a steep slope, the average wave height in shallow water becomes higher, due to breaking of the smaller waves. This way on steep slopes the $H_{2\%}$ can become significantly high, which lead to a high required stone diameter. There results are shown in figure 3.6 Verhagen and Mertens (2010).

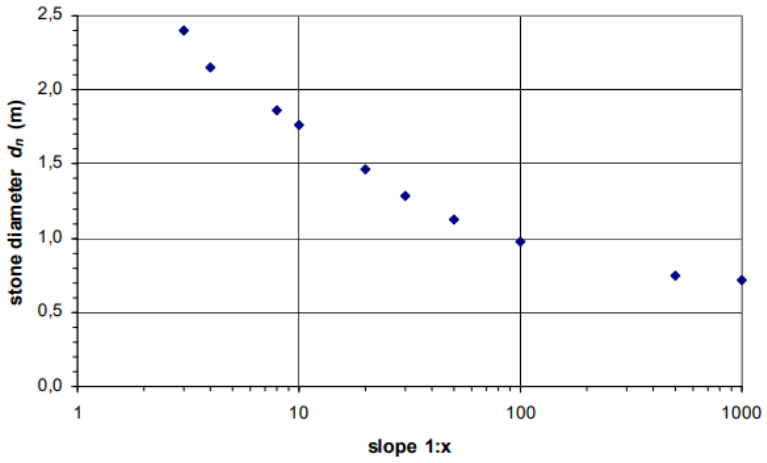

Figure 3.6: Relation between foreshore slope and d_{n50} (Verhagen and Mertens, 2010)

The 1:120 lower foreshore slope in the Eforie case is, looking at figure 3.6, likely not responsible for the observed damage via an increase in $H_{2\%}$. In the research by Lashley, described above, it was mentioned that milder foreshore slopes give rise to infragravity-wave dominance (Lashley, 2021). The presence of infragravity waves and them having an effect on stone stability could place a side note to the research of Verhagen and Mertens of 2010. They used the numerical model SWAN for their research, which does not take into account the IG-wave energy. In table 3.7 the normalized bed slope parameter of the lower foreshore is calculated. Stating again that IG-waves can be generated for β_b<0.3 and for β_b>1. The normalized bed slope parameter of the lower foreshore is smaller than 0.3. The lower

foreshore is therefore a mildly sloping foreshore, where IG-waves grow. This effect could be the cause of the observed IG-wave energy dominance near the coast in the Eforie model test.

Slope-part	β	f_{low}	ω	g	h_b	β_b
Lower foreshore	1/120	1/60	0.105	9.81	7	0.10

Table 3.7: β_b for the lower foreshore and transitional slopes

Cut-off parabolic bay shape
Wave refraction could lead to wave energy focusing. The local bathymetry layout could be important for breakwater stability (Chen et al., 2018).

3.2.3. Conclusion
The main conclusions from this chapter are:

1. The effect IG-wave energy has on the stability of a structure is not known.
2. The transitional slope is not expected to have influenced the SS-wave energy and therefore stone stability. The IG-wave energy can however be increased due to the steep slope.
3. The exclusion of the directional spreading is assumed to have an overestimating effect on the damages measured at the head of the breakwater.
4. Based on the available literature oblique waves are expected to induce less damage than normally incident waves with the same wave height. The hypothesis of this research is that for oblique waves on a shallow foreshore the opposite effect occurs.
5. The 1:120 lower foreshore slope is expected to have limited effect on the SS-wave energy and stone stability, but an increasing effect on the IG-wave energy.
6. The cut-off parabolic bay-shape profile of the bathymetry leads to wave energy focusing, which can affect local stone stability significantly.

3.3. Numerical model
For this research a model is needed that can resolve and account for several important physical phenomena as well as the interaction of waves with porous structures. As stated above it needs to reflect processes induced due to bathymetry and shallow water conditions, such as refraction, shoaling and wave breaking, the presence of infragravity waves and for output it needs to be able to provide a velocity signal. Many different numerical wave models exist, each with their own strengths and applicability based on the numerical schemes incorporated (Holthuijsen, 2007). A division based on phase can be made into phase-resolving and phase-averaging models. Phase resolving models are able to describe sea surface in time and space. For this reason they are recommended for cases such as wave modeling around breakwaters. Although a phase-resolving model is computationally more expensive than a phase-averaging model, a phase-resolving model is required since a breakwater is modelled.

Within phase-resolving models, there are generally two types related to the main set of governing equations each one solves: The Boussinesq type and the Non-Linear Shallow water Equation (NLSW). (Guzman Mardones, 2011). Boussinesq-type models directly account for dispersive properties of waves in deeper water. The NLSW models assume that waves are non-dispersive and are therefore limited to shallow-water applications (Zijlema et al., 2011). However in 2003 Stelling and Zijlema proposed a method to account for dispersion while using the NLSW equations for phase resolving simulations of short waves. A hydrostatic model uses the hydrostatic assumption, while a non-hydrostatic model includes the momentum equation for the vertical-oriented velocity w and the Poisson equation for the non-hydrostatic pressure. By decomposing the pressure in a hydrostatic and a non-hydrostatic part the dispersive properties of the equations improve without neglecting the higher-frequency motions (Stelling and Zijlema, 2003). This is implemented in SWASH and XBEACH-NH and in these models the accuracy and range of applicability of the non-hydrostatic models may be further enhanced by

coarsely dividing the model domain into a fixed number of vertical layers, improving the frequency dispersion (de Ridder, 2018). By increasing the number of vertical layers, models like SWASH may even be extended to the depth-resolving class (Cea et al., 2009). This approach increases the computational demand but allows processes, such as undertow and the shoreward flow near the surface, to be resolved. This hydrostatic pressure assumption has been widely used in studying water movements in shallow waters where the water depth is much smaller than the wave length. It is assumed that the pressure field in a shallow water flow is hydrostatic because the non-hydrostatic pressure component is much smaller than the hydrostatic pressure component and thus be safely neglected in model simulations. With this assumption, a three-dimensional, hydrodynamic model can be significantly simplified because the momentum equation in the vertical direction is reduced to an expression of hydrostatic pressure (Chen, 2005).

Same as the division on phase a division on depth can be made into depth-resolving and depth-averaged models. Depth-averaged means that the balance of mass and momentum equations are integrated along the depth. When looked at larger scales or 3D phenomena a depth-averaged model is more suited for operational use. A depth-resolving model, also called Computational Fluid Dynamics (CFD), is the most complete model. However due to its capabilities it is also computationally the most demanding and therefore restricted to local phenomena. An example is OpenFOAM. OpenFOAM with the waves2Foam toolbox is a free surface modelling tool based on the Reynolds-Averaged Navier-Stokes equations (Zaalberg et al., 2020). As stated this is the most complete, but also computationally demanding model.

Table 3.8 shows the most used model for modelling wave translation. This research requires a model that can translate the full-frequency range from wind-sea swell waves to infragravity waves. Therefore a phase resolving model is required. In 2013 Buckley compared the performance of SWAN with SWASH and XBEACH in predicting wave heights, swell and infragravity, in shallow water coastal environments. His results showed that as expected SWAN was not capable of predicting transformation of energy to the low frequencies. Besides SWASH and XBEACH showed comparable results in predicting the wave energy distribution (Buckley et al., 2014). XBEACH could be a viable option for the numerical task at hand. It comes in two relevant modes. XBEACH-SB is a process based model, so equilibrium follows from balance of forces/transport contributions. The model is a short wave averaged, long wave resolving 2DH model. Because their speed does not depend on wavelength, but only depend on water depth, the waves are said to be non-dispersive. This limitation can be removed by taking a SS-wave averaged approach; however, at the cost of decreased accuracy. The high-frequency waves are averaged, resulting in only motions at the scale of the wave group; thus, reducing the computational demand. It simulates in two dimensions of the horizontal, but no information on variation over depth. It is designed to assess storm impact/erosion on sandy beaches and dune systems. For the application in this research short wave averaging is not desired. XBEACH with the Non-hydrostatic assumption could be a viable option. It shows proper results for similar cases where infragravity wave energy becomes significant near the coast. However the multi-layered version of XBEACH-NH is not sufficient and still under revision. Besides a 3D model is required that can take into account wave refraction and breaking along a 3D breakwater. Using OpenFoam for a 3d model will result in extreme computation time, therefore another model is preferred. SWASH can be applied for wave transformation estimations on shallow foreshores with reasonably low computational costs (Suzuki et al., 2017). This means the wave transformation from offshore to onshore and the interaction between structure and wave is modelled correctly via SWASH. Therefore SWASH is chosen as the model to simulate the physical model test simulations.

Model	Model type		Wave propagation	
			SS waves	IG waves
OPENFOAM	Phase-resolving	Depth-resolving	Directly	
SWASH				
XB-NH		Depth-averaged		
XB-SB	IG wave resolving & SS wave averaged		Action-Balance	Directly
SWAN	Phase-averaged		Action-Balance	Excluded

Table 3.8: Overview of the numerical models considered for comparative analysis (Lashley, 2021)

3.3.1. SWASH

In this research the numerical model SWASH is used to study the influence of different configurations on breakwater stability. SWASH, Simulating WAves till SHore (SWASH), is an open-source non-hydrostatic wave-flow model that is capable of simulating the nearshore wave dynamics. SWASH provides a general basis for describing complex changes to rapidly varied flows and wave transformations in coastal waters. The governing equations are the nonlinear shallow water equations with an added non-hydrostatic pressure correction term as described above (Smit et al., 2013). These provide a good general basis for wave transformation in both surf and swash zones due to nonlinear wave-wave interactions, interaction of waves with currents, and wave breaking as well as runup at the shoreline (Zijlema et al., 2011). SWASH is a phase resolving model, which it makes it suitable for rapidly changing conditions within the scale of the wave length. Since SWASH is not a Boussinesq type wave model, it improves its frequency dispersion by increasing the number of vertical layers, rather than by increasing the order of derivatives of the dependent variables Zijlema et al. (2011). Therefore it can be used in a depth-averaged or multy-layered mode Zijlema and Stelling (2008). SWASH is based on the so called Non Linear Shallow Water equations with the non-hydrostatic pressure term included (Guzman Mardones, 2011). Because the Navier-Stokes equations for water waves are solved, all hydrodynamic processes are by definition included (Rietberg, 2017). Navier-Stokes equations describe every type of fluid motion in three dimensions as a function of time. However many simplifications have to be used to reach different solutions for different cases of fluid motion. (Schiereck, 2017). SWASH has been validated for multiple nearshore processes by studying them under laboratory conditions. As listed by Rijnsdorp et al in 2015; The nearshore evolution of short waves (Zijlema et al., 2011) and infra-gravity waves (Rijnsdorp et al., 2014), the depth-induced breaking of short waves (Smit et al., 2013), the nonlinear wave dynamics in the surf zone (Smit et al., 2014), run-up induced by breaking of irregular waves Ruju et al. (2014). A comprehensive description of the model can be found in (Zijlema et al., 2011) and (SWASH team, 2020). The influence of the porous structure on the waves is taken into account via the volume-averaged Reynolds-averaged Navier-Stokes (VARANS) equations. SWASH is not capable of including breaking induced turbulence. In this research the assumption is made to focus on velocity and exclude turbulence, therefore, this is not an issue. However, if in future research the inclusion of turbulence is required, another model should be used. The final formulas are presented for a 2DV-plane in equations 3.22 to 3.25.

$$\frac{\delta \eta}{\delta t} + \frac{\delta uh}{\delta x} = 0 \tag{3.22}$$

$$\frac{\delta u}{\delta t} + \frac{\delta uu}{\delta x} + \frac{\delta wu}{\delta z} = -\frac{1}{\rho}\frac{p_h + p_{nh}}{\delta x} + \frac{\delta \tau_{xx}}{\delta x} + \frac{\delta \tau_{xz}}{\delta z} \tag{3.23}$$

$$\frac{\delta w}{\delta t} + \frac{\delta uw}{\delta x} + \frac{\delta ww}{\delta z} = -\frac{1}{\rho}\frac{p_{nh}}{\delta z} + \frac{\delta \tau_{zz}}{\delta z} + \frac{\delta \tau_{zx}}{\delta x} \tag{3.24}$$

$$\frac{\delta u}{\delta x} + \frac{\delta w}{\delta z} = 0 \tag{3.25}$$

3.4. Conclusion

The most important takeaways from this chapter are listed below.

1. It is assumed that the governing theory for breakwater stability does not hold for the Eforie case. A new stability formula is composed, which bases stone stability on velocity and calculates the required stone size. The stability formula is shown in 3.26.

$$\Delta d_{n,50} = 0.83 * \frac{u^2}{2g} \tag{3.26}$$

2. The effect IG-wave energy has on stone stability is unknown.

3. The configurations, transitional slope, directional spreading, wave angle, foreshore slope and cut-off parabolic bay shape, are interesting to investigate. Based on the literature they can directly via SS-waves or indirectly via IG-waves influence stone stability.

4. The numerical model that will be used in this thesis is SWASH. It has the identified relevant physical processes included, is computationally usable for the scope of this research and capable of providing velocity signals, necessary for the composed stability formula.

4

Numerical experiments

With the experimental data known the numerical experiments that are capable to perform in this research given the data, resources and time can now be formulated. First these are listed. Then the numerical model set-up for the base case and the alterations for the different simulations is given.

4.1. Experimental program

The experimental program is divided in four different parts, which are listed first and then discussed in more detail below.

1. Part 1: Stone stability
2. Part 2: Eforie modelling choices
3. Part 3: Eforie Layout
4. Part 4: Wave angle

4.1.1. Stone stability

The first part of the research is setting up the numerical model and verifying its accuracy and robustness. In simulation 1.1, the Eforie physical model test is copied, implementing the original Eforie bathymetry, with the transitional slope. In simulations 1.2-1.6 the results from this basecase model are verified, via a sensitivity analysis, resulting in a robust model. After verification the basecase is validated with the Eforie model test data. When the model is proven to be sufficient a velocity signal is obtained. The velocity signal is converted to a required stone size diameter, via the formula derived in the theoretical framework. The stone size is compared to the applied stone size to decide whether it is stable. At the end of part 1 the derived theory regarding breakwater stability based on a numerical model is tested. The velocity results of the validated model serve as the base case for the next steps.

4.1.2. Eforie modelling choices

When the model is verified and validated, the two Eforie model simplifications, namely directional spreading and the transitional slope are tested in separate simulations. In simulations 2.1, directional spreading is added to the numerical model. In simulation 2.2, the influence of the transitional slope is checked by extending the 1:120 slope till the water depth of MN75-23.5m, as is the case at the Eforie coast. In simulation 2.3, both directional spreading as the extended 1:120 slope are implemented. This simulation provides results which would be expected to occur at the Eforie coast.

4.1.3. Eforie Layout

In the third part of the experimental program the two identified layout influences, lower foreshore slope and cut-off parabolic bay shape, are checked. In simulation 3.1 the influence of the lower foreshore

slope will be checked by a steeper slope of 1:30. A 1:30 slope is chosen, since this slope is assumed to only have an impact on stone stability via SS-wave energy and minimally via IG-wave energy. According to the research by Verhagen discussed in chapter 3, shown in figure 3.6 a 1:30 slope has a significant impact on stone size via the SS-wave energy. According to the research by Lashley, the 1:30 slope results in a normalized bed slope between 0.3-1, as shown in table 4.1. This results in the minimum amount of infragravity wave energy in the system (Lashley, 2021). It is assumed that extending the 1:30 slope till the depth of MN75-23.5m gives similar results as applying the 1:30 slope till MN75-13.5m and applying the transitional slope for the last 10 meters of depth. 1:10 and 1:30 are both steep slopes and will similarly affect the wave course over the bathymetry. In simulation 3.2 a gentler slope of 1:500 is applied. For the 1:30 and the 1:500 slope the normalized bed slopes are calculated and shown in table 4.1. In simulation 3.3 the cut-off parabolic bay shape is excluded from the bathymetry.

Slope-part	β	f_{low}	ω	g	h_b	β_b
Simulation 3.1	1/30	1/60	0.105	9.81	7	0.35
Simulation 3.2	1/500	1/60	0.105	9.81	7	0.02

Table 4.1: β_b for the steeper foreshore slope

4.1.4. Wave angle

In the fourth step the wave angle influence on shallow and sloping foreshores is investigated. Therefore a new basecase is created, in simulation 4.1, with a longshore uniform bathymetry. By using the knowledge from part 3, the influence of removing the cut-off parabolic bay shape can be taken into account. This way no refraction occurs and the influence of the wave angle on the stability of the stones can be isolated. By changing the relative angle between the incoming waves and the breakwater from 0 in simulation 4.2, to 30 in simulation 4.3 and 45 in simulation 4.4, this effect is measured.

4.1.5. Conclusion

The final experimental program is shown in table 4.2.

Simulation	Name	Description
Part 1: Stone stability		
Simulation 1.1	Basecase	Basecase
Simulation 1.2-1.5	Sensitivity analysis	Grid size, Vertical resolution, Porosity, Velocity
Part 2: Eforie modelling choices		
Simulation 2.1	Directional spreading	22°Directional spreading
Simulation 2.2	Eforie slope	Eforie slope
Simulation 2.3	Eforie	22°Directional spreading & Eforie slope
Part 3: Eforie Layout		
Simulation 3.1	Steeper lower foreshore	1:30 Lower foreshore
Simulation 3.2	Gentler lower foreshore	1:500 Lower foreshore
Simulation 3.3	Wave focusing	Straight contour lines
Part 4: Wave angle		
Simulation 4.1	Basecase wave angle	13.4°Relative angle
Simulation 4.2		0°Relative angle
Simulation 4.3		30°Relative angle
Simulation 4.4		45°Relative angle

Table 4.2: Simulation plan

4.2. SWASH model set-up

In this research the numerical model SWASH 7.01 (https://swash.sourceforge.io) is used to study the influence of different configurations on breakwater stability (SWASH team, 2020). For the basecase the set-up of the model is explained below. In the different simulations singular adjustments are made to this basecase. These will be discussed next.

4.2.1. Domain and grid

The domain and grid size are important to ensure a good approximation of the solution and must meet certain criteria. It is advised by SWASH to set the boundaries of the domain 2 wavelengths from the area of interest. The domain is chosen as a rectangle with one of the grid axes aligned as much as possible with the dominant wave direction (SWASH team, 2020). For the computational accuracy the grid size is an important aspect. The spatial resolution is chosen fine enough, with sufficient number of grid points per wave length so the energetic wave components can be resolved on the grid, with 50-100 grid cells per wave length.

The horizontal grid axis was chosen aligned with the dominant wave direction. The incoming wave angle was 70°N, thus a counterclockwise rotation of 20 °was applied to the grid. The length of the domain in x-direction is chosen to contain the entire bathymetry with the transitional slope until MN75-23.5m. This way the water depth at the model boundary ≥ 4*$H_{m0,deep}$ to ensure that no depth-induced breaking occurred offshore (Hofland et al., 2017). As can be derived from figure 2.5b, the length results in 1400m. The y-direction is perpendicular to the x-direction. The area of interest for this model is the breakwater. Therefore the height of the domain was set to contain the breakwater and 100 m above and 100 m below the breakwater, which resulted in 300 m in height.

The resulting domain size is 1400m cross-shore and 300 m alongshore. A wave spectrum, which will be discussed later, with a significant wave height of 4.4 mm and peak period of 11.3s is imposed on the offshore boundary. This means the offshore peak wave length is approximately 150 m and at MN75-10m the wavelength is around 125m. This approach used an alongshore grid spacing, 2= 3Δy, which was found to be optimal considering both accuracy and computational demand. A structured rectangular homogeneous grid is used, with a grid size of 3m is in x-direction and 2m in y direction. The total number of grid cells for the computational domain is 466x150. This grid size is tested via a sensitivity analysis and the resulting wave spectra from the model are validated.

The eventual SWASH model is a 3D model with a quite significant dimensions. To reduce computational time, in the vertical plane 2 layers are used. This will result in a relative error of at most 1% as can be concluded from table 4.3 figure 4.1. The use of 1 layer seems to fall within the accepted ranges, a relative error of at most 1%, and will be tested via a sensitivity analysis.

	offshore (MN75-23.5m)	**Foreshore (MN75-10m)**
H (m)	4.40	4.40
T (s)	11.3	11.3
d (m)	24.2	10.7
L (m)	152.7	122.5
c (m/s)	13.45	9.68
k (1/m)	0.04	0.06
kd (-)	1.00	0.62

Table 4.3: Wave climate

K	range	error
1	$kd \leq 0.5$	1%
1	$kd \leq 2.9$	3%
2	$kd \leq 7.7$	1%
3	$kd \leq 16.4$	1%

Figure 4.1: Range of dimensionless depth as function of number of layers K in SWASH (SWASH team, 2020)

For a given number of layers and a water depth, there is a maximum frequency above which a wave component has an incorrect celerity. This means that the phase difference between the concerning harmonics are wrong. This is particularly important when nonlinear effects are dominant. Ideally, the

maximum frequency is about 1.5 to 2 times the peak frequency at a given depth. It is then assumed that all components above this maximum frequency have a little bit amount of energy (SWASH team, 2020). The peak frequency at the wavemaker boundary and at the MN75-10m point is 0.09 Hz, with depths of 24.2m and 10.7m respectively. The required maximum frequency should be at least: 0.09*1.5=0.14 Hz or preferably higher. From figure 4.2 it can be concluded that the use of two layers is sufficient. Also the use of 1 layer might be sufficient.

d (m)	K=1	K=2	K=3
1	0.82	1.37	2.00
5	0.37	0.61	0.89
10	0.26	0.43	0.63
15	0.21	0.35	0.52
20	0.18	0.31	0.45
25	0.16	0.27	0.40

Figure 4.2: Maximum frequency (in Hz) as function of still water depth (in m) and number of layers (SWASH team, 2020)

After the steady-state condition has been reached, the length of this series should at least correspond to the time period during which surface elevation and velocities are outputted. This time period needs to be long enough to give statistically sound wave data. This time period is called the cycle period and the recommended range is between 100-300 wave periods. Equations 4.1 and 4.2 can be used iteratively until a sufficient cycle period is found. The frequency range is such that the highest frequency, f_{max}, equals 3 times the peak frequency, while the lowest one, f_{min}, equals half of the peak frequency. The duration of the time series of surface elevation to be synthesized is set to 25 minutes, which results in 338 wave. During the validation in chapter 5 it is found that this is accurate enough to get sufficient statistics. Making this period longer, means more wave components will be involved at the wavemaker boundary, which can enhance the computing time a lot (SWASH team, 2020).

$$\Delta f = \frac{1}{T_{cycle}} = \frac{1}{1500} = 6.67 * 10^{-5} Hz \tag{4.1}$$

$$N = \frac{f_{max} - f_{min}}{\Delta f} = \frac{0.27 - 0.045}{6.67 * 10^{-5}} = 338 waves \tag{4.2}$$

	East Boundary
T (s)	11.3
f (Hz)	0.09
f_{min} (Hz)	0.045
f_{max} (Hz)	0.27
T_{cycle} (min)	25
N (waves)	338

Table 4.4: Cycle period and wave components

When imposing a spectrum at the boundary, one has to realize that some so-called evanescent modes might be included as well. These modes show exponential decay with distance from the boundary at which the spectrum is imposed. As such, they can not be ”seen” by the model. Evanescent waves are a general property of the underlying model equations. The frequency at which the evanescent modes are generated is the cut-off frequency and is determined by the dispersive properties of the model equations. It is given by figure 4.3. A two layer model is realised, with a depth, uniform along the wavemaker, of approximately 25m. The cut-off frequency is 0.40Hz and the lowest wave period is thus 2.5 s. The f_{max} was determined to be 0.27 HZ, which means no hinder from this cut-off frequency is experienced. For a one layer model, the cut-off frequency is 0.20 Hz. The f_{max} was determined to

be 0.27 HZ, which means (0.27-0.20)/(0.27-0.04)=0.3043. So 30% of the modes on the boundary are evanescent, which can be assumed reasonable. They will be removed from the boundary.

d (m)	K=1	K=2	K=3
1	1.00	1.99	2.99
5	0.45	0.89	1.34
10	0.32	0.63	0.95
15	0.26	0.51	0.77
20	0.22	0.45	0.67
25	0.20	0.40	0.60

Figure 4.3: Cut-off frequency (in Hz) as function of still water depth (in m) and number of layers (SWASH team, 2020)

4.2.2. (Hydraulic) boundary conditions

Bottom level

In the basecase the Eforie model test is copied. The bathymetry was measured and provided by Van oord as a xyz-file, with the breakwater built into the bottom level was obtained. First the transitional slope that was applied in the Eforie model test had to be added correctly to this bathymetry. The test setup of the Eforie model test portrayed a breakwater orientated with an angle of 100°N. In the original bathymetry-file the breakwater has an angle of 83.4°N. Therefore this bottom file was rotated 16.6 °clockwise. In the resulting file, shown in figure 4.4 the transitional slope was applied after 1250m, where the average bottom level was MN75-13.5m. In figure 4.5 the original and the schematization of the bathymetry file is shown. This bathymetry was the bottom input file for the model. In the model the original coordinate system was used to define the origin, besides the bottom file was set to be rotated 16.6 °counterclockwise. This resulted in a correct original orientation in the real coordinate system. The dominant wave angle is 70°N. This means a relative angle of 13.4°between the incoming waves and the breakwater orientation. SWASH performs best when the incoming waves are perpendicular to the grid boundary. Therefore the grid was rotated 20 degrees, compared to the horizontal, giving 70+20=90°angle of the incoming wave compared to the grid boundary. The eventual schematization of the bathymetry contour line is shown in figure 6.13b.

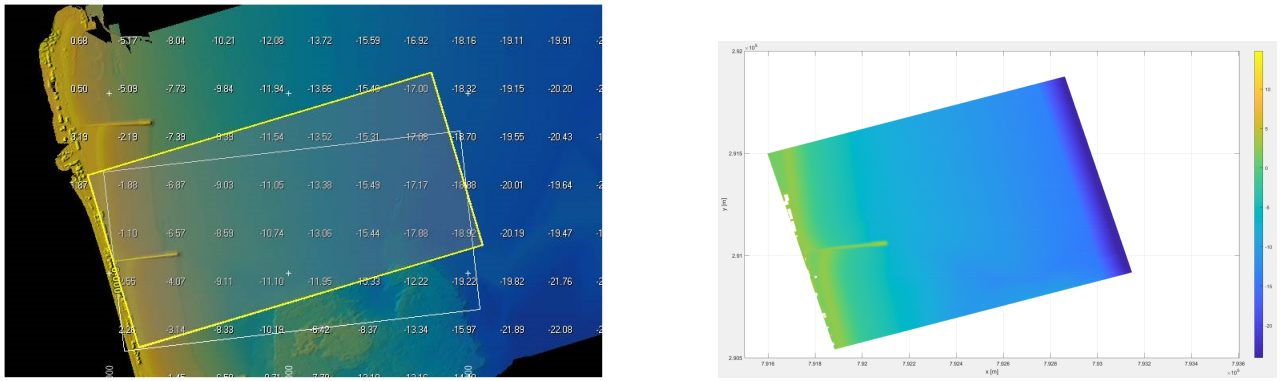

(a) Provided bathymetry file (incl. breakwater

(b) SWASH input bathymetry

Figure 4.4: Transformation bathymetry-file

(a) Basecase sideview

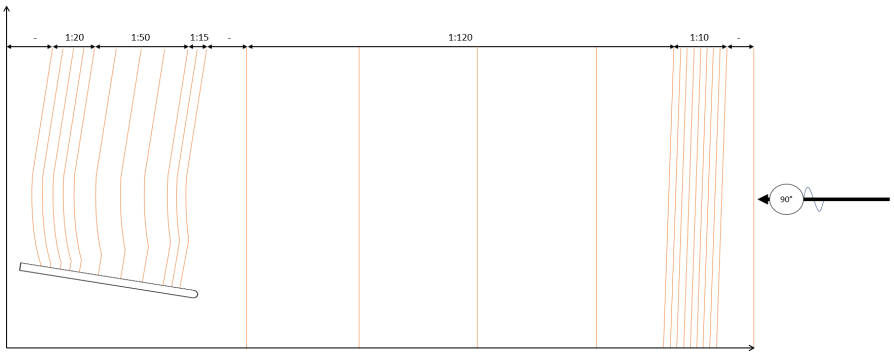

(b) Basecase topview

Figure 4.5: Bathymetry Basecase

Breakwater

In the model a bathymetry file with the breakwater already incorporated was available. The breakwater height is incorporated as an exact copy of the design. The grid size of 3x2 m does influence of the layout of the breakwater, as is visualised in figure 4.6. For breakwater modelling in SWASH the grid resolution should be high enough to suffice that the dimensions of the breakwater are at least four times the grid size of the computational grid. If this is not fulfilled the model can overestimate the transmission and underestimate the reflection (SWASH team, 2020). This requirement is fulfilled in this model.

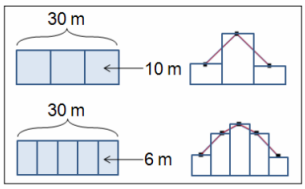

Figure 4.6: Example of increasing accuracy of breakwater definition by means of additional grid cells (Brown and Kraus, 2007)

In SWASH a rubble mound breakwater must be schematized by means of porosity layers to simulate full/partial reflection and transmission. Also the interaction between waves and porous coastal structures can be simulated in this way. The porosity layer must be placed inside the computational domain and can be added to the model by implementing a vertical porosity layer on the bathymetry. The core fill underneath the porous layer is assumed to be impermeable. In the Eforie model test, due to the scaling down the core of the breakwater is also designed as impermeable. Therefore for comparison with the damage values measured in the Eforie model test, this is assumed to be a valid assumption. The porosity of the breakwater is taken into account by applying a porosity layer on the breakwater. This porosity layer is assumed to be 2*dn50, resulting in 1.86 m thick on the slope. In the numerical model the 1.86 m porosity layer on the slope is converted to a 2.2 m thick porosity layer in the vertical, as shown figure 4.7. This is applied in the model by lowering the entire breakwater 2.2m, and then adding a porosity layer of 2.2m layer on these points. The assumed porosity value is 0.5, which was assumed sufficient for breakwater modelling.

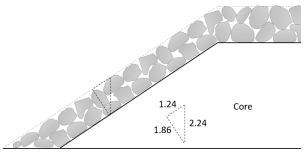

Figure 4.7: Porosity layer thickness in vertical

The mean flow through the porosity layer is described by the volume-averaged Reynolds-averaged Navier-Stokes (VARANS) equations. To describe the flow field inside and outside the porous layer, the velocity is volume averaged. Volume-averaged means that it gives the weighted average velocity over a porous grid element. The influence of porosity (n) is taken into account by SWASH by replacing the velocity (u) with u/n in the shallow water equations (Suzuki et al., 2019). The real pore velocity and free water velocity deviate from this value. In Reynolds-averaged Navier-Stokes equations the velocity field is decomposed into a sum of the average component and of the fluctuating component. In the Volume Averaged RANS-equations a weighted average is taken in the porous medium and in the pure fluid flow field as shown in equations 4.4 and 4.3 (Hsu et al., 2002). Figure 4.8 shows a schematization to explain the way the volume averaging principle is taken into account by SWASH. The porous layer has a permeability of 0.5, as stated before, and water points have a porosity of 1. A fixed porous structure is assumed in SWASH, so porosity does not change with time.

$$u_{layer2} = 100\% * \frac{u_p}{n_{rock}} \tag{4.3}$$

$$u_{layer1} = 75\% * \frac{u_w}{n_{water}} + 25\% * \frac{u_p}{n_{rock}} \tag{4.4}$$

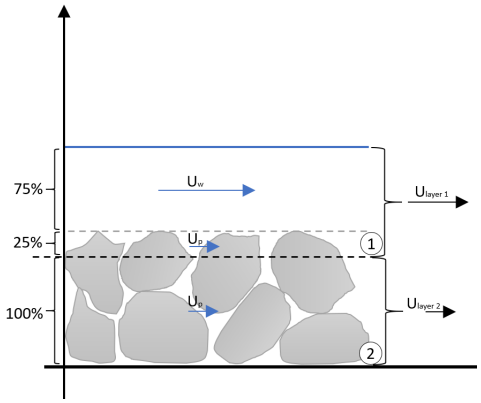

Figure 4.8: Distribution of porous layer over water depth

Wave climate

A time series of surface elevation will be constructed using a Jonswap spectrum with γ=1.5, which is enforced on the boundary. The wave characteristics are determined by the following parameters: the significant wave height, peak period, peak wave direction, and directional spreading. These hydraulic boundary conditions are set as the design 100% SLS HWL storm at the Eforie coast. This means the waterlevel and wave climate that are represented in table 4.5. These will be governing for the next steps of setting up the model. For all simulations the North and South boundary are cyclic lateral repetitive boundaries. Wave energy leaving the South border enters at the Northern border and vice versa.

Run	η (m)	H_{m0} (m)	T_p (s)	β (°N)
Basecase	0.73	4.40	11.3	70

Table 4.5: Basecase input parameters

4.2.3. Data collection

The original bathymetry file can be used, with original coordinates of the measuring devices used in the Eforie model test. Therefore at these locations data output points (W04, W03, W02, W01, G02 & G01) will be identified and asked to measure the waterlevel elevation at every time step. This way afterwards the wave spectra could be constructed and compared to the wave spectra from the Eforie model test. This way the model can be validated. At W04, which is around breakwater chainage 200, there was only infragravity wave energy left, according to the data of the Eforie model test. Therefore it is not necessary to further landward extend data output points along the breakwater to study the wave behaviour.

Location	Output point	Bottom level	Water depth
Chainage 200	W04	MN75-3.0m	3.7 m
Chainage 270	W03	MN75-5.0m	5.7 m
Chainage 370	W02	MN75-7.0m	7.7 m
Head of breakwater	W01	MN75-7.0m	7.7 m
Foreshore	G02	MN75-10m	10.7 m
Offshore	G01	MN75-23.5m	24.2 m

Table 4.6: Ouput locations wave spectra

Next along the breakwater on the slope, at the initial waterline level, from chainage 50 to 310 several data outpoint points are identified as shown in sketch 4.9. These output points are for the basecase positioned at these chainage point. In cetrain simulations where the bathymetry around the breakwater is changed, the output location points are kept constant with respect to water depth. The assumption is that the velocity is dependent on the wave height, which is depth-limited, and neglect the effect of this small distance on wave transformation. Thus keeping the output locations for all the simulations on the same depth will result in similar wave heights and therefore similar velocities, providing comparable and reliable results. Therefore the relevant water depth at the different output locations is given. In the rest of this thesis the output points are mentioned and not the chainages.

Chainage	Output point	Bottom level	Water depth
50	D01	MN75+0.5m	0.2 m
100	D02	MN75-1.0m	1.7 m
150	D03	MN75-2.0m	2.7 m
200	D04	MN75-3.0m	3.7 m
250	D05	MN75-4.5m	5.2 m
300	D06	MN75-6.0m	6.7 m
310	D07	MN75-6.5m	7.2 m

Table 4.7: Ouput locations velocity signal

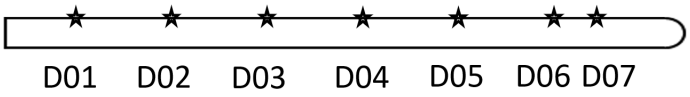

(a) Locations of the output points along the breakwater

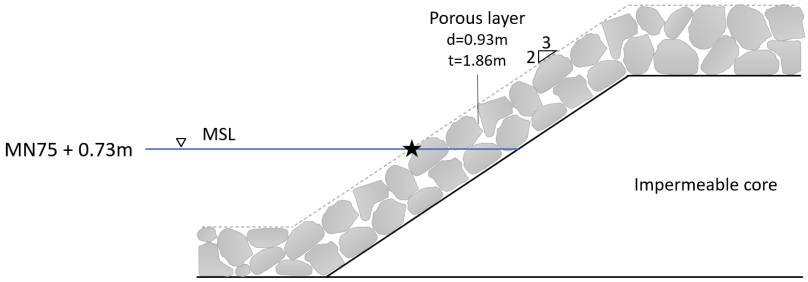

(b) Location on the slope of the output points

Figure 4.9: Output locations topview and sideview

At these points the waterlevel elevation is asked as output, so the change of the wave behaviour along the breakwater can be studied. The wave behaviour of the waves on the slope will be compared to the wave behaviour measured in the output points located next to the breakwater. In addition, in points D01-D07 velocity signal, throughout the simulation, will be asked. In SWASH 7.01 the velocity at certain grid points can be requested as an output in multiple ways.

- VEL: Flow velocity (vector; in m/s)
- VMAG: Velocity magnitude (in m/s)
- VDIR: Velocity direction (in degrees)

The three mentioned velocity signals can also be asked as time-averaged values, as split values per indicated vertical layer or both. In this research two layers in the vertical are assumed to be accurately enough. This will be later tested during a sensitivity analysis. It is chosen to use get the flow velocity per layer. This is the most raw data to get, the velocity magnitude and direction can be obtained from this. The flow velocity will be measured along the breaker at the still waterlevel height. During the validation the choice of how to deal with the two velocities in the vertical and which (averaged) value is governing, was made based on the results of the basecase model and is elaborated in chapter 5. The final basecase layout with measurement points is shown in figure 4.10

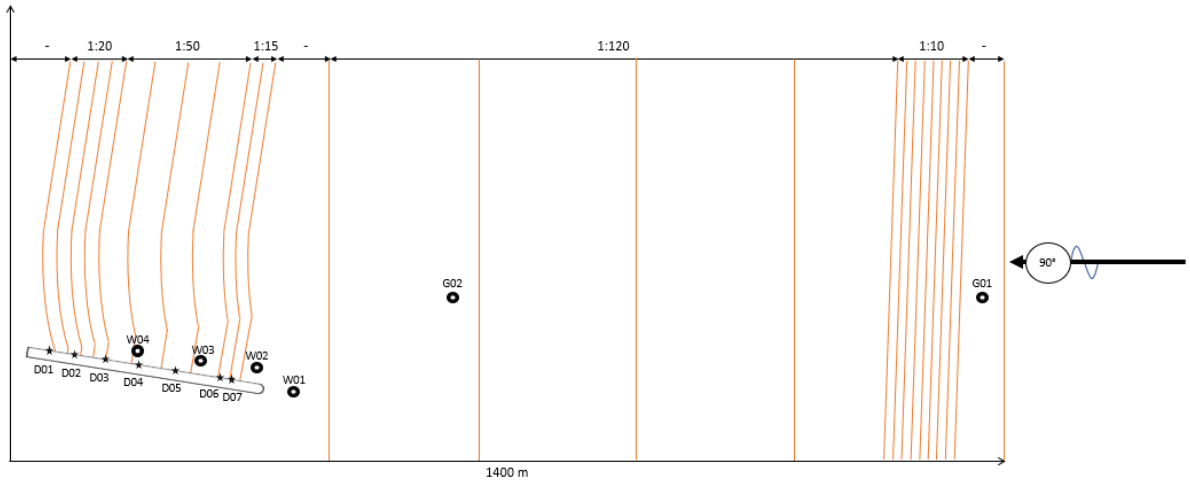

Figure 4.10: Basecase topview with measurement devices

4.2.4. Duration of simulation

For a suitable simulation 500-1000 waves are needed. The cycle period was set to 25 minutes resulting in 338 waves. A steady simulation time of 40 minutes, resulting in 540 waves was assumed to be sufficient. At the start of the simulation the elevation in the domain is zero. The model then begins propagating waves throughout the domain until they are reflected at the shore and propagated back to the wave-maker boundary. The time it takes for the model to get from this zero stage to it's statistical equilibrium is called the spin up time. Before the statistical equilibrium is attained the results are not representative are not taken into account. To determine the spin-up time the calculated wave celerity shown in table 4.3 is used. To be on the safe side a celerity of 9.68 m/s is assumed. The length of the domain is 1370. To calculate the spin up time equation 4.5 is used. This results in a conservative assumed 5 minutes spin-up time. With a spin up time of 5 minutes and a start-up smoothing of 1 minute, this results in a simulation time of 46 minutes. This is tested in the validation in chapter 5 to be sufficient.

$$t = v/s = (2 * 1370)/9.68 = 4.72min \approx 5min \tag{4.5}$$

4.2.5. Numerical parameters

Momentum conservation

The simulation contains breaking waves, hydraulic jumps and bores. Momentum must be conserved via a numerical method which ensures that the wave properties under breaking waves are modelled correctly. The horizontal advection terms of the u- and w-momentum equations are both considered via the central differences scheme. The vertical terms in the u- and w-momentum equations are ressolved via the first order upwinding schemse.

Time intergration

The time integration is explicit. A time step restriction based on the Courant number, associated with the long wave speed, is applied. Since non-linearities such as wave breaking, wave-wave interactions and wave interactions with the steep sloped breakwater occur in the model a maximum Courant number of 0.5 is applied to the model.

4.2.6. Physical parameters

Breaking

In the vertical 2 layers have been assumed. This is sufficient to represent wave physics outside the surf zone, such as refraction, shoaling, diffraction and non-linear wave interactions. Dissipation due to wave breaking in the surf zone requires a finer resolution. Applying this would increase the computational time significantly and therefore the breaking command in SWASH has been used. The pressure distribution under breaking waves is considered to be hydrostatic once the local surface steepness exceeds a maximum value (Lashley, 2021). The breaking command applies a hydrostatic pressure distribution at the front of the wave, which controls the computed location and magnitude of depth-limited wave breaking. At the location where depth-limited breaking would occur, the front quickly transitions into a bore like shape. Due to this command wave breaking is modelled correctly in spite of the coarse vertical resolution.

Subgrid turbulent mixing

For correct computation around the breakwater head the Smagorinsky command has been applied.

Bottom friction

A manning friction coefficient of 0.019 was applied in the model. Numerical experiments have indicated that the Manning formula provides a good representation of wave dynamics in the surf zone, and even better to that returned by other friction formulations (SWASH team, 2020).

Minimal water depth

To avoid unrealistivally high velocity signals on the breakwater slope or possible instabilities a larger threshold of the water depth is applied. The default value of 0.05 mm is increased to 0.01 m.

Infragravity waves
The numerical model assumes bound long waves in the model and does not consider potentially free long waves arriving at the boundary from distant sources. Only the bound long waves created by the wind-sea swell waves, from shoaling and breaking, are taken into account. Due to nonlinearity, sub and super harmonics are formed for high waves. These waves are referred to as bound waves because they are tied to the primary wave and travel at its phase speed rather than the speed of a free wave of the same frequency. At the boundary the model creates free components that are the same magnitude but 180 °out of phase with the bound waves to cancel the bound long wave height. A spatially non-homogeneous wave field will result from the presence of bound and free waves traveling at different speeds, with the wave height changing continually over the domain. This results in more wave energy present in the model, because of the applied suppression and induces less reliable results. In this thesis the presence of infragravity waves is taken into account, so the at the wavemaker boundarie the command to add bound waves is applied. The free long waves are no longer created and the bound long waves are created in the model. These components are determined by the weakly nonlinear, second order, finite-depth wave theory of Hasselmann (1962). The wave field is made up of first order, or primary waves, which correspond to the free wave response, and a second order correction, which corresponds to the bound waves. The assumption of mild non-linearity is used to generate this correction. A weakly reflective condition enabling outgoing waves is applied at the East boundary to simulate entering waves without some reflections at the wavemaker boundary.

4.2.7. Conclusion

	Input	Symbol	Unit	Value
	waterlevel	h	[m]	MN75+0.73
	Spectrum type			Jonswap
Waves	Spectral shape factor	γ	[-]	1.5
	Spectral wave height	H_s	[m]	4.48
	Spectral peak period	T_p	[s]	11.44
	Timestep	Δ t	[s]	0.0250
System	Cycle period	T_{cycle}	[m]	25
	Spin-up duration	$t_{spin,up}$	[m]	5
	Simulation time	$t_{simulation}$	[m]	46
	Viscosity model			Smagorinsky
Physical	Manning friction coefficient	n	[-]	0.019
	Minimal water depth	d	[m]	0.01
Numerical	Time integration	C_{max}	[-]	0.5

Table 4.8: Overview of the inputs used for the simulations

4.3. Data Processing

Velocity signal
The eventual required velocity signal needs to be translated to a governing velocity on which the stone stability and stone size can be based. The two ways that are discussed in this research are via an extreme value analysis of the entire velocity signal or by choosing the top x-% velocity of the entire velocity signal. Both these options will be checked during the validation and the most suitable based on the required velocity signal will be used.

Wave height
The wave heights are determined via data processing. The waterlevel surface elevation time signal is translated to a wave spectrum. From this wave spectrum via H_{m0}=4*$\sqrt{m0}$ the wave height is calculated.

Separation of Sea-Swell and Infragravity Waves
The presence of the infragravity waves is checked throughout the simulations. The influence of the infragravity waves is checked by creating the wave spectra and checking the presence of these waves.

The low frequency signal will be separated from the high frequency. Half the peak frequency ($f_p = \frac{1}{T_p}$ Hz) is taken as the cut-off frequency to separate SS and IG motions (Roelvink and Stive, 1989). This choice of cut-off frequency is based on the tendency that, in deep water, the majority of SS-wave energy is found at frequencies higher than $f_p/2$, while the majority of IG-wave energy lies at frequencies lower than $f_p/2$. (Lashley, 2021).

4.4. Model Simulations

In this chapter the deviations from the basecase are described and shown in sketches of the setup.

4.4.1. Part 2

Simulation 2.1

The influence of directional spreading is investigated. In simulation 2.1, the base case, with the transitional slope, is taken and at the offshore boundary directional spreading is applied to the incoming wave. A sketch of this test setup is shown in figure 4.11. From the metocean study performed for this site a directional spreading of 11°one-sided as standard deviation is found. This is used in the model.

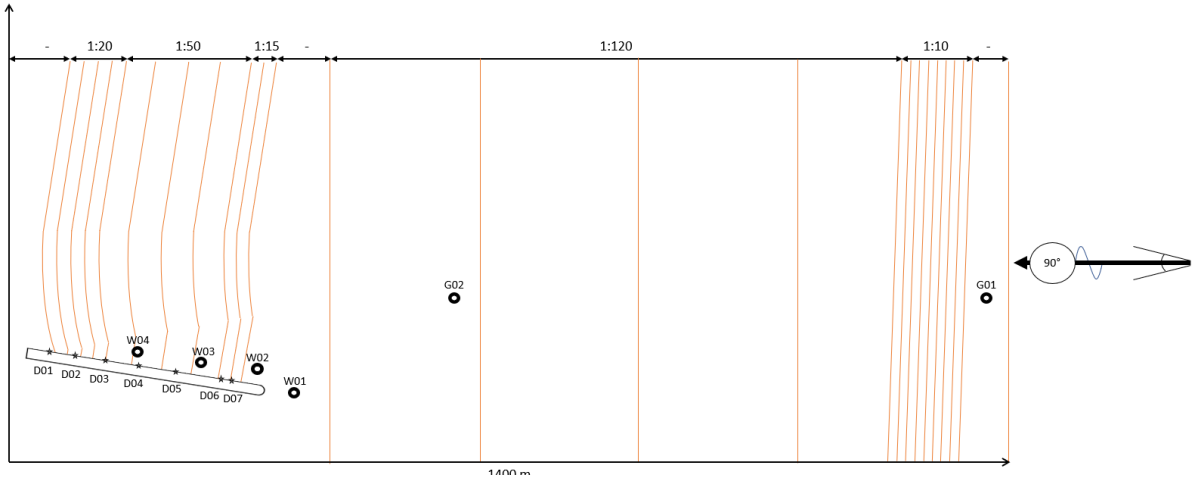

Figure 4.11: setup 2.1 topview

Simulation 2.2

The original Eforie slope is used in the numerical model. Therefore the original Eforie coast bathymetry is used extending the model in x-direction. Figure 4.12 show a top view of this setup.

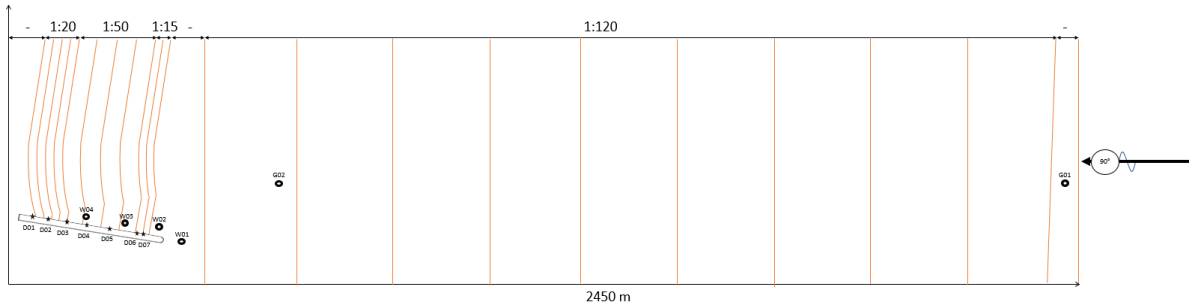

Figure 4.12: setup 2.2 topview

In this simulation the length of the domain was extended to 2450m. Therefore the spin-up time had to be checked or altered for this simulation. To calculate the spin up time equation 4.6 is used. This results in a conservative assumed 9 minutes spin-up time. With a spin up time of 9 minutes, a start-up smoothing of 1 minute and 40 minutes of simulation, this results in a total simulation time of 50 minutes.

$$t = v/s = (2 * 2450)/9.68 = 8.44min \approx 9min \tag{4.6}$$

Simulation 2.3
In this simulation 2.3 the original Eforie slope is implemented and the Eforie wave spectrum with directional spreading is taken into account, as shown in figure 4.13. The spin-up time is taken as 9 minutes, a start-up smoothing of 1 minute and 40 minutes of simulation, thus a total simulation time of 50 minutes.

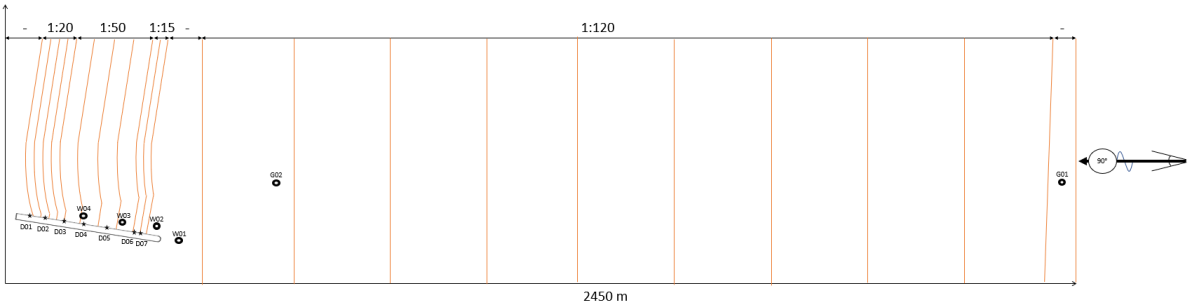

Figure 4.13: setup 2.3 topview

4.4.2. Part 3

Simulation 3.1
In simulation 3.1 a steeper lower foreshore slope is applied, as shown in figure 4.14. Instead of the 1:120 slope a 1:30 slope is applied.

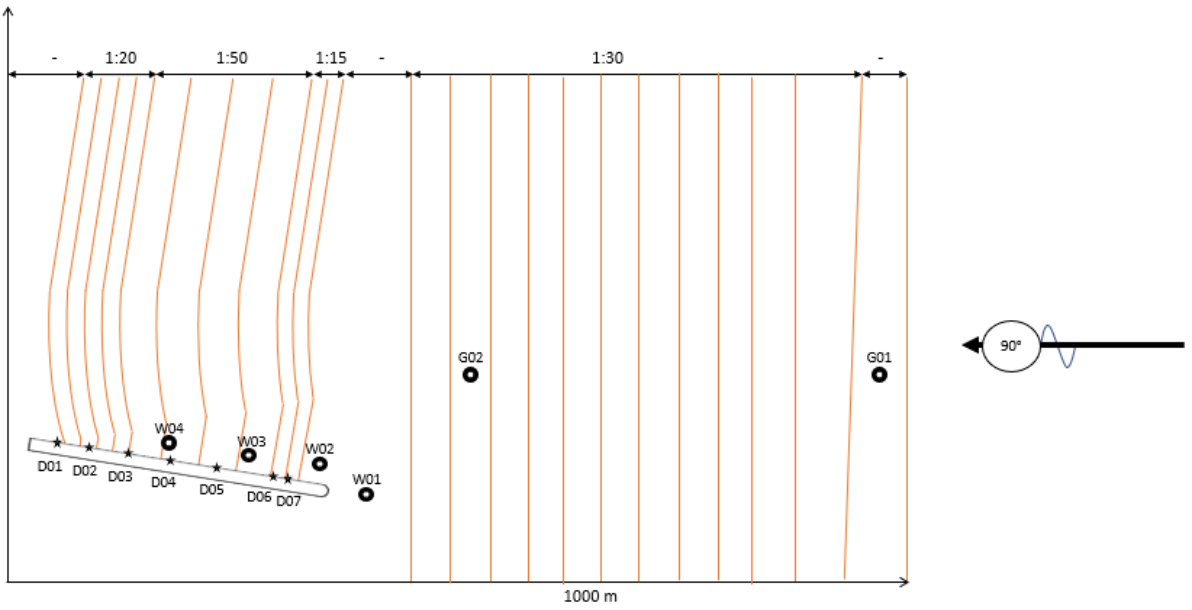

Figure 4.14: setup 3.1 topview

Simulation 3.2
In run 7 the opposite is investigated, as shown in figure 4.15. A slope of 1:500 is applied

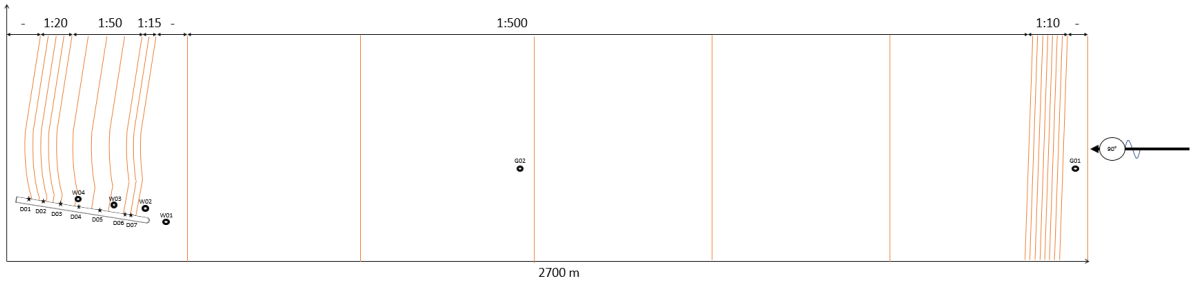

Figure 4.15: setup 3.2 topview

In this simulation the length of the domain was extended to 2961m. Therefore the spin-up time had to be checked or altered for this simulation. To calculate the spin up time equation 4.7 is used. This results in a conservative assumed 9 minutes spin-up time. With a spin up time of 11 minutes, a start-up smoothing of 1 minute and 40 minutes of simulation, this results in a total simulation time of 52 minutes.

$$t = v/s = (2 * 2961)/9.68 = 10.20min \approx 11min \tag{4.7}$$

Simulation 3.3
As shown in figure 4.16 the contour lines are assumed parallel to the beach, excluding the cut-off parabolic bay shape.

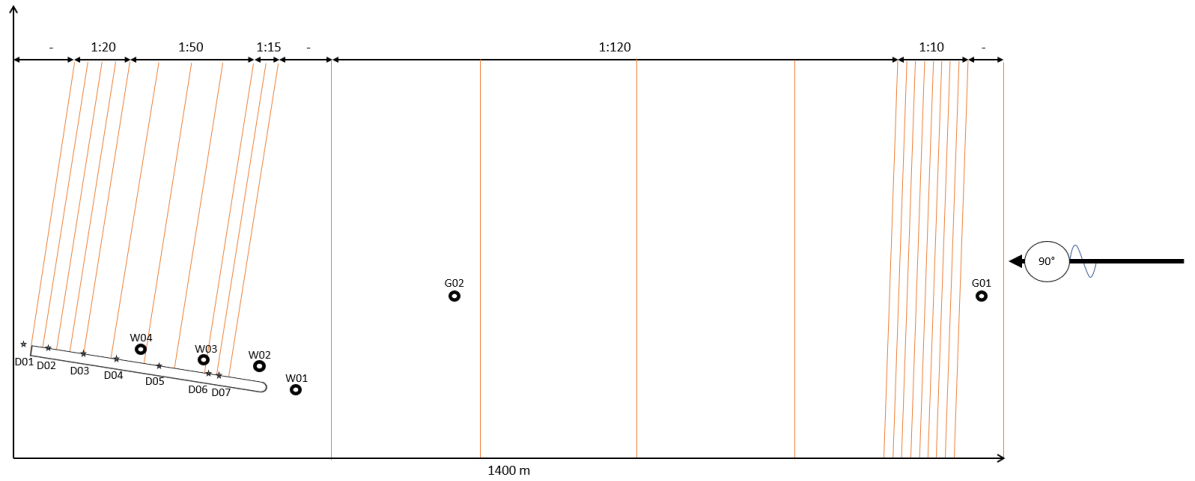

Figure 4.16: setup 3.3 topview

4.4.3. Part 4

In part 4 a new basecase is created where only the relative angle between the incoming waves and the breakwater will be changed. To make sure no refraction or focusing of energy occurs the bathymetry lines are all assumed as parallel to the coast and thus longshore uniform.

The breakwater is assumed as a topside 7m wide breakwater with a constant height of MN75+3m and slope of 2:3. The height of MN75+3m is maintained along the length of the breakwater. A side- and top-view is given in figure 4.17. Three simplifications regarding the original breakwater are the constant height, constant slope and the constant width of the head of the breakwater. This might influence the measured velocity along the breakwater, however this simplification is assumed for all simulations in part 4 and therefore will not affect the outcomes of part relating the influence of the wave angle to breakwater stability.

In simulation 4.1 the new basecase is simulated. This means that a relative angle of 13.4°is applied. Then in simulation 4.2 the relative angle is reduced to 0°, in simulation 3.3 the relative angle is increased to 30°and in simulation 4.4 the relative angle is increased to 45°. Top views of the layout for

these different runs is shown in figure 4.18 and the representation in the simulations is shown in figure 4.19. Just as in simulation 4.3, the output locations along the breakwater are kept constant to the relative depth at 30m above the breakwater. This means that the breakwater is extended in longitudinal direction for simulations 4.3 and 4.4, to maintain constant relative depths at the output points.

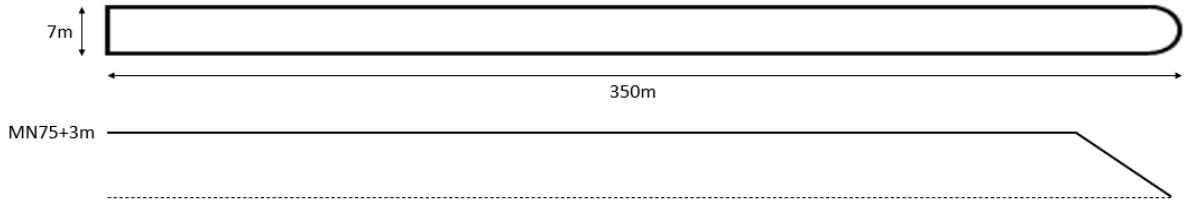

Figure 4.17: Top- and sideview of the modelled breakwater for part 4

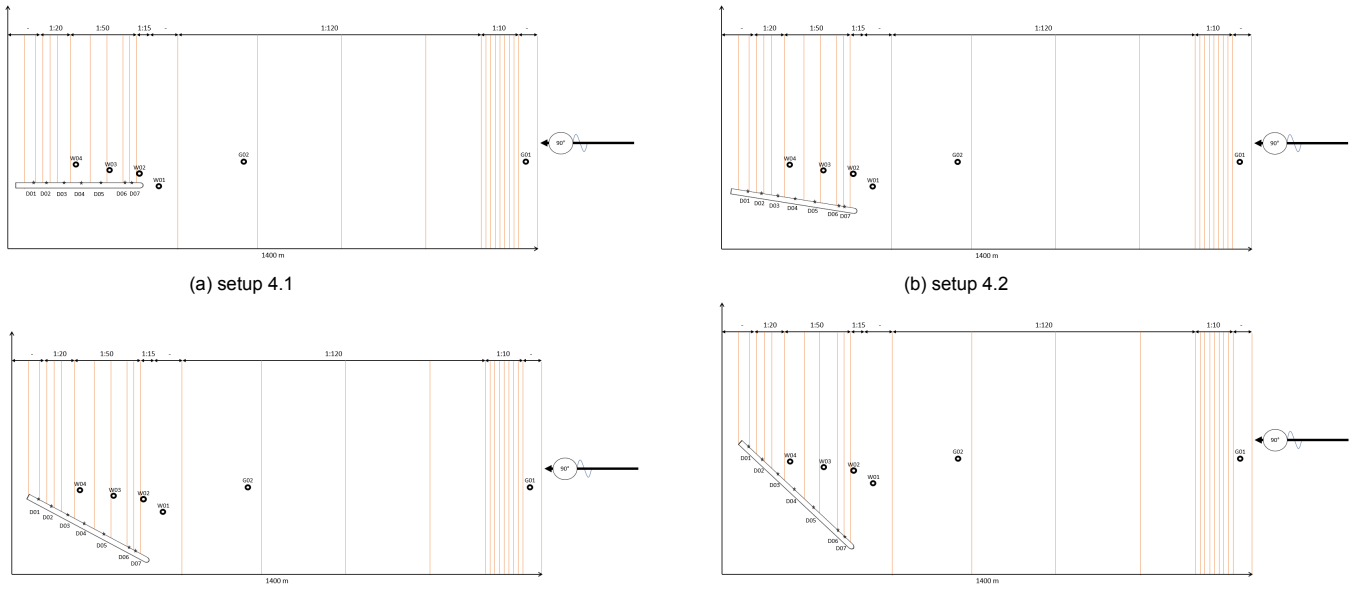

(a) setup 4.1

(b) setup 4.2

(c) setup 4.3

(d) setup 4.4

Figure 4.18: Topview setup simulations 4.1-4.4

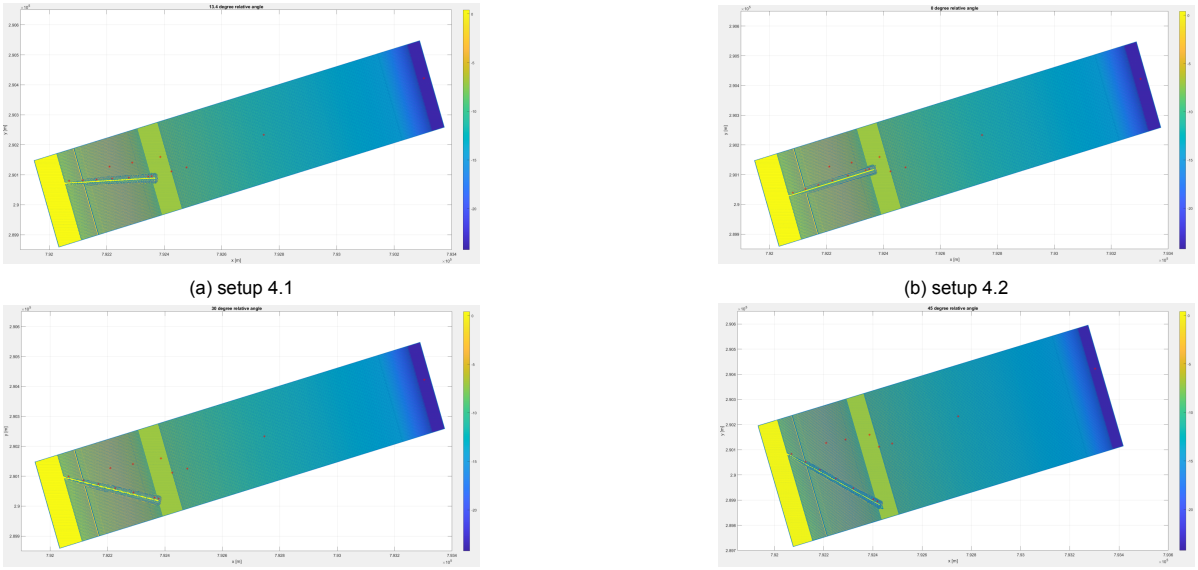

(a) setup 4.1

(b) setup 4.2

(c) setup 4.3

(d) setup 4.4

Figure 4.19: Topview setup simulations 4.1-4.4

Simulation	Relative angle	Incoming wave angle
Simulation 8	13.4	76.6
Simulation 9	0	90
Simulation 10	30	60
Simulation 11	45	45

Table 4.9: γ_β for simulations 8-11

5

Validation & Verification

In this chapter the numerical model is validated and a sensitivity analysis is performed. In the validation it is checked whether the numerical model is logically and semantically correct and coherent to the conceptual model outlined before. The dimensions of the coastal hydrodynamic processes, such as shoaling, refraction, wave breaking etc. are checked. In addition, it is checked whether the outcomes of the numerical model provide sufficient agreement with the data from the physical model test. A sensitivity analysis is performed to check the redundancy and robustness of the numerical model.

5.1. Validation

The correct working of the numerical model is proven by validating the results. The validation is done via multiple subjects:

1. The **coastal hydrodynamics** characteristics are compared with observations from the physical model tests
2. The **wave climate** is checked with the data from the physical model test
3. The **velocities** are compared to be in the order of magnitude as expected via the Ursell number.

5.1.1. Coastal hydrodynamics

The following coastal hydrodynamics are stated to be of importance for this research:

- Correct representation of the wave characteristics, such as wave propagation from East to West, shoaling and wave breaking.
- The faster propagating siderush along the breakwater.
- The refraction pattern, due to the cut-off parabolic bay shape bathymetry.

Wave characteristics

In a 1D side-view of the simulated Eforie coast, shown in figure 5.1a a wave propagating from East to West is visible. In table 5.1 and figure 5.1b the transformation of H_{m0} from offshore (G01) to the coast (W04) is presented.

Output location	W04	W03	W02	W01	G02	G01
H_{m0} for simulation 1.1	2.60	3.67	4.12	3.82	4.25	4.28

Table 5.1: The transformation of H_{m0} for simulation 1.1

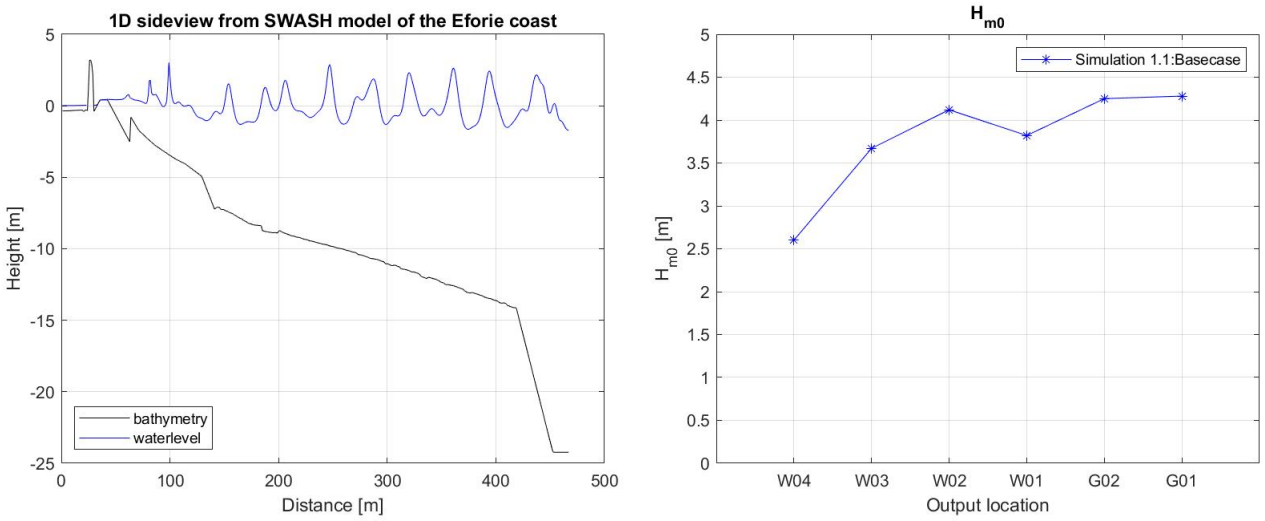

(a) 1D sideview snapshot of the waterlevel

(b) H_{m0} from offhore (G01) to the coast (W04)

Figure 5.1: Wave pattern near the breakwater

In both figures the shoaling effect near the coast and breaking at the beach is visible. The presented wave heights seem to be in the right order of magnitude. When using the water depth along the different output locations, provided in table 4.6, a breaker parameter of around 0.6 is found. This seems correct.

Siderush

When looked closer at the wave pattern near the coast a process which shows a faster propagating wave front at the breakwater, as found in the model tests visualized by figure 2.7b, could not be so clearly identified. Two figures of the wave pattern near the coast are provided in figure 5.2. This may mean that the process that is central for this research is not incorporated in SWASH. This will be discussed further in the discussion.

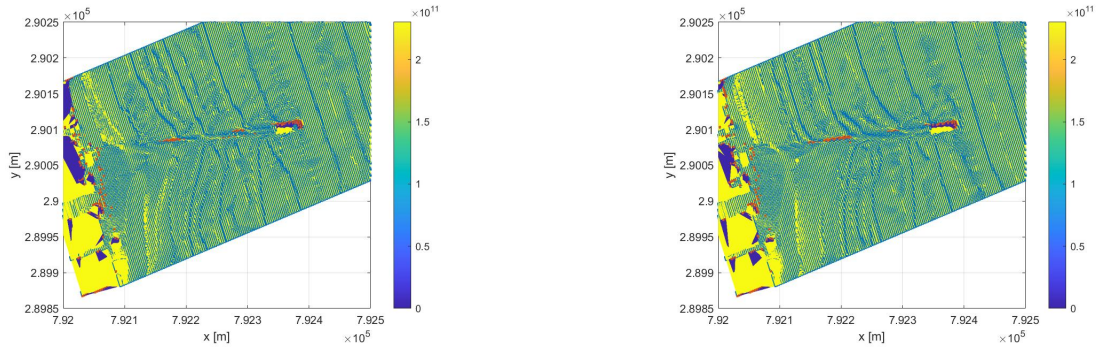

(a) Snapshot at t=35 min

(b) Snapshot at t=45 min

Figure 5.2: Wave pattern near the breakwater

Refraction-pattern

The cut-off parabolic bay shape is visible in the wave patterns shown in the provided top views of the SWASH model, shown in figure 6.14.

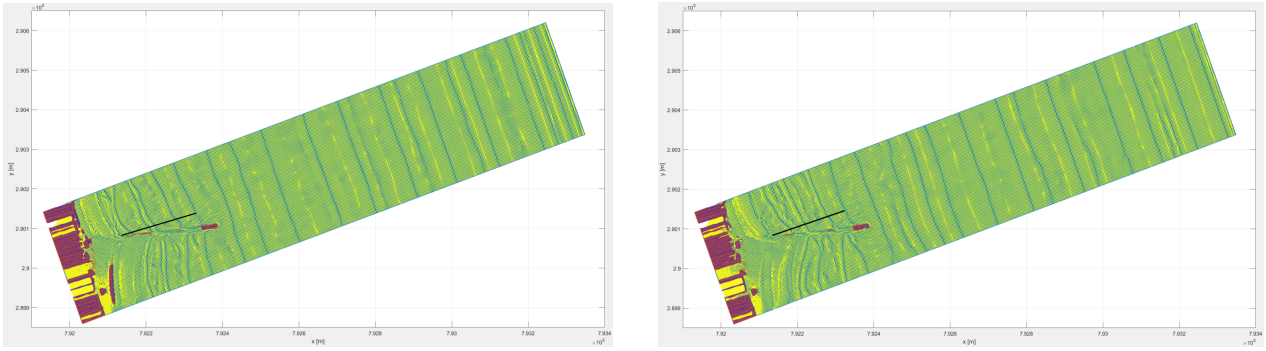

(a) 20 min (b) 35 min

Figure 5.3: Cut-off parabolic bay shape in SWASH model

5.1.2. Wave climate

Figures 5.4 and 5.5 and tables 5.2 and 5.3 present the results for the basecase simulation of the numerical model compared to the results from the physical model test.

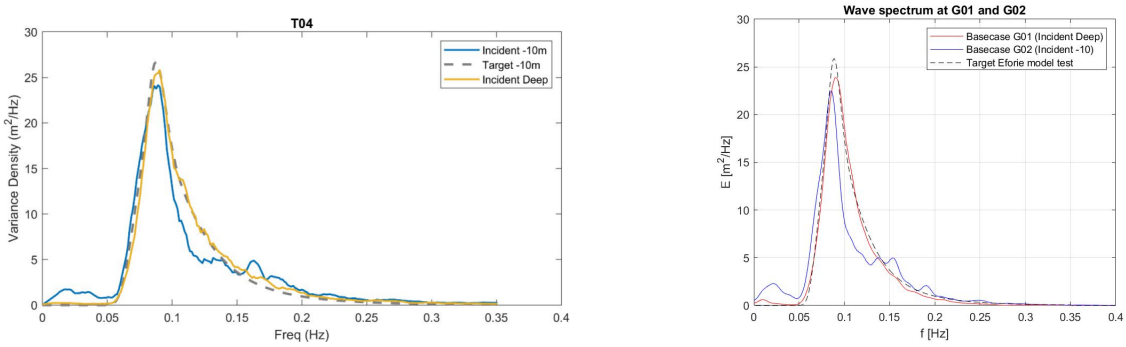

(a) Graph physical model test (b) Target graph

Figure 5.4: Validation G01-02 output locations

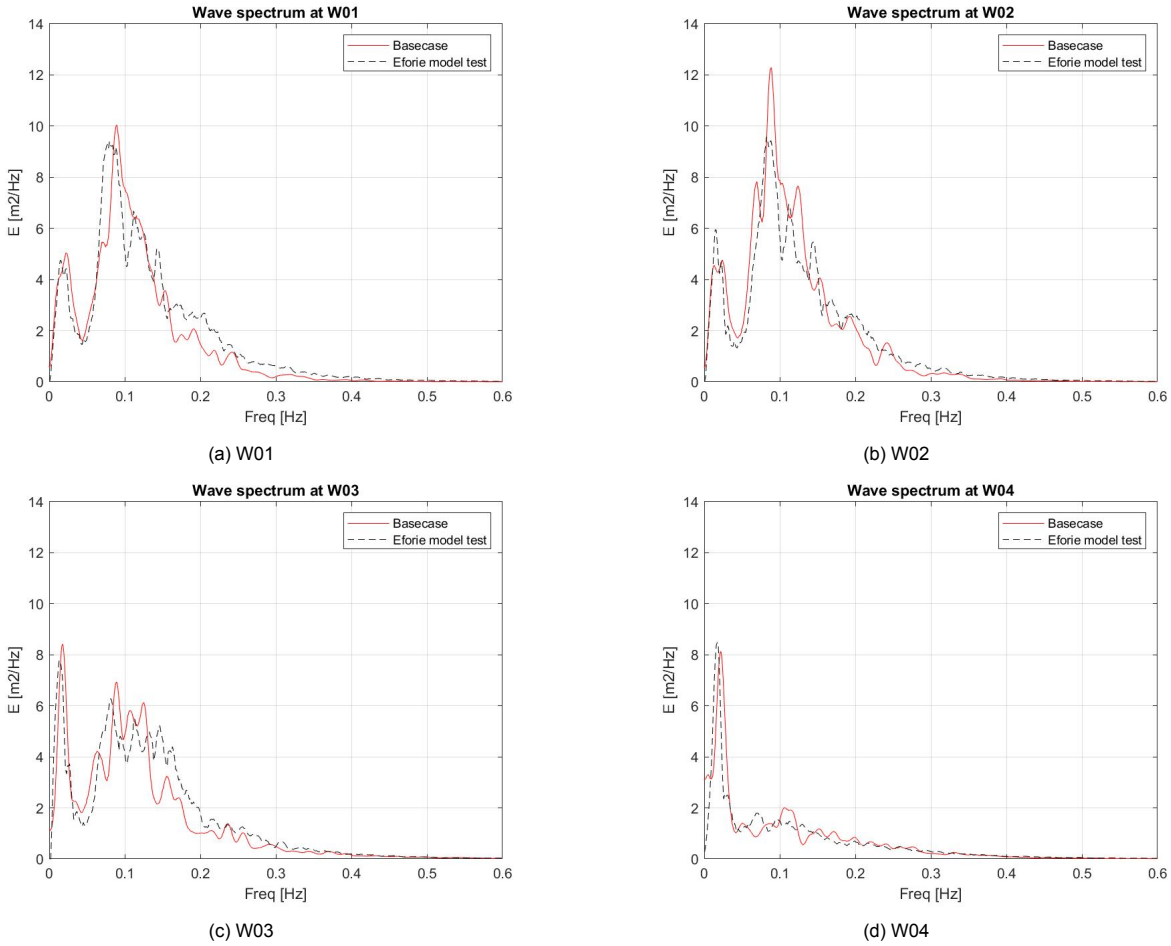

(a) W01 (b) W02

(c) W03 (d) W04

Figure 5.5: Validation W01-04 output locations

TestID	G01		G02	
	H_{m0} (m)	T_p (s)	H_{m0} (m)	T_p (s)
Basecase	4.28	11.1	4.25	11.7
Physical model test	4.40	11.3	4.40	11.3

Table 5.2: Basecase data of G01 and G02 - Full wave spectrum

TestID	W01		W02		W03		W04	
	H_{m0} (m)	T_p (s)	H_{m0} (m)	T_p (s)	H_{m0} (m)	T_p (s)	H_{m0} (m)	T_p (s)
Basecase	3.82	11.3	4.12	11.3	3.67	57.1	2.60	46.2
Physical model test	4.05	13.0	4.01	10.7	3.86	76.1	2.54	62.8

Table 5.3: Basecase data of output locations W01-07 - Full wave spectrum

The wave spectra of the individual wave gauges near the structure show a shift of wave energy towards the lower frequencies due to wave breaking. Therefore, not only the parameters of the complete wave spectra are presented, but also the results without this low frequency component. In these spectra, only energy at frequencies above 0.5 * F_p (peak frequency = 1 / T_p) is used. The peak frequency at the G02 of the base case is used. Thus the dividing frequency is set at 0.5*$\frac{1}{11.7}$=0.043 Hz. Tables tables 5.4 and 5.5 show the results of only the IG-wave energy.

TestID	G01		G02	
	H_{m0} (m)	T_p (s)	H_{m0} (m)	T_p (s)
Base case	0.44	11.1	1.03	11.7
Physical model test	0.30	11.3	0.89	11.3

Table 5.4: Basecase data of G01 and G02 - Only low frequency energy

TestID	W01		W02		W03		W04	
	H_{m0} (m)	T_p (s)	H_{m0} (m)	T_p (s)	H_{m0} (m)	T_p (s)	H_{m0} (m)	T_p (s)
Base case	1.48	11.3	1.48	11.3	1.61	57.1	1.66	46.2
Physical model test	1.37	13.0	1.42	10.7	1.56	76.1	1.55	62.8

Table 5.5: Basecase data of output locations W01-07 - Only low frequency energy

The wave energy transformation of the numerical model seems to represent the physical model test well. Both the total wave energy as the IG-wave energy shows good accordance with the physical model test data. The spectra of the waves show comparable results and shifts in peak frequency.

5.1.3. Velocity

With the results from the basecase the governing velocity can be chosen. In the sensitivity analysis it is found that two velocity layers are required and sufficient to provide a robust model. In figure 5.6 the measured water height during the later chosen velocity is displayed relative to the porosity layer thickness. This shows how the different velocity layers are proportioned relative to the porosity layer. The two vertical layers of the water depth are compared to the porosity layer for the different output locations along the breakwater. These figures are snapshots of the water levels during the later chosen velocity at that output location.

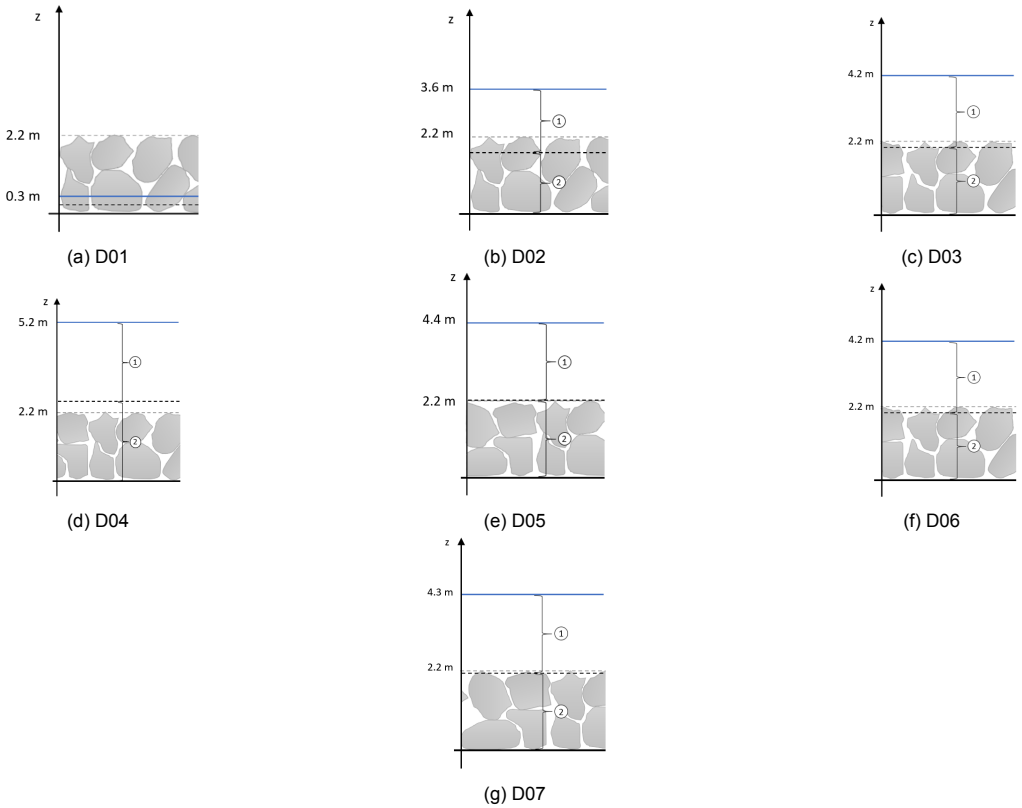

Figure 5.6: Relative velocity layers over the depth

Figure 5.6a shows the relative waterlevel during the governing velocity. It can easily be observed that this waterlevel is well below the porosity layer and thus will be affected significantly by this porosity

layer. The eventual velocity that would be found for output location D01 is approximately 0.08 m/s. This value is too small to relatively compare with D01 values of the other simulations. The D01 output location will therefore be left out of the further analysis.

In chapter 3 it was discussed that the Izbash stability formula required the velocity close to the rocks. The formulated stability formula for this thesis is based on the Izbash formula and therefore also required the velocity close to the stone. From the different figures of figure 5.6 it can be concluded that in this thesis the layer 1 velocity is governing for stone Stability.

For further analysis the velocity signals of layer 1 are used. As discussed before the traditional formulas in the rock manual link the highest velocity under the highest wave. In that case by performing an extreme value analysis and choosing velocity corresponding to the $H_{1\%}$ for example results in a robust and repeatable way to analyze velocity data. In this SWASH research the waterlevel and wave height approximately coincide as indicated in figure 5.7a. However, when looked closely at the graph it can be seen that the highest waves do not necessarily provide the highest velocities. Looking at figure 5.7b a delay between the peak of the waterlevel and the peak of the velocity can be identified.

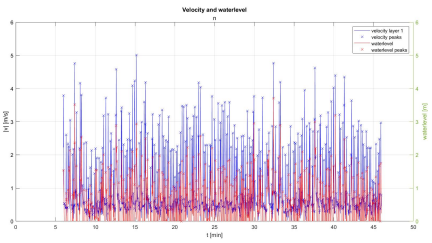

(a) Velocity and waterlevel plot in one graph

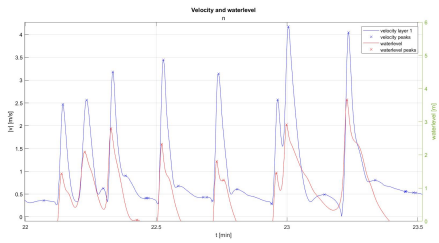

(b) Close up of velocity and waterlevel in one graph

Figure 5.7: D04

The link between highest velocity occurring during the highest waterlevel does not hold for the results of this numerical model. To ensure a robust and consistent processing of the data is applied, the velocity signals of layer 1 are listed topdown and the $v_{0.2\%}$, the 192th largest value, is chosen as governing. This value is assumed as it ensures outliers are neglected. It resembles a velocity that occurs approximately 5 seconds per storm of 40 minutes, which can be related to a peak velocity governing for stone stability. Approaching the data per velocity output point and per run this way, makes sure that a structured data-processing is performed with every point at every run. Whether the $v_{0.1\%}$, $v_{0.2\%}$ or the $v_{0.5\%}$ provides better answers is checked via a sensitivity analysis and the $v_{0.2\%}$ provides reliable results. In table 5.6 the $v_{0.2\%}$ for the two layers are presented. This shows the significant (expected) difference between the two velocities and supports the choice to link stone stability to the velocity of layer 1.

Chainage	Velocity layer 1	Velocity layer 2
D02	3.72	0.27
D03	3.71	0.31
D04	4.17	0.65
D05	4.31	0.83
D06	5.30	0.61
D07	6.21	1.19

Table 5.6: Measured velocity of layer 1 & 2

In 1984 Dean and Dalrymple used the shallow water asymptotic forms to derive to an equation for water particle velocities of long waves, stated in equation 5.1 (Dean and Dalrymple, 1984). This equation, combined with the known formula 5.2 can be rewritten to equation 5.3. This equation can provide an estimate of the particle velocity of a long wave and are applied in this thesis to provide an order of

magnitude for the expected velocities along the breakwater. The expected velocities based on equation 5.3 are compared to the measured velocities in table 5.7. The results from table 5.7 provide confidence in the measured velocities along the breakwater.

$$u = \frac{\eta * c}{h} \tag{5.1}$$

$$c = \sqrt{gh} \tag{5.2}$$

$$u = \frac{\eta * \sqrt{g}}{\sqrt{h}} \tag{5.3}$$

Output location	Depth	waterlevel	Expected velocity	Measured velocity ($v_{0.2\%}$)
D02	1.71	1.5	3.58	3.72
D03	2.36	1.93	3.94	3.71
D04	3.33	2.44	4.20	4.17
D05	2.70	2.10	3.99	4.31
D06	2.31	1.57	3.24	5.30
D07	2.47	1.63	3.24	6.21

Table 5.7: Measured velocity and Dean expected velocity

5.2. Sensitivity Analysis

In the model set-up and the data processing a large number of parameters and numerical schemes were included. These where assumed or estimated based on the Eforie coast, the physical model test and on literature. A sensitivity analysis is required to find the best settings and to check the robustness of the results. This to optimize the SWASH output and simulation duration. The model results were compared by altering the model properties of the grid size, the vertical resolution and the cycle period, shown in table 5.8. The impact of these alterations on the wave climate and wave spectra along the shore and breakwater was evaluated.

	Parameters	Description
A	Grid Size	Size of the computational grid in alongshore and cross-shore direction
B	Vertical resolution	The amount of vertical layers applied in the model
C	Porosity	The thickness of the applied porosity layer
D	Velocity	The velocity which is taken as governing for the critical stone size

Table 5.8: Sensitivity analysis

5.2.1. Grid size

An important choice for a numerical model is the grid size. As elaborately described in chapter 4 the grid size needs to be big enough to correctly calculate hydrodynamic processes. The grid size needs to be small enough so the model is computationally usable for the intended use. Table 5.9 and figure 5.8 show the velocity signal from the SWASH model for different grid sizes.

Case	Gridsize (m)	D02	D03	D04	D05	D06	D07
A1	2x2	3.61	3.42	4.03	4.29	5.02	5.93
A2	3x2	3.72	3.71	4.17	4.31	5.30	6.21
A3	3x3	3.25	3.51	4.13	4.10	4.56	5.43
A4	4x3	2.99	3.37	4.09	4.39	4.77	5.25

Table 5.9: Grid size

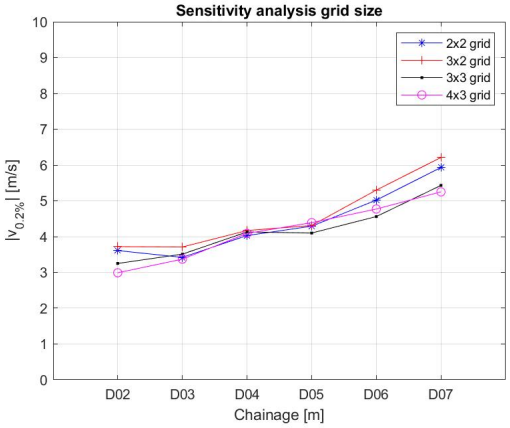

Figure 5.8: Sensitivity analysis grid size

Table 5.9 and figure 5.8 do not show a unanimous connection between grid resolution and velocity. A grid of 2x2 provides smaller velocities than a 3x2. A bigger grid 3x3 and 4x3 also provide smaller values. The resolution of 2 meters in the vertical can be assumed as important. The output points are located on the slope of the breakwater. This slope is between 4 and 10 meters along the breakwater. Therefore a high enough resolution is required to retrieve reliable data. Increasing to a resolution of 3 meters will retrieve averaged data for the output locations. Especially when comparing the basecase with the simulations this will affect the deviations. The same holds for a resolution of 4 meter in the horizontal direction. Grid resolutions 2x2 and 3x2 both show a similar course along the breakwater. However the 2x2 grid is computationally significantly more demanding. Therefore a 3x2 grid is a correct and reliable resolution to use.

5.2.2. Vertical resolution

As discussed before the two layers in the vertical are crucial to retrieve reliable velocities along the breakwater. Table 5.10 and figure 5.9 show the velocity signal from the SWASH model for different vertical resolutions.

Case	Vertical layers	D02	D03	D04	D05	D06	D07
B1	1	0.95	1.36	1.81	1.76	1.75	2.29
B2	2	3.72	3.71	4.17	4.31	5.30	6.21

Table 5.10: Vertical resolution

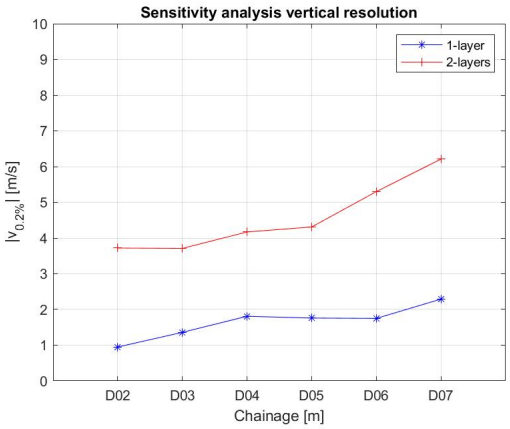

Figure 5.9: Sensitivity analysis vertical resolution

In the simulation where 1 vertical layer is applied, the bottom has to much influence, bringing down the

averaged velocity over the vertical. Figure 5.9 and the check performed earlier in this chapter shows that 2-layers in the vertical is able to calculate plausible velocity signals. In this thesis 2-layers are assumed in the vertical.

5.2.3. Porosity layer

Checking a smaller porosity layer is interesting because it was expected to influence the measured velocity significantly. In the model a constant porosity thickness of 1.86m, resulting in 2.2m in the vertical, is assumed. In the Eforie case from output locations D01 to in between D02 and D03 the outer layer is made of smaller rocks and thus has a smaller porosity thickness of 1.30m, resulting in 1.6m in the vertical. From output location D07 to the head of the breakwater the outer layer has a bigger porosity thickness of 2.44m, resulting in 2.9m in the vertical. In addition, a bigger porosity layer is interesting to check, since the core is assumed as impermeable. In the physical model test the core was assumed impermeable as well, however in the Eforie case the core is constructed out of core fill 1-500kg, which is not impermeable. Table 5.11 and figure 5.10 show the velocity signal from the SWASH model for different porosity layer thicknesses.

Case	thickness (m)	D02	D03	D04	D05	D06	D07
C1	1.6	4.62	4.84	4.93	5.48	7.04	7.74
C2	2.2	3.72	3.71	4.17	4.31	5.30	6.21
C3	2.9	2.48	2.89	3.60	3.79	4.19	4.95

Table 5.11: Porosity layer

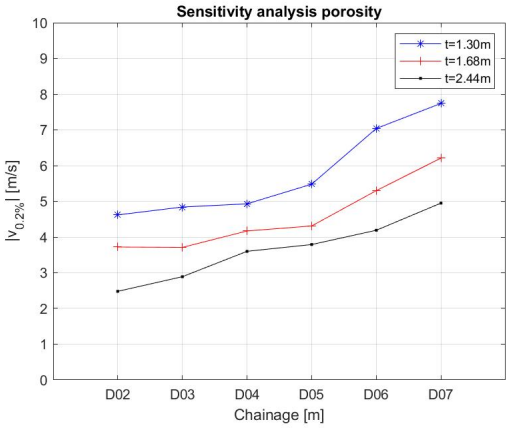

Figure 5.10: Sensitivity analysis porosity layer

The results presented in figure 5.10 show that the porosity has a significant effect on the value of the calculated velocity.

5.2.4. Velocity

Table 5.12 and figure 5.11 show the velocity signal from the SWASH model for different %-velocities.

Case	Velocity (m/s)	D02	D03	D04	D05	D06	D07
D1	$v_{0.1\%}$	3.98	3.85	4.37	4.80	5.51	6.59
D2	$v_{0.2\%}$	3.72	3.71	4.17	4.31	5.30	6.21
D3	$v_{0.5\%}$	3.24	3.39	3.83	4.00	4.85	5.57

Table 5.12: Velocity

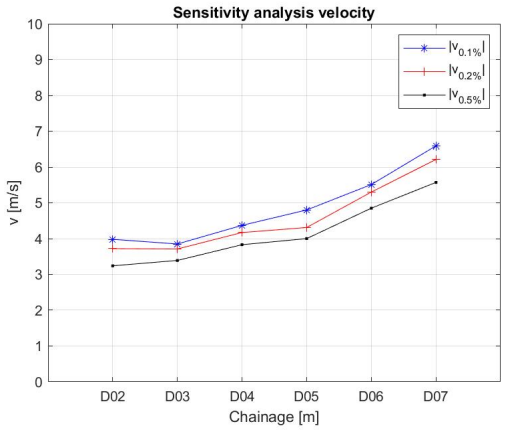

Figure 5.11: Sensitivity analysis velocity

Using the 0.1%, 0.2% or the 0.5% maximum velocity does not influence the outcome of the research much. Of course the 0.1% maximum velocity results in a higher critical required stone size. The shape of the graphs are however the same, indicating no outliers and reliable data. The choice for 0.2% depends on the desire that the velocity is approximately 5 seconds per storm of 40 minutes higher than the given velocity. In this research the 0.2% maximum velocity is used.

5.3. Conclusion

The most important takeaways from this chapter are listed below.

1. The model resembles the wave climate from the physical model test well and provides reliable velocity values. The model is validated and found to be sufficient for the numerical model study of this thesis.
2. The sensitivity analysis discussed the effect of certain assumptions and parameters on the results in this study.
    - A minimal resolution of 2m in the y-direction was required for reliable results throughout the simulations.
    - A vertical resolution of 2 vertical layers was required for reliable results throughout the simulations.
    - A porosity thickness of 2.2m in the vertical is found to provide reliable results. In needs to be notices that the porosity layer thickness has a significant effect on the obtained velocity signal and thus on the results from this research. This will be taken into account when discussing the results.
    - The $v_{0.2\%}$ is chosen to be a good representative of a governing velocity.

6

Results & Analysis

In this chapter the results of the performed SWASH simulations in the numerical study will be shown. In the previous chapter the numerical model was verified and validated. In this chapter first the found governing velocities for the basecase will be presented and linked to breakwater stability with the theory proposed in this thesis. The velocity values from the basecase provide the benchmark-values for the rest of the simulations. Secondly, the results of the simulations in which the Eforie modelling choices are treated are discussed. Thirdly, the simulations treating the influence of bathymetry layout are presented. Fourthly, a new basecase is created that neglects all the above checked influences and focuses on the influence of wave angle. The distribution of wave energy between long and short waves is discussed throughout the different simulations.

6.1. Stone stability

6.1.1. Velocity

The velocity that is chosen as governing in this study is the $v_{0.2\%}$ value of layer 1. Table 6.1 shows the velocity signal for the different output locations for the basecase. The velocity values from the basecase provide the benchmark-values for the rest of the simulations.

Output point	D02	D03	D04	D05	D06	D07
$v_{0.2\%}$ (m/s)	3.72	3.71	4.17	4.31	5.30	6.21

Table 6.1: Governing velocity

6.1.2. Stability

In chapter 3 a stability formula is composed that links velocity to a required stone diameter. From the measured velocities in the numerical model the required stone diameter is calculated, with equation 6.1 and compared to the applied stone size in the Eforie physical model test. This is shown in table 6.2 and figure 6.1.

$$\Delta d_{n,50} = 0.83 * \frac{u^2}{2g} \tag{6.1}$$

Output point	D02	D03	D04	D05	D06	D07
$v_{0.2\%}$ (m/s)	3.72	3.71	4.17	4.31	5.30	6.21
$d_{n,50}$ (m)	0.37	0.37	0.47	0.50	0.76	1.04

Table 6.2: Measured velocity and calculated d_{n50}

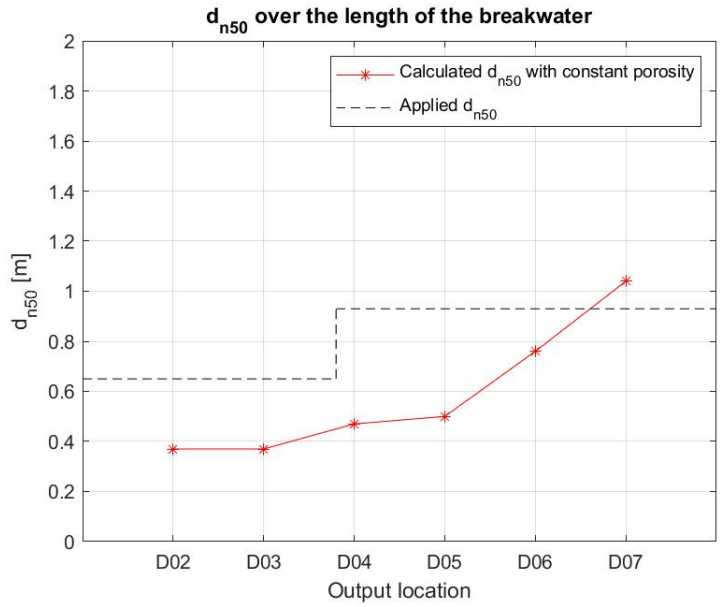

Figure 6.1: Critical $d_{n,50}$

In chapter 2 the qualitative description of the damage measured during the physical model test is given. Here it is restated with the chainage point translated to the output location as: The measured damage during the model test shows two trajectories. Between D02 and D03 the damage value increases from approximately 0 till just below 2. Around D03 the stone size decreases. Then between D04 and D07 the damage value increases again from approximately 0 till just below 2.

If it is assumed that reaching a damage value of 2 is comparable to exceeding the calculated required stone size, figure 6.1 shows that the second trajectory from D04 to D07 is predicted reasonably well. Around D07 the calculated $d_{n,50}$ exceeds the applied $d_{n,50}$, which corresponds with the measured damage value of 2 from the physical model test. For the first trajectory, output locations D02-D03, the observed peak in the measured damage is not well represented. This can be explained by the constant assumed porosity thickness. In the physical model test at output locations D02-D03 a different stone size, with a lower porosity thickness of 1.6m in stead of 2.2m was applied.

In the sensitivity analysis it was shown that this porosity layer thickness has a significant effect on the obtained velocity signal. Taking the 2.2m thickness as the governing thickness the relative percentage change in velocity for a thickness of 1.6m and 2.9m is shown in table 6.3.

Case	thickness (m)	D02	D03	D04	D05	D06	D07	Average	σ
C1	1.6	24	30	18	27	33	25	26	4
C2	2.2	0	0	0	0	0	0	0	-
C3	2.9	-33	-22	-14	-12	-21	-20	-20	7

Table 6.3: Percentage change in velocity relative to thickness 2.2m

Combining the velocity results from the cases C1(thickness of 1.6m) and C2 (basecase, thickness of 2.2m) a more representative presentation of the breakwater can be given. For D02-D03 the velocity values obtained in the sensitivity analysis for a porosity thickness of 1.60m were used and for D04-D07 the velocity values obtained in the sensitivity analysis for a porosity thickness of 2.2m were used. Applying this provides the results presented in table 6.4 and figure 6.2.

Output point	D02	D03	D04	D05	D06	D07
$v_{0.2\%}$ (t=2.2) (m/s)	3.72	3.71	4.17	4.31	5.30	6.21
$v_{0.2\%}$ (t=1.6) (m/s)	4.62	4.84	4.93	5.48	7.04	7.74
$v_{0.2\%}$ (t=correct) (m/s)	4.62	4.84	4.17	4.31	5.30	6.21
$d_{n,50}$ (m)	0.57	0.63	0.47	0.50	0.76	1.04

Table 6.4: Measured velocity and calculated d_{n50}

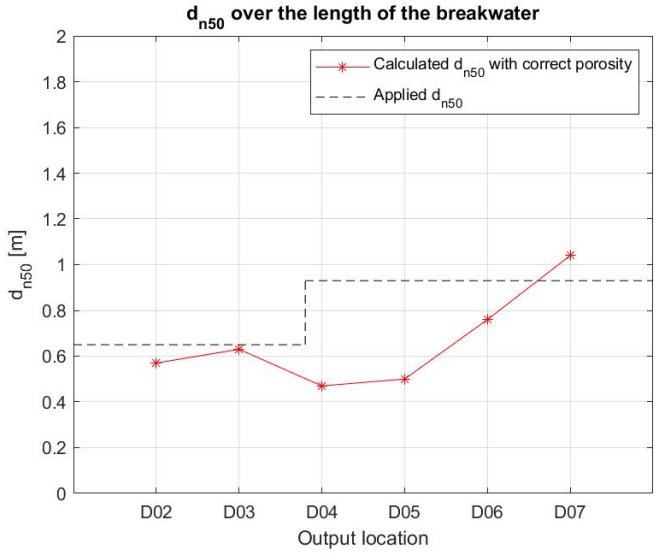

Figure 6.2: Critical $d_{n,50}$ with correct porosity

Figure 6.2 shows that when the correct porosity is applied, also the first trajectory from D02 to D03 is predicted reasonably well. Around D03 the calculated $d_{n,50}$ reaches the applied $d_{n,50}$, which corresponds with the measured damage value of 2 from the physical model test. It is important to note that the values for a porosity of 1.6m give an overestimation of the actual results, since in this simulation the entire porosity layer is assumed as 1.60m. This results in less friction along the offshore part, D03-D07, of the breakwater.

The calculated stone size is linked to the measured velocity via equation 6.1. In the next steps of this thesis the velocity signals of the different simulations will be compared. These will not be calculated to a stone size, to keep the presented results clear of possible errors in the setup theory.

6.1.3. Conclusion

The main conclusions of part 1 are:

1. A reliable velocity signal can be obtained from SWASH. The breakwater needs to be modelled with a permeable core and an impermeable porosity layer as outer layer. It is important to notice that the applied thickness of this porosity layer significantly influences the obtained velocity signal velocity and therefore needs to be modelled well. In the vertical two layers need to be applied. It needs to be checked whether the top layer (layer 1) is sufficiently above the applied porosity layer. If this is the case the 0.2% value of the velocity signal of layer 1 can be obtained as a reliable governing velocity.
2. The calculated stone sizes show that breakwater stability can be predicted reasonably well from a velocity signal obtained from SWASH. If the correct porosity is applied both trajectories, visible in the measured damage, are represented by the calculated $d_{n,50}$. The formula to translate the measured velocities to a required stone size is presented in equation 6.2

$$\Delta d_{n,50} = 0.83 * \frac{u^2}{2g} \tag{6.2}$$

6.2. Eforie modelling choices

6.2.1. Directional spreading

The first check that is performed is the influence of directional spreading at the Eforie coast. As discussed directional spreading with a standard deviation of 11 degrees is applied in the model. This results in a total directional spreading of 22 degrees. Based on the literature research the following results were expected:

- For multi-directional waves lower velocities are expected along the breakwater (Matsumi et al., 1995).
- For multi-directional waves, H_{m0} was expected to be smaller (Briggs and Grace, 1988).
- For multi-directional waves, $H_{m0,IG}$ was expected to be smaller (Hofland et al., 2017).

Velocities

In table 6.5 and figure 6.3 the measured velocities of the simulation and the basecase are shown.

Output point	D02	D03	D04	D05	D06	D07
Simulation 2.1	3.74	3.75	4.17	4.16	5.07	6.15
Basecase	3.72	3.71	4.17	4.31	5.30	6.21
Δ v (m/s)	0.02	0.03	0.00	-0.15	-0.23	-0.06

Table 6.5: Simulation 2.1 and base case velocities

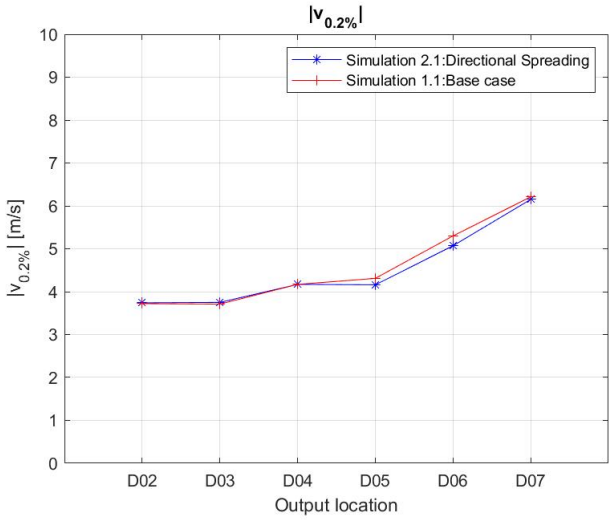

Figure 6.3: Velocity for simulation 2.1 and the basecase

The measured velocities largely overlap for the different output locations along the breakwater. Around the head of the breakwater between D05-D07, the results show a minor deviation, where unidirectional waves result in a higher velocity along the breakwater.

Wave Climate

Figure 6.4 shows the wave energy of simulation 2.1 compared to the basecase. In figure 6.4d the difference between the wave energy and velocity values of the simulation and the basecase is presented.

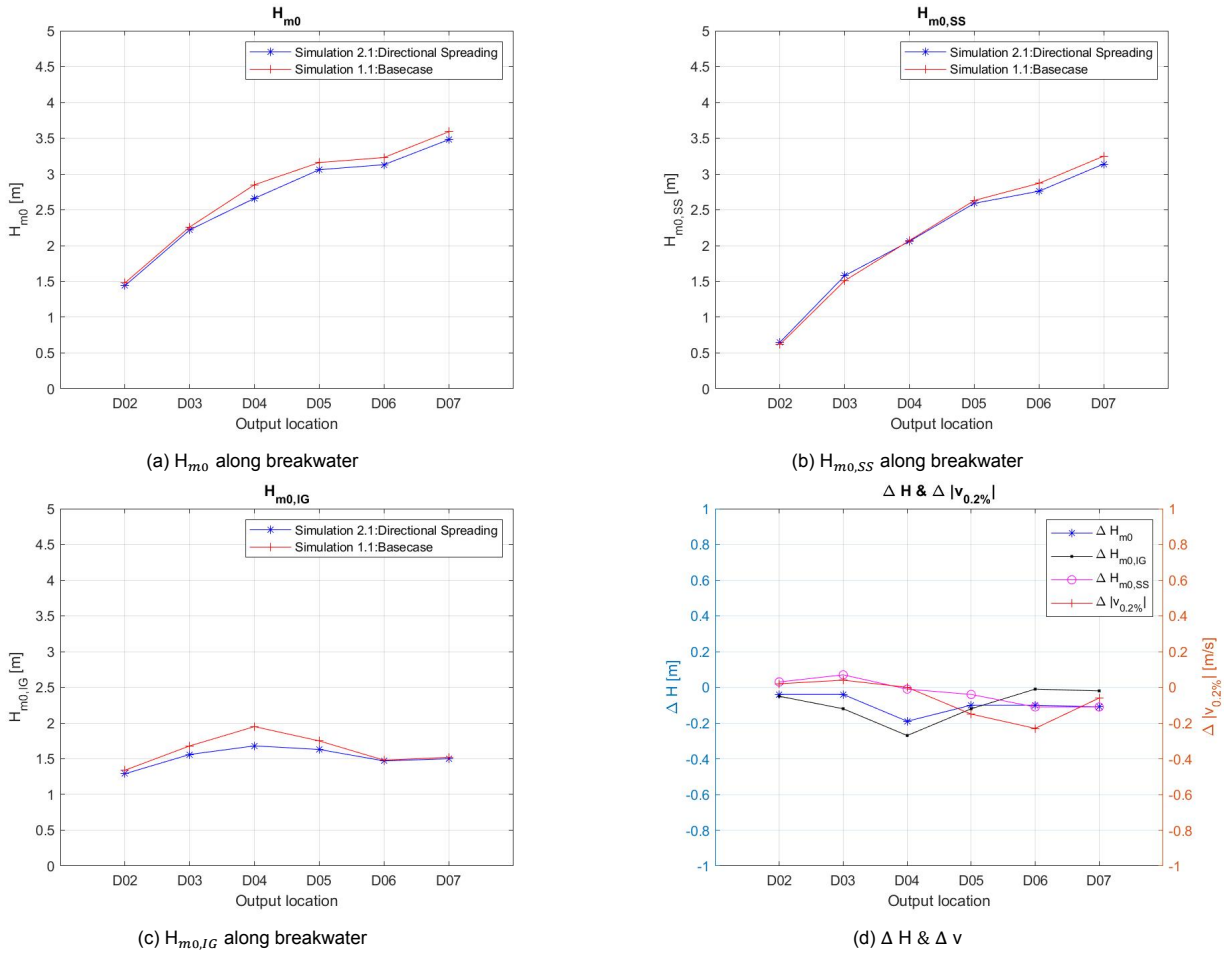

(a) H_{m0} along breakwater

(b) $H_{m0,SS}$ along breakwater

(c) $H_{m0,IG}$ along breakwater

(d) Δ H & Δ v

Figure 6.4: Wave height for simulation 2.1 and the basecase

Along the breakwater the multi-directional case, simulation 2.1, showed a slight decrease in IG-wave energy. From figure 6.4d the results show that a difference in infragravity wave energy does not directly lead to a reduction in velocity along the breakwater. A clear relation between change in wave (component) energy and velocity can not be found.

Conclusion
The most important takeaways from this simulation are listed below.

1. Directional spreading seems to have minor influence on the velocity measured along a breakwater.
2. SWASH represents both the decrease in wave energy as in IG-wave energy that was expected from the literature.
3. No clear relation between wave energy (component) and velocity can be identified in the results.

6.2.2. Eforie slope

The next check is removing the transitional slope from the simulation. The 1:120 lower foreshore slope is applied and the transitional slope is removed from the model. Based on the literature research the following results were expected:

- The transitional slope has no effect on the velocities measured along the breakwater.
- The transitional slope has minor influence on the SS-wave energy.
- The transitional slope increases the generation of IG-waves.

Velocities
In table 6.6 and figure 6.5 the measured velocities of the simulation and the basecase are shown.

Output point	D02	D03	D04	D05	D06	D07
Simulation 2.2	3.52	3.02	4.08	4.26	5.41	6.12
Basecase	3.72	3.71	4.17	4.31	5.30	6.21
Δ v (m/s)	-0.19	-0.70	-0.09	-0.05	0.11	-0.09

Table 6.6: Simulation 2.2 and base case velocities

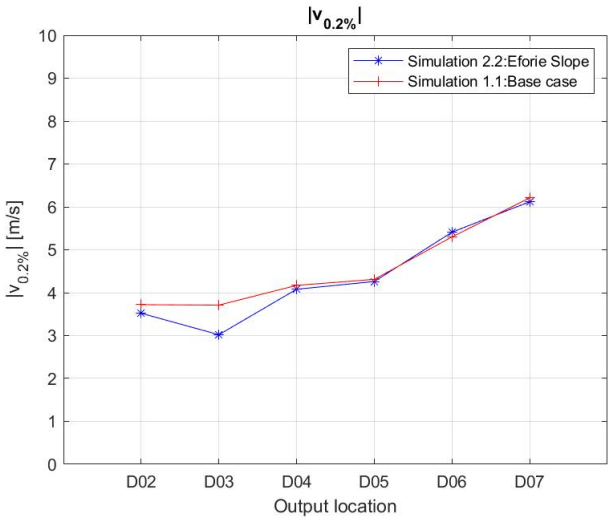

Figure 6.5: Velocity for simulation 2.2 and the basecase

When looked at the velocities along the breakwater in figure 6.5 a reduction in the velocity is measured at output location D03. This could be a one-time outlier. Investigating a possible link with wave energy could perhaps elaborate on this.

Wave Climate
Figure 6.6 shows the wave energy of simulation 2.2 compared to the basecase. In figure 6.6d the difference between the wave energy and velocity values of the simulation and the basecase is presented.

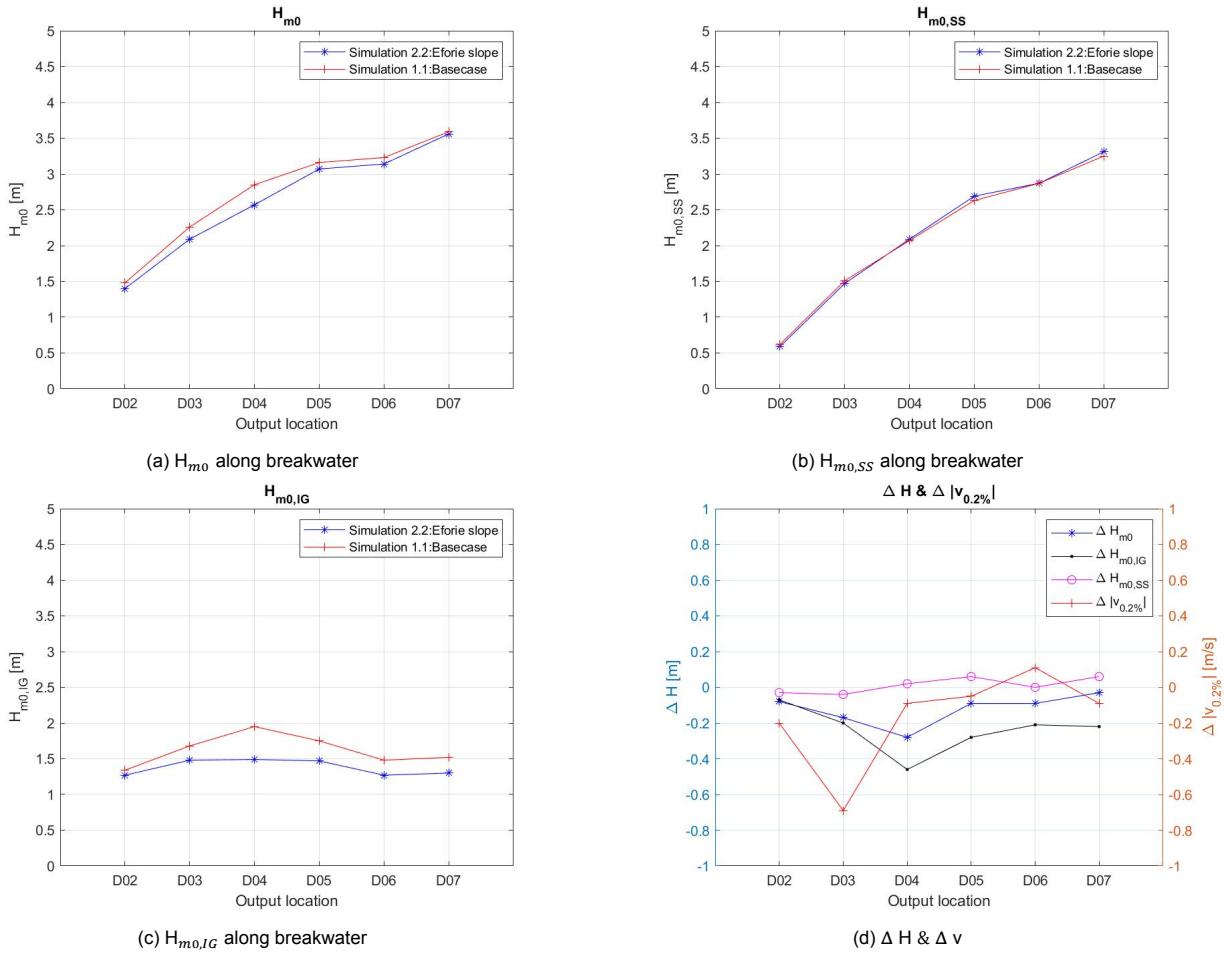

(a) H_{m0} along breakwater

(b) $H_{m0,SS}$ along breakwater

(c) $H_{m0,IG}$ along breakwater

(d) Δ H & Δ v

Figure 6.6: Wave height for simulation 2.2 and the basecase

Figure 6.6 shows a significant reduction in the infragravity wave energy, while the wind-sea swell wave energy remains constant. The exclusion of the transitional slope, and implementation of the 1:120 slope, thus induces a reduction in infragravity wave energy. The reduction in the velocity measured at output location D03, could be perceived as a one-time outlier. Investigating figure 6.6d a clear relation between IG-wave energy and velocity could be identified. Near the shore the IG-wave energy of the basecase is dominant over simulation 2.2. The velocity signal shows that the velocity measured at this location is also higher. However, when comparing the differences between the wave energy and comparing this to the differences in velocity a clear correlation can not be identified. The results suggest that IG-wave energy near the coast is correlated with the higher velocities. An exact causality can not be identified.

Extending the 1:120 slope (thus excluding the transitional slope) does not affect the wind-sea swell wave energy present in the waves. However a reduction in low frequency wave energy is visible throughout the different output locations. This hypothesis is confirmed by the wave spectrum observation at output location G02, which is around the MN75-10m bathymetry line, shown in figure 6.7b. At G02 the spectrum from simulation 2.2 shows a bigger spectral width and a less defined peak. This means that more waves are present of different frequencies, which reduces the clear interaction between the short waves that generates the infragravity waves. Figure 6.7a shows that at the head of the breakwater, output location W01, the decrease in IG-wave energy for simulation 2.2 is already visible. Figure 6.8 and table 6.7 compare the IG-wave energy propagation along the breakwater foreshore. At G02 the amount of IG-wave is comparable. At W01 the total energy difference is approximately the same as it was at G02. The amount of IG-wave energy however has decreased significantly for simulation 2.2.

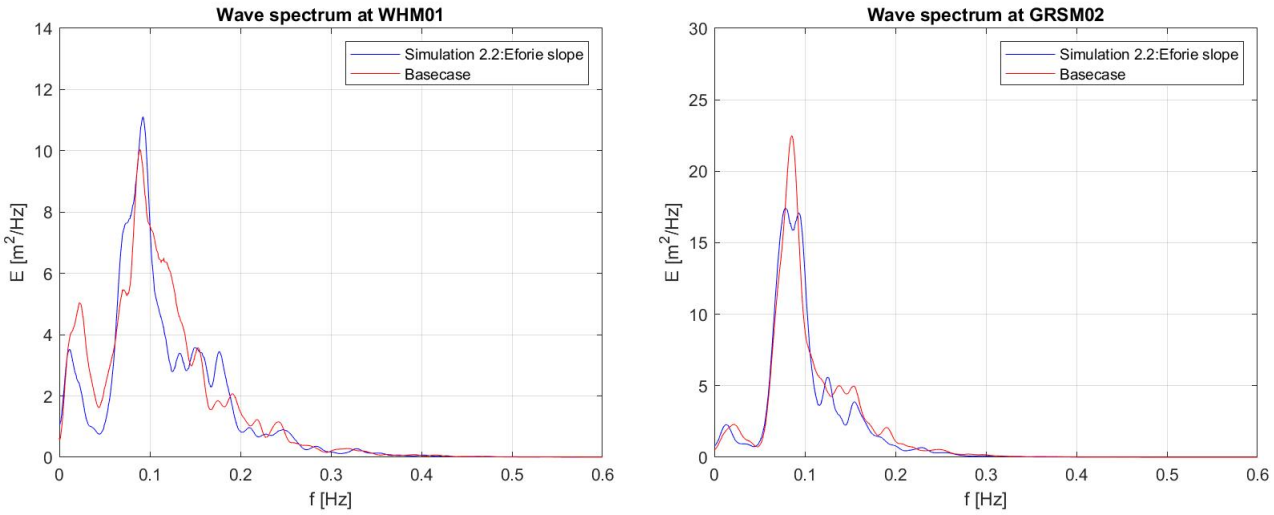

(a) Wave spectrum at W01

(b) Wave spectrum at G02

Figure 6.7: Wave height for simulation 2.2 and the basecase

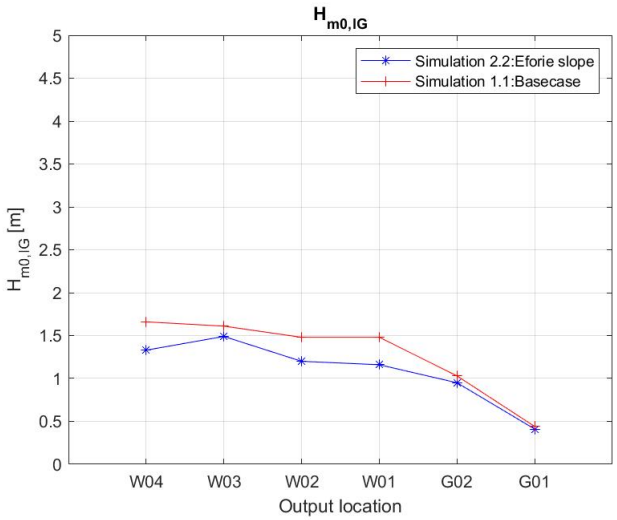

Figure 6.8: $H_{m0,IG}$ along the upper and lower foreshore

	W01			G01		
	H_{m0}	$H_{m0,ss}$	$H_{m0,IG}$	H_{m0}	$H_{m0,ss}$	$H_{m0,IG}$
Simulation 2.2	3.65	3.46	1.16	4.07	3.96	0.95
Basecase	3.82	3.52	1.48	4.25	4.13	1.03
Δ H	-0.17	-0.06	**-0.32**	-0.18	-0.17	-0.08

Table 6.7: Simulation 2.2 and base case wave heights at W01 and G02

Conclusion

The most important takeaways from this simulation are listed below.

1. The transitional slope seems to have minor influence on the velocity measured along a breakwater.

2. The results show no influence on SS-wave energy as expected from the literature.

3. The results represent the decrease in IG-wave energy as expected from the literature.
4. The results suggest that IG-wave energy near the coast is correlated with the higher velocities. An exact causality can not be identified.

6.2.3. Eforie

The next check is removing the transitional slope from the simulation and applying directional spreading to the model boundary, thus combining the adaptations of simulations 2.1 and 2.2. Based on the literature and the results of simulations 2.1 and 2.2, the following results were expected:

- The added effect of both the transitional slope and directional spreading on the velocity is expected. A minor effect around the head of the breakwater, with a decrease in velocity and around D03 a decrease in velocity.
- A decrease in wave energy, represented in the IG-wave energy component.

Velocities

In table 6.8 and figure 6.9 the measured velocities of the simulation and the basecase are shown.

Output point	D02	D03	D04	D05	D06	D07
Simulation 2.3	2.82	3.10	4.12	4.08	4.98	6.19
Basecase	3.72	3.71	4.17	4.31	5.30	6.21
Δ v (m/s)	-0.89	-0.61	-0.05	-0.23	-0.32	-0.02
%-difference	-24	-16	-1	-5	-6	0

Table 6.8: Simulation 2.3

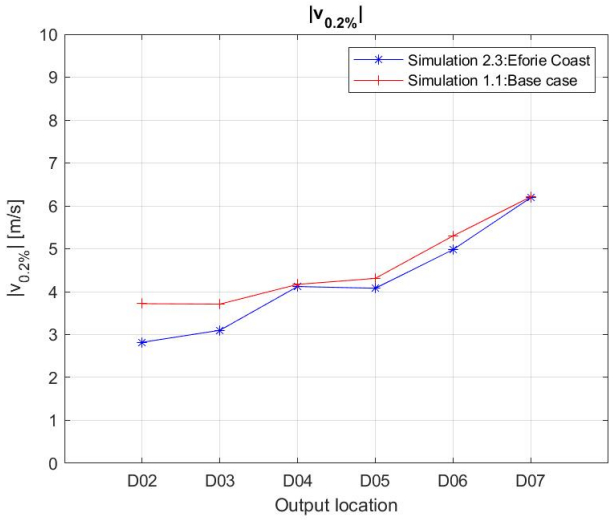

Figure 6.9: Velocity for simulation 2.3 and the basecase

The velocity along the breakwater shows the combined effect of simulations 2.1 and 2.2. A reduction in velocity along the entire breakwater is measured, increasing towards the shore. In the nearshore part, D02-D03, a velocity reduction between 16-24 % is measured, while a reduction between 0-6% is measured for D04-D07. The applied modelling choices by Deltares resulted in a somewhat conservative design, especially for the nearshore part of the breakwater.

Wave Climate

Figure 6.10 shows the wave energy of simulation 2.2 compared to the basecase. In figure 6.10d the difference between the wave energy and velocity values of the simulation and the basecase is presented.

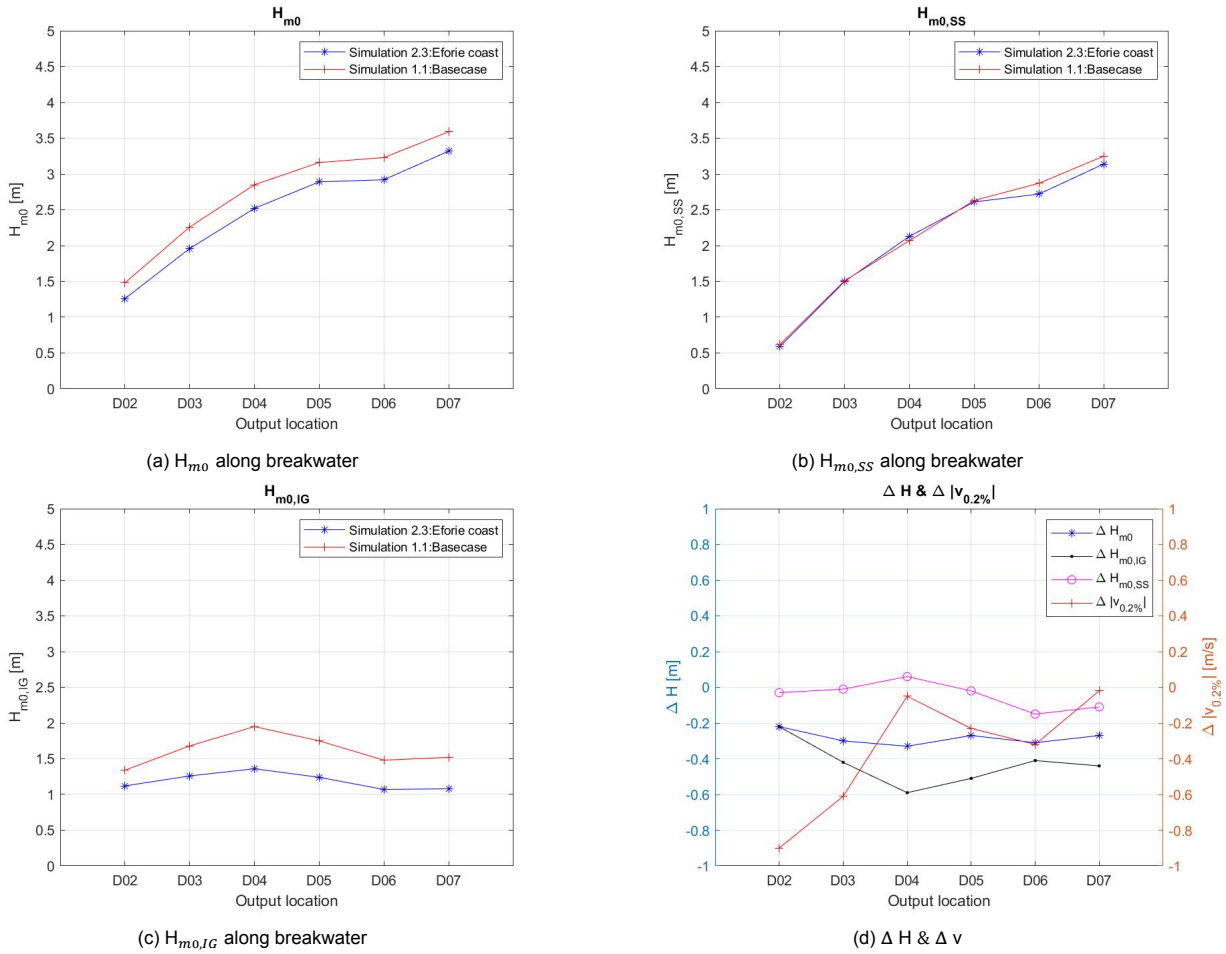

(a) H_{m0} along breakwater

(b) $H_{m0,SS}$ along breakwater

(c) $H_{m0,IG}$ along breakwater

(d) Δ H & Δ v

Figure 6.10: Wave height for simulation 2.3 and the basecase

The wave energy along the breakwater shows a significant reduction, which is largely due to a reduction in IG-wave energy. The SS-wave component only shows a minor reduction at the head of the breakwater. The results suggest that at the head of the breakwater the SS-waves are governing, resulting in lower velocities for simulation 2.3. Near the shore the IG-waves are governing providing the increased waterlevel which results in higher waves that induce more damage, as was discussed in chapter 1.

Conclusion
The most important takeaways from this simulation are listed below.

1. The added effect of directional spreading and the transitional slope is visible in the velocity and wave energy signal. An average overestimation of the velocity along the entire length of the breakwater is measured. In the nearshore part, D02-D03, a significant velocity reduction between 16-24% is measured.

2. The significant reduction in measured velocity for the nearshore part seems to be correlated with the expected IG-wave dominance in this part. Simulation 2.3 has less IG-wave energy, which can be linked to the lower velocity.

6.2.4. Conclusion

The most important takeaways from part 2 are listed below.

1. For the physical model test Deltares choose to neglect the effect of directional spreading and apply a transitional slope at the offshore boundary. Based on the results of part 2 it can be concluded that Deltares was correct to choose for this. The modelling choices resulted in an underestimation of the breakwater stability and therefore a somewhat conservative design along

the entire length of the breakwater. This underestimation of the velocity was minimal, 0-6%, for locations D04-D07, but significant, 16-24%, for locations D02-D03.

2. Both the transitional slope as the assumption of long-crested waves lead to more IG-wave energy in the system.

3. The increase in velocity at D02-D03 due to the applied modelling choices seems to be linked to the indirect effect on velocity via IG-wave energy. The proposed theory suggests that near the shore the IG-waves are governing providing a temporary increase in waterlevel, which results in higher waves that induce more damage. A correlation between IG-wave energy and velocity along the D02-D03 segment is suggested, however conclusive evidence for a direct relation between IG-wave energy and velocity could not be found.

6.3. Eforie layout

In part 3 the two identified configurations of the Eforie layout are tested. The foreshore slope angle and the cut-off parabolic bay shape.

6.3.1. Lower foreshore

In simulations 3.1 and 3.2 the angle of the foreshore slope is increased and decreased as discussed in chapter 4. Based on the literature research the following results were expected:

- The average SS-wave height becomes higher for steeper slopes, due to breaking of the smaller waves (Verhagen and Mertens, 2010)
- For a gentler foreshore slope, the surf zone becomes wider and waves break further offshore, increasing dissipation, resulting in more IG-wave energy (Lashley, 2021)
- Based on the literature and the results of part 1 and part 2, due to the expected changes in wave-energy as listed above, the velocities along the breakwater are expected to change accordingly. For the steeper slope, higher velocities are expected at the breakwater head and lower near the shore. For the more gentler slopes, this effect is expected to be reversed, a lower velocity at the head and a higher velocity near the coast.

Velocities

In table 6.9 and figure 6.11 the measured velocities of the simulation and the basecase are shown.

Output point	D02	D03	D04	D05	D06	D07
Simulation 3.1	2.71	3.17	4.39	4.99	5.85	6.65
Simulation 3.2	4.34	4.13	4.79	4.77	4.97	5.41
Basecase	3.72	3.71	4.17	4.31	5.30	6.21
Δ $v_{3.1}$ (m/s)	-1.00	-0.54	0.22	0.68	0.55	0.45
%-difference$_{3.1}$	-27	-15	5	16	10	7
Δ $v_{3.2}$ (m/s)	0.62	0.41	0.62	0.45	-0.33	-0.79
%-difference$_{3.2}$	60	30	9	-5	-15	-19

Table 6.9: Simulation 3.1& 3.2

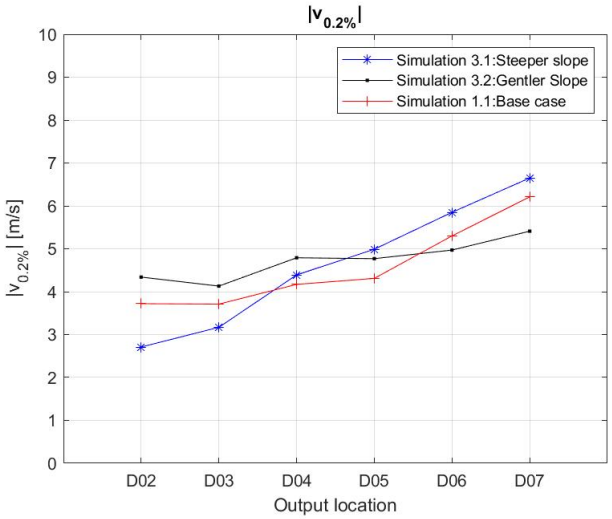

Figure 6.11: Velocity for simulations 3.1, 3.2 and the basecase

In figure 6.11 a trend could be identified where around the head of the breakwater the simulation with the most gentle slope results in the lowest velocity and the simulation with the steepest slope results in the highest velocity. At the landward side this is the other way around. Both observations correspond to the expectations.

Wave Climate
Figure 6.12 shows the wave energy of simulations 3.1 and 3.2 compared to the basecase.

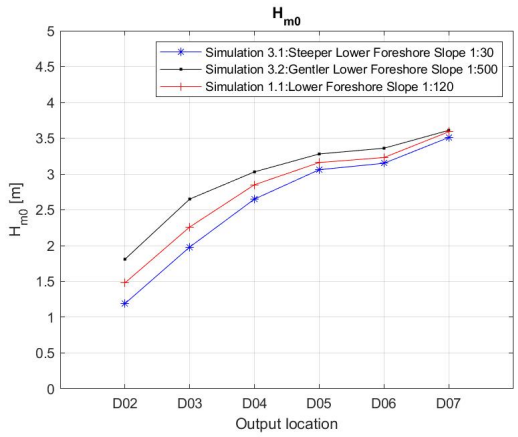

(a) H_{m0} along breakwater

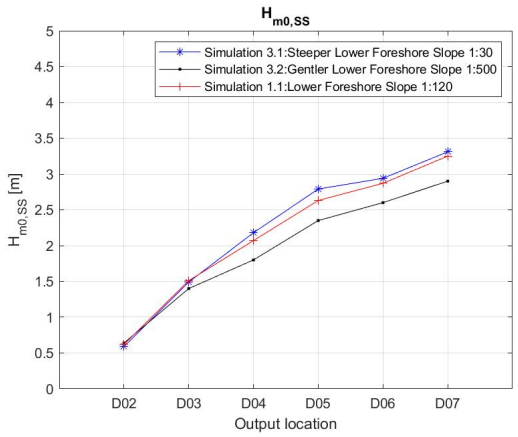

(b) $H_{m0,SS}$ along breakwater

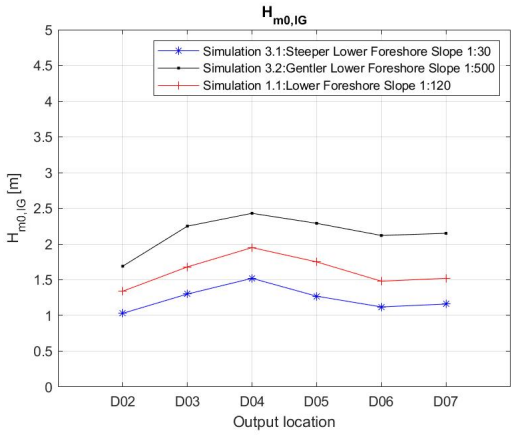

(c) $H_{m0,IG}$ along breakwater

Figure 6.12: Wave height for simulations of 3.1 and 3.2 the basecase

The influence of IG waves increased for milder foreshore slopes. This is visible in the figures above. In chapter 4 the 1:30 slope was chosen since it would have an impact on stone stability via SS-wave energy, but would be gentle enough to induce minimal IG-wave energy. It shows that the 1:30 wave is still mild enough that no significant IG-wave generation on the steep slope has occurred. Figure 6.12 reveals that the SS-wave energy becomes more dominant with a steeper slope and the IG-wave energy becomes more dominant with a more gentle slope.

Comparing 6.12 with figure 6.11 suggests that at the head of the breakwater the SS-waves are governing for the velocity. Around D05-D07 the SS-waves of simulation 3.1 are highest and simulation 3.1 provides the highest velocity. Around D05 the depth is approximately 5.2m and the wave height is approximately 3.2m. Due to depth-limited breaking, the short (waves) break around D05. After D05 the IG-waves then become governing for the velocity. Around D02-D04 the IG-waves of simulation 3.2 are highest and simulation 3.2 provides the highest velocity. Figure 6.12a shows that the H_{m0} at D07 is approximately the same for the different foreshore slopes. The $H_{m0,IG}$ differs as described above, with higher $H_{m0,IG}$ along the entire breakwater for simulation 3.2. Since at D07 the H_{m0} is the same and the $H_{m0,IG}$ is higher for simulation 3.2, the $H_{m0,SS}$ is lowest for this simulation. This also results in lower velocities at the head.

Conclusion

The most important takeaways from these simulations are listed below.

1. The foreshore slope angle is correlated to SS- and IG- wave energy. As expected a steeper slope results in more SS-wave energy in the system and a more gentle slope results in more IG-wave energy in the system.

2. In line with the conclusion of part 2, at the head of the breakwater the SS-waves are governing for the velocity. Around D05 the SS-waves break and the IG-waves become governing for the velocity.

3. At point D07 the results show that more IG-wave energy, results in less SS-wave energy, which leads to a lower velocity.

6.3.2. Wave focusing

In simulation 3.3 the cut-off parabolic bay shape is excluded from the bathymetry. The contour lines are assumed straight and perpendicular to the breakwater, as shown in figure 6.13. Based on the observations of chapter 2 the following results were expected:

- A decrease of the wave focusing effect.
- Resulting from the above a decrease in wave velocity along D02-D03.

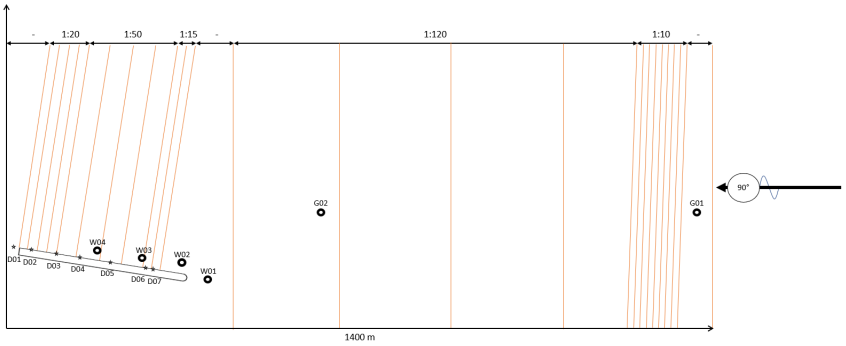

(a) $setup_{3.3}$ topview

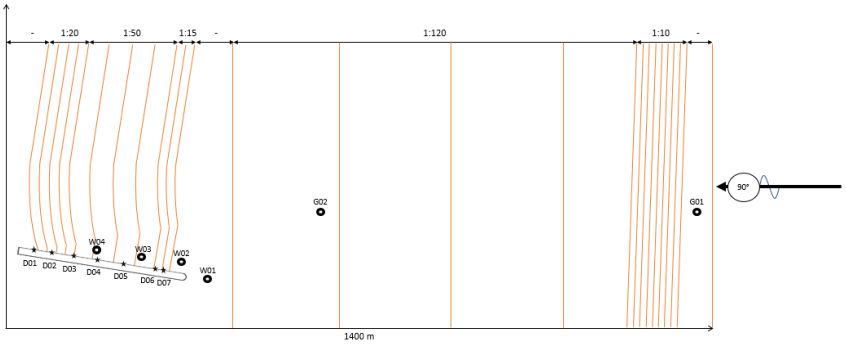

(b) Basecase topview

Figure 6.13: Bathymetry 3.3

Wave-focusing

In figure 6.14 a top view of the simulation 3.3 and basecase is shown.

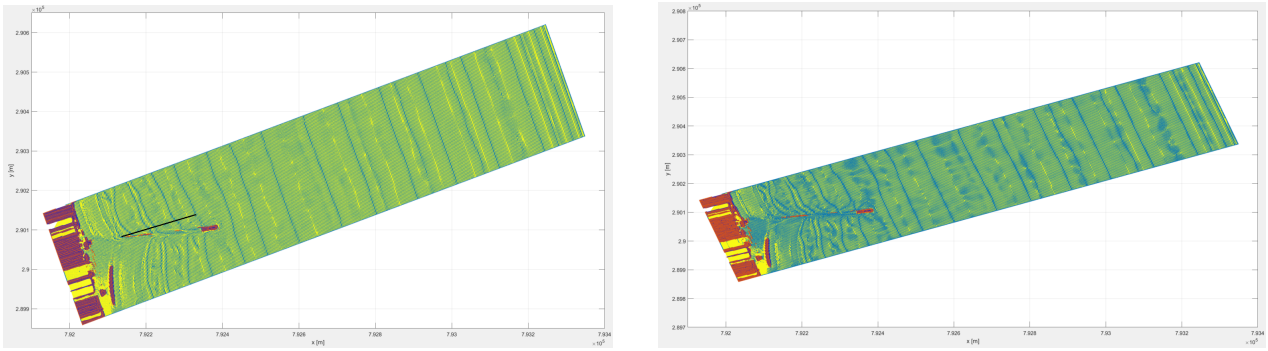

(a) Basecase (b) Simulation 3.3

Figure 6.14: Cut-off parabolic bay shape in SWASH model

In chapter 2 it was verified that the wave focusing effect of the cut-off parabolic bay shape was visible in the SWASH top view. Figure 6.14 shows that in simulation 3.3 this wave-focusing effect is not visible when the cut-off parabolic bay-shape is excluded. The wave in simulation 3.3 now interacts with the structure along the length of the breakwater. In figure 6.14b it can be seen that therefore the wave slows down near the structure, which is expected due to the roughness of the structure. This effect is not visible in figure 6.14a.

Velocities

In table 6.10 and figure 6.15 the measured velocities of the simulation and the basecase are shown.

Output point	D02	D03	D04	D05	D06	D07
Simulation 3.3	3.32	3.43	4.26	4.33	5.20	6.10
Basecase	3.72	3.71	4.17	4.31	5.30	6.21
Δ v (m/s)	-0.39	-0.29	0.19	0.01	-0.10	-0.11
%-difference	-11	-8	2	0	-2	-2

Table 6.10: Simulation 3.3 and base case velocities

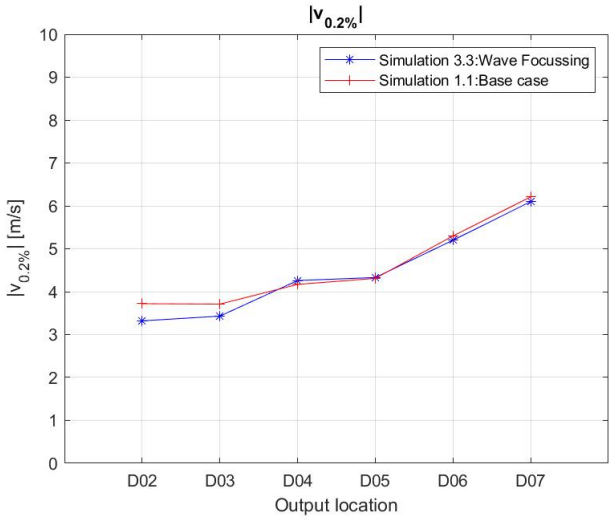

Figure 6.15: Velocity for simulation 3.3 and the basecase

As expected for simulation 3.3, by excluding the cut-off parabolic bay shape, the wave-focusing was excluded as well. This resulted in lower velocities around output locations D02 and D03 of around 8-11% depending on depth. This is visible in figure 6.15, where the velocities of simulation 3.3 and the basecase are shown.

A remark needs to be made regarding the output locations. As explained in chapter 4 all the output locations are shifted more landward to remain on the same water depth. When the velocity results of simulation 3.3 are checked it can be seen that the velocity signal stays the same and only deviates at output locations D02 and D03. This leads to believe that scaling the output locations with the water depth, and thus the relative position of the output locations on the breakwater length, has minor influence on the velocity signal. Therefore it can be stated that the cut-off parabolic bay shape has an influence at the shore-ward side of the breakwater, which has some effect on stone stability.

Conclusion
The most important takeaways from this simulation are listed below.

1. Excluding the cut-off parabolic bay shape excludes the wave-refraction pattern and results in lower velocities around output locations D02 and D03 of around 8-11% depending on depth.

6.3.3. Conclusion
The main conclusions from part 3 are:

1. The foreshore slope affects breakwater stability (in)directly. Due to the foreshore slope the IG- and SS- wave energy components are affected. A steeper slope results in more SS-wave energy in the system and a more gentle slope results in more IG-wave energy in the system. This results in more instability at the head of the breakwater for steeper slopes and more instability nearshore for the more gentle slopes. In line with the conclusion of part 2, at the head of the breakwater the SS-waves are governing for the velocity. Around D05 the SS-waves break and the IG-waves become governing for the velocity.

2. Excluding the cut-off parabolic bay shape excludes the wave-refraction pattern and results in lower velocities around output locations D02 and D03 of around 8-11% depending on depth.

6.4. Wave angle
In this section the comparison is made between different relative angles between the incoming waves and the breakwater. Therefore a new basecase is modelled, where all the bathymetry contour lines are adjusted as parallel to the coast. The effects of this simplification on the measured velocity is discussed by comparing the outcomes of simulation 4.1 to simulation 3.3. Then the influence of the wave angle is checked and its effect is described in more detail.

6.4.1. Basecase wave angle
In simulation 4.1 a new basecase for the wave angle part is constructed. The contour lines are assumed straight so refraction effects do not occur in the system. This new basecase is therefore compared to the results of simulation 3.3. Based on the results of simulation 3.3 and the remarks made regarding simulation 4.1 in chapter 4 the following results were expected:

- Comparable velocities around output locations D02 and D03.
- Minor changes in velocity along the breakwater due to simplifications regarding the breakwater head, slope and height.

Velocities
In table 6.11 and figure 6.16 the measured velocities of the simulation and the basecase are shown.

Output point	D02	D03	D04	D05	D06	D07
Simulation 4.1	3.32	3.43	4.26	4.33	5.20	6.10
Simulation 3.3	3.33	3.42	3.65	4.11	6.21	6.58
Δ v (m/s)	0.00	0.01	0.70	0.22	-1.01	-0.48

Table 6.11: Simulation 4.1 compared with simulation 3.3

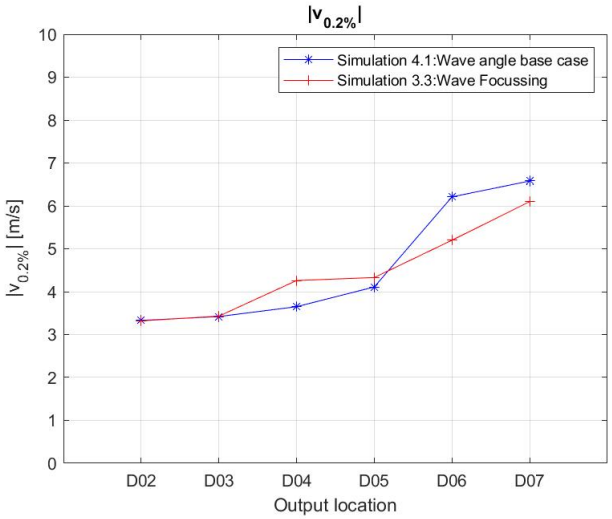

Figure 6.16: Velocity for simulations 4.1 and simulation 3.3

Along the shore-part of the breakwater, D02-D03, the velocity is comparable between simulation 4.1 and 3.3. This means the conclusion of simulation 3.3 also holds for simulation 4.1. However, in the offshore-part of the breakwater a different pattern of velocity is visible. Between output location D03-D05 the velocity in simulation 3.3 is higher, between output location D05-D07 the velocity measured in simulation 4.1 is higher. This could be due to the fact that the head of the breakwater is now visualised as a 2:3 slope till a height of MN75+3m instead of a 3:4 slope with a height of MN75+4m. This means the waves will be reduced less by the porous breakwater and therefore result in higher velocities along the breakwater.

Conclusion
The most important takeaways from this simulation are listed below.

1. No effect of wave focusing is visible
2. The velocity of simulation 4.1 differs from 3.3, but forms a reliable basis to compare the influence of incoming wave angle

6.4.2. Wave angle

The final step of this research is comparing different wave angles. As described in chapter 4, a relative angle of 0°, 13.4°, 30°, 45°between the breakwater and the incoming waves is applied. Based on the theory presented in chapter 3 and the results from part 2 and 3 the following results were expected:

- An increase in velocity along the breakwater for more oblique incoming wave angles. Thus a decrease in velocity along the breakwater for more perpendicular incoming waves.
- A change in wave-energy (component) is not expected based on the relative wave angle.

Velocities
In table 6.12 and figure 6.17 the measured velocities of the simulations are shown.

Output point	D02	D03	D04	D05	D06	D07
Simulation 4.2	2.45	2.38	2.77	3.21	4.54	5.61
Simulation 4.1	3.33	3.42	3.65	4.11	6.21	6.58
Simulation 4.3	4.16	4.26	4.40	5.39	6.53	6.76
Simulation 4.4	4.53	4.49	4.62	5.84	6.78	6.92

Table 6.12: Part 4

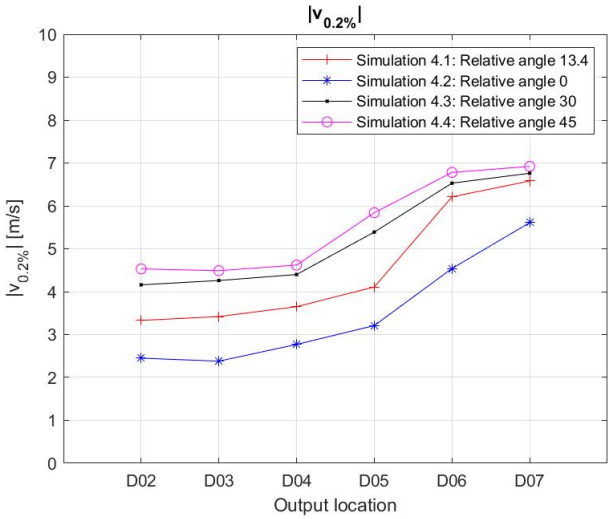

Figure 6.17: Velocity for simulations 4.1-4.4

In figure 6.17 the velocities of simulation 4.1, 4.2, 4.3 and 4.4 are shown. A clear relation between relative angle and measured velocity in the SWASH can be identified. The velocities increase according to the relative angle between the breakwater and the incoming waves. This is in line with the theory of Van Gent listed in chapter 3. However, the hypothesis that for very oblique wave angles in shallow water a different relation between wave angle and breakwater stability would show is not represented by the model and can therefore not be concluded based on the results from this SWASH numerical model research. This could have multiple explanations, which are discussed chapter 7.

Below it will be investigated whether only the relative relation between wave angle and stone stability is shown via the theory used in this research or that the exact found relation between wave angle and stone stability, identified by Van Gent, can be reproduced with the results of this model. To check the level of performance of the model, the obliqueness factors of Van Gent is compared to the outcomes of the model. Important for this is to restate that Van Gent performed his tests is relatively deep water conditions at the toe of the breakwater and no wave breaking occurred on the horizontal foreshore Van Gent (2014). The h/H_s ratio during the Van Gent model tests was between 2.38-33.33. For simulations 4.1,4.3 and 4.4 that are compared with this method the h/H_s ratio does not reach these values, but remains around 1. This analysis is therefore not fully applicable, but it gives an extra check for the possible use of the proposed method.

For the conditions Van Gent performed his tests, he expressed that it provided reasonable estimates for wave angles between β = 0°(perpendicular waves) and β = 90°(parallel waves). D_β is the required armour size for oblique waves and D_0 is the required armour size for perpendicular waves. The obliqueness factors of Van Gent can be calculated with equation 6.3. For this research this equation is rewritten to equation 6.5.The slope factor is for this comparison not taken into account, because it can not be stated how the wave flows over the breakwater for the different incoming angles. The c_β=0.35 for rock slopes with long-crested waves. Table 6.13 shows the Van Gent obliqueness factors for the different incoming wave angles. Table 6.14 shows the squared velocity signal of the different simulations. In table 6.16 the velocities of different simulations are divided by each other and the obliqueness factors of different simulations are divided by each other.

$$\gamma_\beta = (1 - c_\beta) * cos^2(\beta) + c_\beta \tag{6.3}$$

$$\gamma_\beta = \frac{D_\beta}{D_\perp} \rightarrow \frac{D_{\beta,1}}{\gamma_{\beta,1}} = \frac{D_{\beta,2}}{\gamma_{\beta,2}} \rightarrow \frac{D_{\beta,1}}{D_{\beta,2}} = \frac{\gamma_{\beta,1}}{\gamma_{\beta,2}} \tag{6.4}$$

$$\Delta D = \frac{1}{K} * 0.42 * \frac{u^2}{2g} \rightarrow \frac{D_{\beta,1}}{D_{\beta,2}} = \frac{u^2_{\beta,1}}{u^2_{\beta,2}} = \frac{\gamma_{\beta,1}}{\gamma_{\beta,2}} \tag{6.5}$$

Simulation	Relative angle	Incoming wave angle	c_β	$\gamma_{\beta,VanGent}$
Simulation 4.1	13.4	76.6	0.35	0.38
Simulation 4.2	0	90	0.35	0.35
Simulation 4.3	30	60	0.35	0.51
Simulation 4.4	45	45	0.35	0.68

Table 6.13: $\gamma_{\beta,VanGent}$ for simulations 4.1-4.4

	D02	**D03**	**D04**	**D05**	**D06**	**D07**
Simulation 4.1	11.07	11.69	13.35	16.87	38.53	43.30
Simulation 4.2	6.03	5.64	7.66	10.29	20.64	31.42
Simulation 4.3	17.31	18.15	19.33	29.05	42.64	45.70
Simulation 4.4	20.53	20.16	21.30	34.06	45.95	47.84

Table 6.14: Squared velocity for simulations 4.1-4.4

	D02	D03	D04	D05	D06	D07	Average	σ
sim 4.4/sim 4.3	1.19	1.11	1.10	1.17	1.08	1.05	**1.12**	0.05
sim 4.4/sim 4.1	1.85	1.72	1.60	2.02	1.19	1.10	**1.58**	0.66
sim 4.3/sim 4.1	1.56	1.55	1.45	1.72	1.11	1.06	**1.41**	0.36

Table 6.15: Calculated ratio for simulations 4.1-4.4

	$\frac{\gamma_{\beta,VanGent}}{\gamma_{\beta,VanGent}}$	Average	σ
sim 4.4/sim 4.3	1.32	**1.12**	0.05
sim 4.4/sim 4.1	1.75	**1.58**	0.33
sim 4.3/sim 4.1	1.33	**1.41**	0.25

Table 6.16: Calculated ratio for simulations 4.1-4.4

Comparing the average value of the ratios of the velocities and the Van Gent γ_β-factor, presented in table 6.16, they seem to coincide reasonably well. The standard deviation is however significant for some comparisons. I addition, as stated above, the depth conditions the different tests were performed in differs. The theory of basing stone stability on a velocity signal from a numerical model can therefore give a good order of magnitude value for the ratios between different wave angles, in line with the Van Gent theory. However, it is recommended that first research is performed in applying this theory, in which a numerical model is setup to acquire velocity signals to determine stone stability.

Wave Climate

Figure 6.18 shows the wave energy of simulations 4.1-4.4.

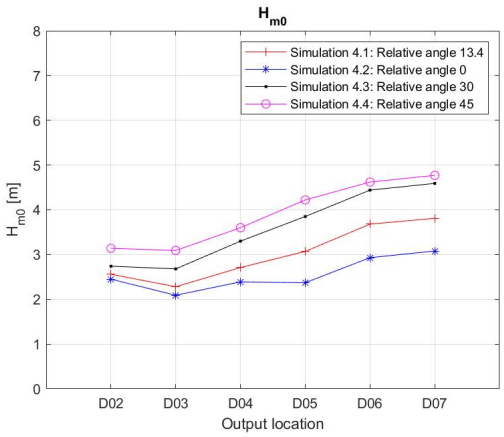

(a) H_{m0} along breakwater

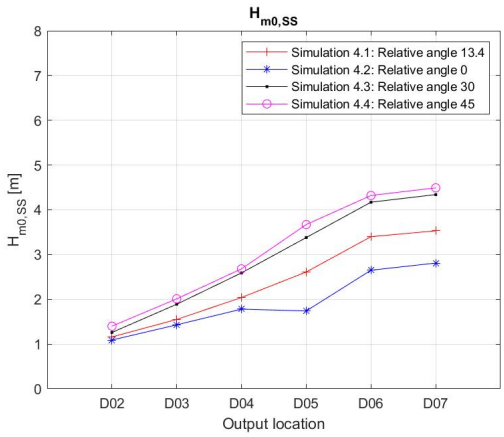

(b) $H_{m0,SS}$ along breakwater

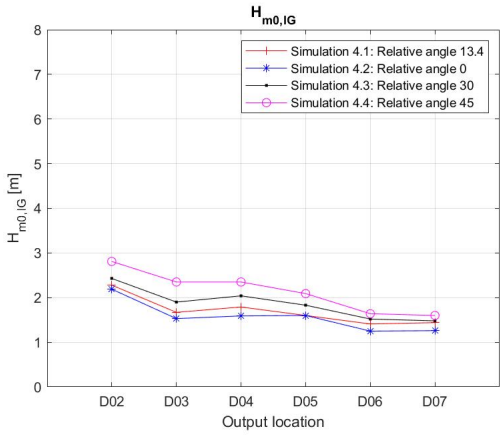

(c) $H_{m0,IG}$ along breakwater

Figure 6.18: Wave height for simulations of 3.1 and 3.2 the basecase

In figure 6.18 the wave energy components show that the wave energy is higher at all output locations along the breakwater for a higher relative angle. This is represented in both the SS- as the IG-wave energy component. This does not match the stated hypothesis. This means that there is more energy present in the system in simulations with a higher relative angle. A possible explanation for this could be due to reflecting waves. In case of parallel waves relative to the breakwater, hardly any waves will be reflected. The waves travel along the breakwater and break at the beach. For less oblique incoming waves, wave energy can be reflected introducing more energy in the system.

6.4.3. Conclusion

The most important takeaways from part 4 are listed below.

1. A clear relation between relative angle and measured velocity in SWASH can be identified. The velocities increase according to the relative angle between the breakwater and the incoming waves.
2. The Van Gent obliqueness factors, listed in chapter 3, can reasonably be reproduced by the outcomes of this model.
3. The hypothesis that for very oblique wave angles another relation between wave angle and breakwater stability would show can not be concluded based on the results from this SWASH numerical model research.
4. A shift to IG-wave energy is observed for larger relative angles, so less oblique waves.

5. Both the SS- as the IG-wave energy is higher at all output locations along the breakwater for a higher relative angle. This can be due to reflected wave energy.

6.4.4. IG-wave

In the previous sections it was consistently found that at the head of the breakwater the SS-waves are governing and at the shore-ward side of the breakwater the IG-waves become governing. To test the direct effect of a long wave on the velocity along the breakwater a final simulation is performed, simulation 5.1. In this simulation a long wave with wave characteristics presented in table 6.17 is applied to the basecase model. The hypothesis, as described in 1, is that the IG-waves by themselves do not inflict damage to a breakwater, but indirectly increase velocity via the SS-waves. The velocities measured along the breakwater and the wave climate in the system is presented in figure 6.19.

Run	η (m)	H_{m0} (m)	T_p (s)	β (°N)
Simulation 5.1	0.73	0.5	50	70

Table 6.17: Simulation 5.1 input parameters

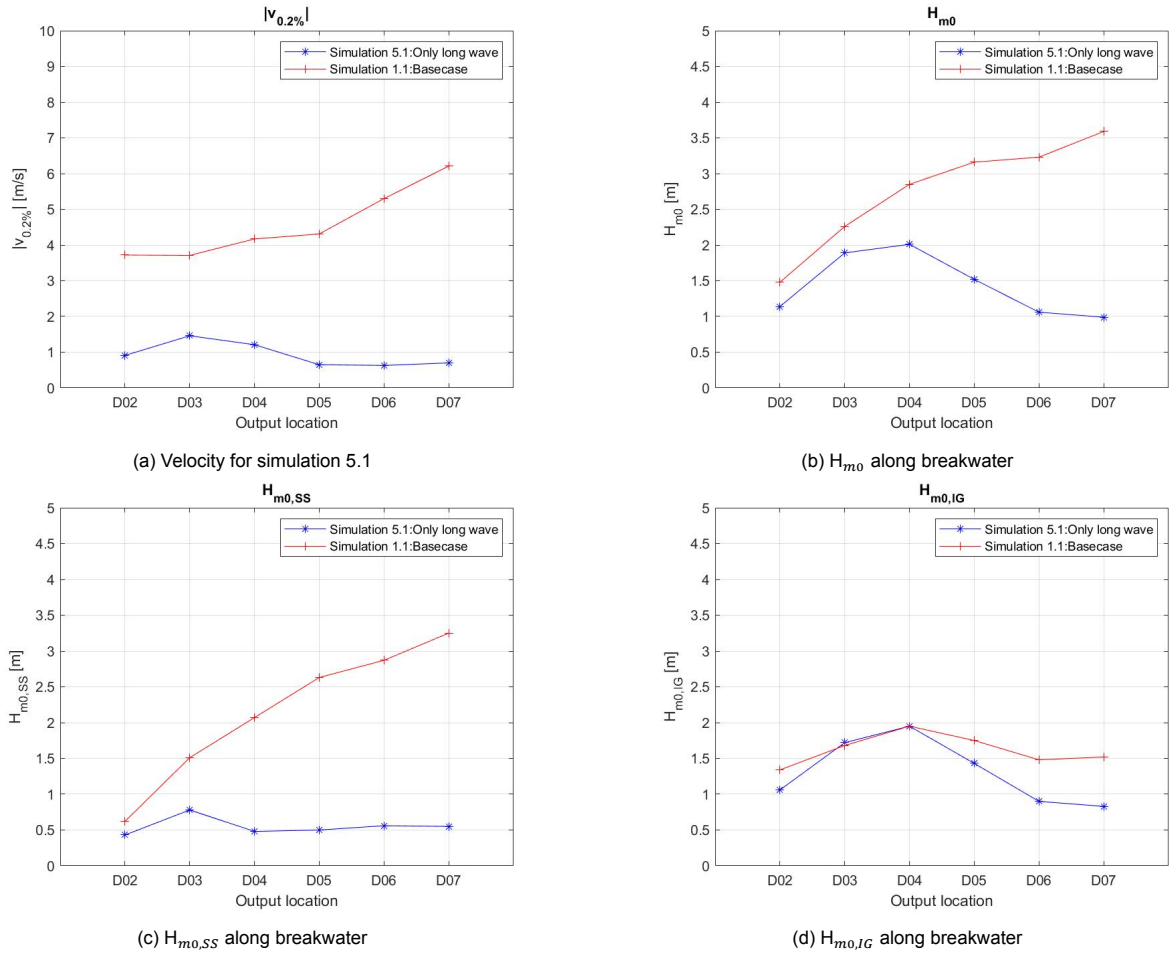

(a) Velocity for simulation 5.1

(b) H_{m0} along breakwater

(c) $H_{m0,SS}$ along breakwater

(d) $H_{m0,IG}$ along breakwater

Figure 6.19: Wave height for simulation 2.3 and the basecase

Figure 6.19 shows the indirect effect IG-waves have on the velocity and thus damage of a breakwater. A IG-wave by itself does not lead to high velocities along the breakwater. Figure 6.19d shows that around D02-D04 the IG-wave energy in the system is the same between simulation 1.1 and 5.1. When looked at figure 6.19a the velocity is still much larger for simulation 1.1. This is because in simulation 5.1 with only a long wave present, there is too little SS-wave energy. The $H_{m0,SS}$ is therefore larger for simulation 1.1, resulting in higher velocities, both at the head as near the coast. Simulation 5.1

reinforces the theory that an IG-wave induces a temporary increase in waterlevel. This allows the depth-limited SS-waves, if present, to become bigger resulting in a higher velocity and more damage on the breakwater.

6.4.5. Conclusion

The main conclusions from this section are:

1. Only a IG-wave does not result in high velocities along the breakwater, also not around D02-D03.
2. Simulation 5.1 reinforces the theory that an IG-wave induces a temporary increase in waterlevel. This allows the depth-limited SS-waves, if present, to become bigger resulting in a higher velocity and more damage on the breakwater.

7

Discussion

This chapter discusses various aspects that are relevant for interpretation of the previous shown results of the numerical model study. The next sections will present the discussion on the key findings, put them in perspective and discuss their applicability and limitations. The most influential assumptions and limitations of the research are discussed and finally an overview concerning the conditions that shape this research is provided.

The theory presented in this thesis is the first research that proposes to use SWASH to determine breakwater stability. In order to formulate this theory and perform the numerical model study, multiple assumptions had to be made regarding the existing theory on breakwater stability, the capabilities of SWASH and the correctness of the numerical model input and output.

7.1. Model theory

The stability equation that is formulated for this thesis is based on the relation stated by Izbash (1935) and scaled with the theory from Shields (1936). Uniform flow conditions were assumed above the stone, neglecting increased turbulence and accelerations (Hoffmans, 2006). This allowed to assume that the obtained velocity from the numerical model was governing for the stone stability. In chapter 3 it was presented that stone stability can be investigated via turbulence, shear stress and velocity and many more influential processes. It could be argued that the conditions of the waves flowing over and breaking on the breakwater do not fully resemble uniform flow conditions. As van Gent already demonstrated with his model tests in 2003, the fact that waves break due to the shallow depth has an affect on the stone stability (Van Gent et al., 2003). For nonuniform flow, the influence of turbulence and acceleration should also be taken into account (Steenstra et al., 2016).

It could be argued that the due to the surface roller turbulence should be taken into account. This could be done via the theory of Izbash. In this thesis under the assumption of uniform flow the relative fluctuation intensity, r, is assumed as 0.1. The observed wave moving along the breakwater resembled a sort of hydraulic jump or bore. For bores an r-value of 0.15 could be used and implemented, which results in a K_v of approximately 1.3 (Shi et al., 2020). However, the effect a hydraulic jump has on breakwater stability is assumed to be negligible (Schiereck, 2017).

In 2006 Verhagen et al. stated that the stability of rock on a slope depends on the velocity and the acceleration of the flow (Verhagen et al., 2006). In deep water, because of the phase shift between maximum velocity and maximum acceleration of $\pi/2$, the influence of acceleration can be neglected. However in shallower water, with shoaling waves, the influence of acceleration becomes relevant. Due to shoaling both acceleration as velocity increase. In addition, due to the increasing wave asymmetry the acceleration increases even more than the velocity (Verhagen et al., 2006). This effect is even greater in case of steeper foreshore slopes (Ciria et al., 2006). This means that next to velocity also acceleration is of significance for breakwater stability.

As stated above due to the assumption of uniform flow conditions, acceleration has not been taken into account in this thesis and it was assumed that drag force was dominant (Te Velde, 2022). Since this is a first step investigation assuming uniform flow conditions was a justifiable assumption (Hofland, 2005).

7.2. SWASH capabilities

SWASH physical phenomena

This numerical model study is performed in SWASH. SWASH is a well-known numerical model that has multiple hydraulic and coastal mechanisms incorporated. In previous research SWASH has been validated to correctly take into account multiple physical phenomena as presented and elaborated in chapter 3 (SWASH team, 2020). In this thesis it was assumed that the responsible process is incorporated in the numerical equations that are implemented in SWASH. This means that it is assumed that the observed phenomena is not a new process, such as a Mach-stem wave, briefly discussed in chapter 3. It should therefore be an existing effect such as refraction, shoaling or breaking. Refraction and shoaling are both incorporated in SWASH and investigated and modelled. This leaves the type of breaking mechanism as a possible cause.

In chapter 5 the numerical model was validated. It was found that in the wave pattern near the coast a process with a faster propagating wave front at the breakwater could not be so clearly identified. This may mean that the process that is central for this part of research was not incorporated in SWASH. In the SWASH model the grid size was 3m x 2m. On each grid cell, with these dimensions, there could only be one water surface. The breaking wave flowing along the breakwater length resembled a plunging wave. For a plunging wave the front of the wave is steep, resulting in large pressure gradient under the wave and large temporary accelerations (**?**). The large pressure gradients could result in pressure differences in the outer layer of the breakwater and 'push' a stone out of the armour layer. The SWASH model does not take this effect of the breaking plunging wave sufficiently into account, due to the grid dimensions. In this thesis several potential causes of the observed damage during the Eforie physical model test have been disproved. However, this effect needs to be investigated further and will therefore be discussed in the recommendations.

SWASH velocity capabilities

It is assumed that SWASH is capable of calculating reliable velocity signals along a porous breakwater. This entails that SWASH correctly incorporates the influence of a porous structure via the VARANS-equations and that SWASH is capable of calculating reliable velocity signals for these complex points. SWASH is capable and often used in research to calculate the cross-shore flow components in the vertical, however calculating the velocity on a slope with a porous layer induces extra complexities. The measured velocity signal was validated, seemed to be in the correct order of magnitude and resulted in reliable stone sizes. Therefore, this assumption seems, based on the results of this thesis, reliable.

7.3. Model Input

Grid size

The grid size in this numerical model resulted in 40 grid cells per wave length for the MN75-10m point, output location G02. It is advised to take between 50-100 grid cells per wave length. During the validation and the sensitivity analysis this resolution was found to provide reliable and sufficient results. When the waves approach the coast and the depth decreases the waves become shorter. At the head of the breakwater for example the peak period is 11s and the water depth is approximately 7m. This means a wavelength of approximately 90 meters, which means 30 grid cells per wave length. Along the breakwater this declines even further. In the SWASH manual a rule of thumb near the coast of 15 to 20 grid cells per wave length is advised (SWASH team, 2020). As tested in the verification and validation this coarser grid does result in reliable wave spectra for the output points located next to the breakwater. However, the grid resolution on the breakwater influences the representation of the breakwater in the model. This influences the authenticity of the required velocity signal.

Porosity
The breakwater was assumed as an impermeable core with a constant porous outer layer of 1.86m thick. Both the assumed impermeable core as the constant porosity thickness of 1.86m influence the velocity signal as indicated in the sensitivity analysis. As the sketches in figure 2.4 show the original breakwater does not have an impermeable core. This assumption leads to an overestimation of the velocity along the breakwater. Near the coast the original breakwater has a porous layer thickness of 1.30m and near the head the actual thickness is 2.44m. The constant porosity thickness therefore leads to an overestimation of the velocity along the head part and an underestimation along the nearshore part.

Number of vertical layers
SWASH was used with 2 layers in the vertical. In the sensitivity analysis 1 vertical layer was tested, but was found to be not sufficient enough. The use of 3 layers in the vertical was not computationally feasible. As the comparisons between the basecase and measured data in the physical model test showed great agreement, it was decided that 2 vertical layers was sufficient. For the wave spectra 2 layers were sufficient, however for the required velocity along the breakwater just above the rocks a more defined vertical resolution would have resulted in more reliable velocity results along the breakwater. Especially due to the interaction with the porous layer and its significant impact on the velocity results.

7.4. Model output

Output location scaled with water depth
The output location points are kept constant with respect to water depth. The assumption was that the velocity was dependent on the wave height, which is depth-limited. Thus keeping the output locations for all the simulations on the same depth resulted in comparable and reliable results regarding that. However this also meant that the output locations would be more shoreward on the breakwater. When a wave propagates over the breakwater it experiences friction due to the bed and the porous layer. This is expected to reduce the velocity.

Choice of velocity
The 0.02% velocity of layer 1 is chosen as the governing velocity for this research, as is discussed and substantiated in chapter 5. Most research in the theory regarding overtopping and stability make a link to a governing wave height, such as $H_{2\%}$. This link could not be made in this research, which make the conclusions from this thesis less easily repeatable and transferable.

8

Conclusions & Recommendations

This chapter deals with the conclusions that can be drawn from this research. The findings of this research are placed and linked to the literature and it is elaborated whether they support, extend or contradict with the governing theories. Lastly, recommendations for further research are presented, based on the discussion and conclusions of this study.

In this thesis SWASH was used to determine breakwater stability. The Eforie physical model situation was simulated and various alterations to the wave characteristics and the coastal layout were applied. This in order to evaluate, quantify and analyze the effect on the wave spectral energy and the breakwater stability, via the velocity along the breakwater, of several potentially influencing factors. The data from the physical model test was used to validate the basecase of the numerical model. These basecase velocity values where contrasted with the results from the different simulations, in which the before mentioned configurations where altered separately. The results from this research show interesting relations regarding the capabilities of SWASH for the use in determining breakwater stability, the relation between wave height (component) and velocity and the relation between certain configurations on the velocity.

8.1. Conclusions

The objective of this research was to propose a method that can link breakwater stability to SWASH and to assess whether the identified configurations resulted in the damage along the statically stable rubble mound breakwater, measured during the Eforie physical model test. To achieve this objective five sub-questions were formulated. These sub-questions will be treated first in separate sections, then the main research question will be answered.

8.1.1. Stone stability

In this section the goal was to propose a method that could link a velocity signal from SWASH to stable stone sizes. First, a equation was needed to be formulated that linked velocity to stone stability. Secondly, a sufficient velocity signal needed to be retrieved from SWASH.

In chapter 3 an equation is formulated, based on the theory of Izbash (1935) and Shields (1936) that links a velocity signal to stone stability. It is provided in equation 8.1. By inserting a velocity, which can be obtained from SWASH, a minimum required stone size results from the model.

$$\Delta d_{n,50} = 0.83 * \frac{u^2}{2g} \tag{8.1}$$

A reliable velocity signal was obtained from SWASH. The breakwater was modelled as a permeable core with an impermeable porosity layer as outer layer. In the vertical two layers were applied and it was checked whether the top layer (layer 1) was sufficiently above the applied porosity layer. This was

the case and therefore the velocity signal of layer 1 could be used as the governing velocity above the stones in the Izbash-type equation. To account for the governing velocity the 0.2% value of the velocity signal was used. Implementing this velocity in the proposed equation resulted in the minimum required stone size calculated for this research. From theses results it can be concluded that stone stability can be predicted reasonably well from a velocity signal obtained from SWASH. If the correct porosity is applied the trajectories, that were visible in the measured damage, were represented by the calculated $d_{n,50}$. In the sensitivity analysis it was shown that this porosity layer thickness has a significant effect on the obtained velocity signal of a 20-26% increase/reduction for an reduction/increase in porosity layer thickness of 30% or 0.6m. A difference in porosity layer thickness of 0.6m can easily occur in a single breakwater design, due to the different stone sizes that are used for different parts of the breakwater.

8.1.2. Influence modelling choices

In this section the conclusions are drawn on the influence of the modelling choices applied by Deltares during the physical model test.
The Eforie case has been adjusted to fit in the wave basin for the physical model test. This required certain modelling choices, that reduced the needed dimensions of the basin. The most important ones identified in this are listed below:

- Appropriate scaling relations where applied.
- The layout of the Eforie coast was simplified in three notable ways.
  - The foreshore was an immobile concrete foreshore, of which the guiding properties are assumed the same as the prototype situation.
  - Around the model, a conical shaped wave damping gravel beach was applied which prevented unwanted reflections.
  - From the bottom of the basin, located at MN75-23.5m, towards the first modelled depth contour a 1:10 transitional slope was used.
- For the hydraulic boundary conditions, directional spreading was not taken into account and only long-crested waves where applied during the test.

During the investigation presented in chapters 2 and 3 it was concluded that the implementation of a transitional slope and the assumption of long crested unidirectional waves could have an effect on breakwater stability. The influence of these two simplifications has been tested in the numerical model. Based on the results of this thesis it can be concluded that Deltares was correct to apply these choices. The modelling choices resulted in an underestimation of the breakwater stability and therefore a somewhat conservative design along the entire length of the breakwater. Applying directional spreading reduced the velocity around the head of the breakwater and excluding the transitional slope reduced the velocity along the breakwater nearshore. Together this effect was combined and all along the breakwater a reduction of velocity was measured. This underestimation of the velocity was minimally between 0-6%, around the head of the breakwater for output locations D04-D07 (h/Hs = 2.5-4.8), but significantly between 16-24%, for locations D02-D03 (h/Hs = 1.1-1.8). The increase in velocity at D02-D03 due to the applied modelling choices seemed to be linked to the indirect effect on velocity via IG-wave energy. The offshore transitional slope is too far away and in deep water to directly impact stone stability. However, both the transitional slope as the assumption of long-crested waves lead to more IG-wave energy in the system. The effect of infragravity wave on breakwater stability will be discussed in section 8.1.5.

8.1.3. Influence Eforie layout

In this section the conclusions are drawn on the influence of the layout of the Eforie case.

The layout of the Eforie case has been discussed in detail in chapter 2. Several layout characteristics were identified, of which the most important parts for this thesis are listed below:

- The Eforie coast contains a steep upper foreshore slope along the breakwater, which induces continuous breaking along the breakwater.
- The Eforie coast has a 1:120 lower foreshore slope in front of the breakwater, which induces shoaling and generation of bound infragravity waves.
- Along the North-side of the breakwater the contour lines are in a cut-off parabolic bay shape form near the breakwater.

In chapter 2 a bathymetry file was presented that contained both the exact Eforie layout, with the breakwater included. This resulted that only the lower foreshore slope and the cut-off parabolic bay shape could be investigated in this research. In chapter 3 it was found that a lower foreshore slope could affect breakwater stability directly via the SS-wave energy and indirectly via generation of IG-wave energy. In addition the refraction pattern of the cut-off parabolic bay shape could lead to wave focusing and increased wave impact. The influence of these two layout characteristics has been tested in the numerical model. The lower foreshore slope of 1:120 is neither steep nor gentle and therefore the SS-waves do not significantly influence breakwater stability. The lower foreshore slope does affect breakwater stability indirectly, via generation of IG-waves. This effect is significant and influences stone stability closer to the shore, where IG-waves become dominant. This will be discussed further in section 8.1.5. This configuration can in reality not be altered by the contractor, so needs to be taken into account in the design. The upper foreshore slope is not investigated and might be interesting to inspect in further research. The cut-off parabolic bay shape is responsible for the wave-refraction pattern and wave focusing which results in higher velocities around output locations D02 and D03 of around 8-11% depending on depth. It is however not responsible for the extreme difference in damage expectation and observation.

8.1.4. Influence wave angle

In this section the conclusions of the influence of oblique incoming wave angles on a shallow foreshore on the stability of a breakwater will be presented.

In chapters 2 and 3 it was found that the Eforie case entails a situation that has not been investigated before. A sloping foreshore along the breakwater, with very oblique breaking waves impacting the breakwater. In chapter 3 it was concluded that a Mach-stem wave did not occur in the Eforie case and was therefore not responsible for the measured damage. The faster propagating siderush of the wave over the breakwater could be responsible. The hypothesis was that due to the oblique waves another relation between wave angle and breakwater stability would show, where more oblique waves would induce more damage to a breakwater. Based on the results from this SWASH numerical model research the theory behind the Van Gent obliqueness factor is strengthened. Oblique waves approaching a breakwater on a shallow foreshore show a similar decrease in impact in this research as was observed by Van Gent for deep straight foreshores. In addition, it is found in this thesis that both the SS- as the IG-wave energy is higher at all output locations along the breakwater for a higher relative angle, which means also a shift to IG-wave energy is observed for larger relative angles. This can be due to reflected wave energy.

8.1.5. Influence infragravity wave energy

In this section the conclusions of the influence of infragravity wave energy on the stability of a breakwater will be presented.

The results from the simulations performed in this research showed that SWASH correctly calculated the wave transformation along a breakwater on a slope. All the simulations showed the expected results regarding infragravity wave generation. The IG-wave energy in the system could be influenced by multiple of the identified configurations:

- An offshore transitional slope leads to more IG-wave energy in the system.
- Assuming unidirectional waves leads to more IG-wave energy in the system.

- A steeper lower foreshore slope leads to less IG-wave energy in the system.
- A gentler lower foreshore slope leads to more IG-wave energy in the system.
- A higher relative angle between the breakwater and incoming waves leads to more IG-wave energy in the system.

The simulations regarding the modelling choices suggested that the measured velocity around D02-D03 (h/Hs = 1.1-1.8) was indirectly linked to the IG-wave energy in the system. From the simulations regarding the foreshore slope, it was concluded that the foreshore slope can affects breakwater stability indirectly. Due to the foreshore slope the IG- and SS- wave energy components are affected. A steeper slope results in more SS-wave energy in the system and a more gentle slope results in more IG-wave energy in the system. This results in more instability at the head of the breakwater for steeper slopes and more instability nearshore for the more gentle slopes. At the head of the breakwater the SS-waves are governing for the velocity. Around D05 (h/Hs = 1.7) the SS-waves break and the IG-waves become governing for the velocity.

Based on the simulations performed in this thesis it can be concluded that IG-waves have an indirect effect on breakwater stability. A IG-wave by itself does not lead to high velocities along the breakwater. However, an IG-wave induces a temporary increase in waterlevel. This allows the depth-limited SS-waves, if present, to become bigger resulting in higher velocities and more damage on the breakwater. This effect is mostly visible along D02-D03 (h/Hs = 1.1-1.8).

8.1.6. Breakwater stability

In this section the conclusions for the main objective of this thesis are presented. The objective of this research was to propose a method that can link breakwater stability to SWASH and to assess whether the identified configurations resulted in the damage along the statically stable rubble mound breakwater, measured during the Eforie physical model test.

The results of this research show that breakwater stability can be predicted reasonably well from a velocity signal obtained from SWASH. The velocity signal, obtained from SWASH, results in reliable stone sizes. The configurations could be investigated with the proposed method and the results provided reliable and useful insights. The proposed method was able to identify the effect infragravity wave energy has on the stability of a breakwater. The method is also tested by calculating the relative obliqueness factors for different incoming wave angles. The Van Gent tests were performed for relatively deep water conditions at the toe of the breakwater and no wave breaking occurred on the horizontal foreshore. In the numerical model these conditions differ strongly. Still relatively the change in damage resembles the Van Gent obliqueness factor, derived for deep water, however the standard deviation is significant for some comparisons. This analysis is therefore not fully applicable, but it gives an extra check for the possible use of the proposed method and proposes a recommendation for further research.

It needs to be stated that in the proposed formula, the required stone size is only based on the flow velocity and a slope factor. Multiple factors, identified in the literature, such as turbulence, acceleration and depth-influence are not taken into account. The theory to base stone stability on a velocity signal from a numerical model seems therefore valid to give an indication and order of magnitude value for the required stone size. It provides a promising basis for further research. However, basing the entire stone stability only on velocity might result in deviations. It is recommended that first further research is performed in applying the theory in which a numerical model is setup to acquire velocity signals to determine stone stability.

8.2. Recommendations

From the work provided in this report suggestions for further research and recommendations about the Eforie cae arose based on the discussion and conclusion. The study's recommendations for additional research are divided into three divisions.

1. The first set of suggestions focuses on the use of the **theory** that is central in this research using numerical models to determine stone stability. It focuses on the theory to link numerical model outcomes to breakwater stability.
2. The second category focuses on applying **SWASH** as the numerical model to use for this application and thus the use of SWASH in relation to breakwater stability. It offers suggestions for additional SWASH development and entails practical recommendations for future research and development that is required to improve its performance for breakwater stone stability techniques.
3. The third set of recommendations provides suggestions regarding the **Eforie** coast. In this thesis several potential causes have been investigated and (partially) identified/debunked as part of the cause for the observed damage during the physical model test. Recommendations can be presented regarding further steps into this new phenomena are provided.

Theory

In this research a first step is made into using numerical models to determine breakwater stability. This theory shows promising results, but first needs research focused on the theory itself, before it can be confidently used for applications such as the case treated in this thesis. The formula is based on theory of Izbash (1935), which is a balance of forces, scaled with Shields (1936). The way it is proposed in this thesis, the formula bases stone stability on velocity as the driving force for stone (in)stability, including wave propagation direction on the slope as an influential factor. This theory can be enhanced in two ways. On the one hand multiple research has indicated that other factors, such as turbulence, acceleration and depth influence, are of influence on stone stability in the environment of shoaling and breaking waves as well. It is therefore recommended to perform additional literature research increasing the confidence in the proposed method and the parameters it should contain. Once a sufficient and reliable equation has been set-up, it is recommended to first validate and scale the equation by repeating the model tests of Van der Meer and Van Gent for shallow water and Van Gent for oblique waves in deep water, measuring the velocities at multiple points along the breakwater. This can be done with the numerical model SWASH, but then for the known conditions of the above proposed tests. This to link this measured velocity to their identified damage values. By performing this, the applicability of the used theory assumed in this research is investigated. A basis and scaling framework can be constructed to explain and scale its applicability. Once the theory is proven to work, then applying the validated theory on a new subject will reduce uncertainties in the required outcomes. Further numerical experiments reproducing the results from physical model tests should be done to verify the use of this theory linking breakwater stability to numerical model outcomes. On the other hand the Izbash formula is a balance of forces. Simplifying the theory to this and choosing a numerical model that can calculate shear stresses allows the theory to base stone stability on the calculated shear stress as driving force for stone (in)stability.

SWASH application

This thesis investigates the abilities of SWASH to reproduce velocities along a breakwater. An assumption is made regarding the capabilities of SWASH. SWASH has shown to be a useful tool for analyzing wave transformation on a shore and taking into account the effect of IG-waves. It has great capabilities of calculating reliable velocity signals along a breakwater. Nonetheless, recommendations can be made for further SWASH development and points of interest when SWASH is used for this application. During the verification of the numerical model not all observed phenomena from the physical model test seemed to be repeated by the model. Perhaps the governing failure mechanism, responsible for the observed damage is not correctly incorporated in the SWASH model used for this thesis. This could be the reason that the exact reason for the observed higher damage is not conclusively found in this research. As some causes of the increased damage have been disproved, it seems likely that the different oblique wave breaking process that was not modelled in detail leads to the increased damage. The

SWASH model used in this thesis does not take this effect of the breaking plunging wave sufficiently into account, due to the grid dimensions. It is recommended to investigate the required grid size and the amount of vertical layers that is required to correctly take this phenomenon into account. This can be done via a more elaborate numerical model study investigating the Eforie case. Increasing the grid size and the amount of vertical layers will result in longer computation time. This can be reduced by using more powerful computers. In addition, the effect of oblique waves on a shallow foreshore could be investigated in a physical model test study. In this study the four cases presented in part 4 of this thesis could be tested in a wave basin. For this study the bathymetry can even be further simplified to one or two constant slopes that induce shallow water conditions near the breakwater.

Eforie recommendations
For the design of future structures on the Eforie coast or areas with similar coastal features, some recommendations for further projects can be made.

- Based on the results of this thesis it can be concluded that it was correct of Deltares to apply the modelling choices. These resulted in a slight underestimation of the breakwater stability and therefore a somewhat conservative design along the entire length of the breakwater. Especially near the shore the breakwater is somewhat oversized, due to the fact that both the transitional slope as the assumption of unidirectional waves increases the IG-wave energy in the system. For future projects it is recommended to apply the same modelling choices. The Deltares modelling choices did not provide the full explanation for the larger observed damage during the physical model tests.

- The lower foreshore slope induces the generation of IG-waves in the system. This increased the velocity near the coast, however the lower foreshore slope is not responsible for the larger observed damage during the physical model tests. This configuration can in reality not be altered by the contractor, so needs to be taken into account in the design.

- The cut-off parabolic bay shape is responsible for the wave-refraction pattern and wave focusing which results in higher velocities around output locations D02 and D03 of around 8-11% depending on depth. In future projects applying a cut-off parabolic bay shape or an extended parabolic bay shape should be discussed, since it can influence the required stone size for the breakwater.

- Based on the results of this research, oblique waves on a shallow foreshore do not show a different effect than oblique waves on a deep foreshore. This suggests that the wave angle is therefore not responsible for the observed damage. It is however concluded that the effect this wave angle has, has not been correctly taken into account by the numerical model. As some causes of the increased damage have been disproven, it seems likely that the different oblique wave breaking process that was not modelled in detail leads to the increased damage. This could be investigated via the proposed physical model test study as described above.

- In this research multiple configurations and characteristics of the numerical model setup have been investigated. However due to the data that was available, the upper foreshore slope is not investigated in detail. Since this is a steep(er) slope, it could be responsible for the higher damage. Therefore investigating the influence of a steep slope along the breakwater is interesting to investigate in further research. This can be done by setting up a new longshore uniform simplified basecase, as was done in part 4 of this thesis. Performing multiple simulations with an upper foreshore slope of 1:30, 1:50 and 1:70 should provide a proper insight in the effect this upper foreshore has on the wave behaviour along the breakwater. It is important to note that the output points should be kept at similar depths for the different simulations. In addition the 1:15 slope around the head of the breakwater, that connects the sand profile to the existing bed, should be investigated. This steep slope around the head of the breakwater could function as a ramp for the waves to shoal on an induce heavy wave breaking. Excluding this slope, by steepening other parts of the slope could be an interesting topic to investigate.

- Several of the configurations investigated in this thesis affect the presence of IG-wave energy close to the shore. Based on the simulations performed in this thesis it can be concluded that

IG-waves have an indirect effect on breakwater stability. A IG-wave by itself does not lead to high velocities along the breakwater. However, an IG-wave induces a temporary increase in waterlevel, which allows the depth-limited SS-waves, if present, to become bigger resulting in higher velocities and more damage on the breakwater. This affects the breakwater stability closer to shore and this needs to be taken into account when designing a breakwater in these conditions. It is recommended to further investigate the influence of IG-waves on coastal structures, such as breakwaters, in shallow water. Currently real scale tests are performed investigating the effect of IG-wave energy on dune erosion. Perhaps this could also be performed to investigate the effect of IG-waves on breakwater stability.

- It is advised to further investigate what could be the explanation of the observed wave transformation along the breakwater and investigate whether this phenomena is included in SWASH or another numerical model. In this thesis it was derived that a Mach-stem wave did not occur, but perhaps it did. Another phenomena could also be responsible. This needs to be identified before proper research and mitigation measures can be taken.

Bibliography

Baart, Stephan , Ebbens, Reinder , Nammuni-Krohn, Julia , and Verhagen, Henk Jan (2011). TOE ROCK STABILITY FOR RUBBLE MOUND BREAKWATERS. *Coastal Engineering Proceedings*, 1 (32). ISSN 0589-087X. doi: 10.9753/icce.v32.structures.35.

Battjes, Jurjen A. and Groenendijk, Heiko W. (2000). Wave height distributions on shallow foreshores. *Coastal Engineering*, 40(3). ISSN 03783839. doi: 10.1016/S0378-3839(00)00007-7.

Beakawi Al-Hashemi, Hamzah M. and Baghabra Al-Amoudi, Omar S. (2018). A review on the angle of repose of granular materials. ISSN 1873328X.

Bertin, Xavier , de Bakker, Anouk , van Dongeren, Ap , Coco, Giovanni , André, Gael , Ardhuin, Fabrice , Bonneton, Philippe , Bouchette, Frédéric , Castelle, Bruno , Crawford, Wayne C. , Davidson, Mark , Deen, Martha , Dodet, Guillaume , Guérin, Thomas , Inch, Kris , Leckler, Fabien , McCall, Robert , Muller, Héloïse , Olabarrieta, Maitane , Roelvink, Dano , Ruessink, Gerben , Sous, Damien , Stutzmann, Éléonore , and Tissier, Marion (2018). Infragravity waves: From driving mechanisms to impacts. ISSN 00128252.

Bijker (1967). Some Considerations about scales for Coastal Models with movable Bed. *DELFT Hydraulics laboratory Nº50*.

Bosboom, Judith and Stive, Marcel J.F. (2021). *Coastal Dynamics*. TU Delft Open, Delft.

Briggs, Michael J. and Grace, Peter J. (1988), Influence of frequency and directional spreading on wave transformation in the nearshore region. doi: 10.1109/oceans.1988.794962.

Brown, Mitchell and Kraus, Nicholas (2007). Tips for Developing Bathymetry Grids for Coastal Modeling System Applications.

Buckley, Mark , Lowe, Ryan , and Hansen, Jeff (2014). Evaluation of nearshore wave models in steep reef environments Topical Collection on the 7th International Conference on Coastal Dynamics in Arcachon, France 24-28 June 2013. *Ocean Dynamics*, 64(6). ISSN 16167228. doi: 10.1007/s10236-014-0713-x.

Bux, Imraan . *THE EFFECTS OF FORESHORE SLOPE ON BREAKWATER ARMOUR UNIT STABILITY*. PhD thesis, UNESCO-IHE Institute for Water Education, Delft (2007).

Cea, L. , Stelling, G. , and Zijlema, M. (2009). Non-hydrostatic 3D free surface layer-structed finite volume model for short wave propagation. *International Journal for Numerical Methods in Fluids*, 61 (4). ISSN 02712091. doi: 10.1002/fld.1961.

Chen, Jia Lin , Ralston, David K. , Geyer, W. Rockwell , Sommerfield, Christopher K. , and Chant, Robert J. (2018). Wave Generation, Dissipation, and Disequilibrium in an Embayment With Complex Bathymetry. *Journal of Geophysical Research: Oceans*, 123(11). ISSN 21699291. doi: 10.1029/2018JC014381.

Chen, Xin Jian (2005). A comparison of hydrostatic and nonhydrostatic pressure components in seiche oscillations. *Mathematical and Computer Modelling*, 41(8-9). ISSN 08957177. doi: 10.1016/j.mcm.2004.08.005.

Ciria, Cur, and Cetmef (2006). *The Rock Manual. The use of rock in hydraulic engineering.*

de Bruin, Robert (2019). Roemeens kustversterkingsproject gegund aan Van Oord. URL https://www.vanoord.com/nl/updates/roemeens-kustversterkingsproject-gegund-aan-van-oord/.

De Heij, J . *The influence of structural permeability on armour layer stability of rubble mound breakwaters*. PhD thesis, TU Delft, Delft (2021).

de Ridder, Menno . *Non-hydrostatic wave modelling of coral reefs with the addition of a porous in-canopy model*. PhD thesis, TU Delft, Delft (2018).

Dean, R. G. and Dalrymple, R. A. (1984). Water wave mechanics for engineers and scientists. ISSN 0096-3941. doi: 10.1029/eo066i024p00490-06.

Diwedar, Al I. , Abdelhaleem, F. S. , and Ali, A. M. (2019), Wave parameters influence on breakwater stability. In *IOP Conference Series: Earth and Environmental Science*, volume 326. doi: 10.1088/1755-1315/326/1/012013.

Froehlich, David C. (2011). Mass Angle of Repose of Open-Graded Rock Riprap. *Journal of Irrigation and Drainage Engineering*, 137(7). ISSN 0733-9437. doi: 10.1061/(asce)ir.1943-4774.0000316.

Gagarina, E. , Van Der Vegt, J. , and Bokhove, O. (2013). Horizontal circulation and jumps in hamiltonian wave models. *Nonlinear Processes in Geophysics*, 20(4). ISSN 10235809. doi: 10.5194/npg-20-483-2013.

Galland, J. C. (1995), Rubble mound breakwater stability under oblique waves: an experimental study. In *Proceedings of the Coastal Engineering Conference*, volume 1. doi: 10.1061/9780784400890.078.

Guzman Mardones, Cesar . *Impact of access channel geometry on wave penetration in harbours*. PhD thesis, Delft University of Technology, Delft (2011).

Hedges, T. S. (1995). Regions of validity of analytical wave theories. *Proceedings of the Institution of Civil Engineers: Water, Maritime and Energy*, 112(2). ISSN 17537819. doi: 10.1680/iwtme.1995.27656.

Herbers, T. H.C. , Elgar, Steve , and Guza, R. T. (1999). Directional spreading of waves in the nearshore. *Journal of Geophysical Research: Oceans*, 104(C4). ISSN 21699291. doi: 10.1029/1998jc900092.

Herrera, Maria P. , Molines, Jorge , and Medina, Josep R. (2016). Hydraulic stability of nominal and sacrificial toe berms for mound breakwaters on steep sea bottoms. *Coastal Engineering*, 114. ISSN 03783839. doi: 10.1016/j.coastaleng.2016.05.006.

Hoffmans, Gijs J.C.M. (2006). Stability of stones under non-uniform flow. Technical report, Rijkswaterstaat, Delft.

Hofland, Bas (2005). Rock & roll: Turbulence-induced damage to granular bed protections. ISSN 01696548.

Hofland, Bas , Chen, Xuexue , Altomare, Corrado , and Oosterlo, Patrick (2017). Prediction formula for the spectral wave period Tm-1,0 on mildly sloping shallow foreshores. *Coastal Engineering*, 123. ISSN 03783839. doi: 10.1016/j.coastaleng.2017.02.005.

Holthuijsen, Leo H. (2007). *Waves in oceanic and coastal waters*, volume 9780521860284. doi: 10.1017/CBO9780511618536.

Hsu, Tian Jian , Sakakiyama, Tsutomu , and Liu, Philip L.F. (2002). A numerical model for wave motions and turbulence flows in front of a composite breakwater. *Coastal Engineering*, 46(1). ISSN 03783839. doi: 10.1016/S0378-3839(02)00045-5.

Izbash, S.V. (1935). Construction of Dams by Dumping Stones into Flowing Water. Technical report, Leningrad.

Kobayashi, N (1986). Numerical Simulation Of Wave Run Up And Armor Stability . *Offshore Technology Conference*.

Lashley, Christopher H. . *The Influence of Infragravity Waves on Overtopping at Coastal Structures with Shallow Foreshores*. PhD thesis, TU Delft, Delft (2021).

Longuet-Higgins, M. S. and Stewart, R. w. (1964). Radiation stresses in water waves; a physical discussion, with applications. *Deep-Sea Research and Oceanographic Abstracts*, 11(4). ISSN 00117471. doi: 10.1016/0011-7471(64)90001-4.

Mares-Nasarre, Patricia and van Gent, Marcel R.A. (2020). Oblique wave attack on rubble mound breakwater crest walls of finite length. *Water (Switzerland)*, 12(2). ISSN 20734441. doi: 10.3390/w12020353.

Mase, Hajime , Memita, Tetsu , Yuhi, Masatoshi , and Kitano, Toshikazu (2002). Stem waves along vertical wall due to random wave incidence. *Coastal Engineering*, 44(4). ISSN 03783839. doi: 10.1016/S0378-3839(01)00038-2.

Matsumi, Y. , Mansard, E. P.D. , and Rutledge, J. (1995), Influence of wave directionality on stability of breakwater heads. In *Proceedings of the Coastal Engineering Conference*, volume 2. doi: 10.1061/9780784400890.102.

Monteban, Dennis . *Numerical modelling of wave agitation in ports and access channels*. PhD thesis, TU Delft, Delft (2016).

Muttray, Markus and Reedijk, Bas (2009), REANALYSIS OF BREAKWATER STABILITY WITH STEEP FORESHORE. doi: 10.1142/9789814277426{_}0277.

Ottenheim, E.S.A.P. . *Stability of stones in the surf zone*. PhD thesis, TU Delft, Delft (1997).

Paintal, A. S. (1971). Concept Of Critical Shear Stress In Loose Boundary Open Channels. *Journal of Hydraulic Research*, 9(1). ISSN 0022-1686. doi: 10.1080/00221687109500339.

Recking, A. and Pitlick, J. (2013). Shields versus Isbash. *Journal of Hydraulic Engineering*, 139(1). ISSN 0733-9429. doi: 10.1061/(asce)hy.1943-7900.0000647.

Rietberg, D.C. . *WAVE DYNAMICS BEHIND A SHORE-NORMAL BREAKWATER*. PhD thesis, Delft University of Technology, Delft (2017).

Rijnsdorp, Dirk P. , Smit, Pieter B. , and Zijlema, Marcel (2014). Non-hydrostatic modelling of infragravity waves under laboratory conditions. *Coastal Engineering*, 85. ISSN 03783839. doi: 10.1016/j.coastaleng.2013.11.011.

Roelvink, Dano , Reniers, Ad , van Dongeren, Ap , van Thiel de Vries, Jaap , McCall, Robert , and Lescinski, Jamie (2009). Modelling storm impacts on beaches, dunes and barrier islands. *Coastal Engineering*, 56(11-12). ISSN 03783839. doi: 10.1016/j.coastaleng.2009.08.006.

Roelvink, J. A. and Stive, M. F.J. (1989). Bar-generating cross-shore flow mechanisms on a beach. *Journal of Geophysical Research*, 94(C4). ISSN 01480227. doi: 10.1029/JC094iC04p04785.

Ruju, Andrea , Lara, Javier L. , and Losada, Inigo J. (2014). Numerical analysis of run-up oscillations under dissipative conditions. *Coastal Engineering*, 86. ISSN 03783839. doi: 10.1016/j.coastaleng.2014.01.010.

Schiereck, Gerrit J. (2017). *Introduction to Bed, Bank and Shore Protection*. doi: 10.1201/9781315274935.

Shi, Rui , Leng, Xinqian , and Chanson, Hubert (2020). On turbulence and turbulent events in a breaking bore. *Mechanics Research Communications*, 104. ISSN 00936413. doi: 10.1016/j.mechrescom.2020.103478.

Smit, Pieter , Zijlema, Marcel , and Stelling, Guus (2013). Depth-induced wave breaking in a non-hydrostatic, near-shore wave model. *Coastal Engineering*, 76. ISSN 03783839. doi: 10.1016/j.coastaleng.2013.01.008.

Smit, Pieter , Janssen, Tim , Holthuijsen, Leo , and Smith, Jane (2014). Non-hydrostatic modeling of surf zone wave dynamics. *Coastal Engineering*, 83. ISSN 03783839. doi: 10.1016/j.coastaleng.2013.09.005.

Steenstra, Remco , Hofland, Bas , Smale, Alfons , Paarlberg, Andries , Huthoff, Fredrik , and Uijttewaal, Wim (2016). Stone Stability under Stationary Nonuniform Flows. *Journal of Hydraulic Engineering*, 142(12). ISSN 0733-9429. doi: 10.1061/(asce)hy.1943-7900.0001202.

Stelling, G. and Zijlema, M. (2003). An accurate and efficient finite-difference algorithm for non-hydrostatic free-surface flow with application to wave propagation. *International Journal for Numerical Methods in Fluids*, 43(1). ISSN 02712091. doi: 10.1002/fld.595.

Suzuki, Tomohiro , Altomare, Corrado , Veale, William , Verwaest, Toon , Trouw, Koen , Troch, Peter , and Zijlema, Marcel (2017). Efficient and robust wave overtopping estimation for impermeable coastal structures in shallow foreshores using SWASH. *Coastal Engineering*, 122. ISSN 03783839. doi: 10.1016/j.coastaleng.2017.01.009.

Suzuki, Tomohiro , Hu, Zhan , Kumada, Kenji , Phan, L. K. , and Zijlema, Marcel (2019). Non-hydrostatic modeling of drag, inertia and porous effects in wave propagation over dense vegetation fields. *Coastal Engineering*, 149. ISSN 03783839. doi: 10.1016/j.coastaleng.2019.03.011.

SWASH team (2020). User Manual SWASH version 7.01. URL https://swash.sourceforge.io/download/zip/swashuse.pdf.

Takahashi, Shigeo (2002). Design of vertical breakwaters. *PHRI reference document nr. 34*.

Te Velde, Esmee . *An experimental study on the drag and inertia forces due to mussel growth on vertical poles exposed to waves*. PhD thesis, TU Delft, Delft (2022).

Van den Bos, Jeroen , Verhagen, Henk Jan , and Olthof, Jelle (2011). LOW-MOBILITY TRANSPORT OF COARSE-GRAINED BED MATERIAL. *Coastal Engineering Proceedings*, 1(32). ISSN 0589-087X. doi: 10.9753/icce.v32.sediment.13.

van den Bos, J.P. and Verhagen, H.J (2018). *Breakwater Design - Lecture notes CIE5308*.

van der Meer, J. W. (1988). Rock slopes and gravel beaches under wave attack. *DELFT, THE NETHERLANDS, DELFT HYDRAUL. LAB., NOV. 1988*, (396)).

van der Meer, Jentsje W. . Application and stability criteria for rock and artificial units. In *Dikes and Revetments: Design, Maintenance and Safety Assessment* (2017). doi: 10.1201/9781315141329.

van der Werf, Ivo (2021). Physical modelling of Eforie protection works_Measurement report 3D physical modelling of ECn2. Technical report, Deltares, Delft.

Van Dongeren, Ap , Reniers, Ad , Battjes, Jurjen , and Svendsen, Ib (2003). Numerical modeling of infragravity wave response during DELILAH. *Journal of Geophysical Research: Oceans*, 108(9). ISSN 21699291. doi: 10.1029/2002jc001332.

Van Gent, Marcel R.A. (2014). Oblique wave attack on rubble mound breakwaters. *Coastal Engineering*, 88. ISSN 03783839. doi: 10.1016/j.coastaleng.2014.02.002.

van Gent, Marcel R.A. (2021). Influence of oblique wave attack on wave overtopping at caisson breakwaters with sea and swell conditions. *Coastal Engineering*, 164. ISSN 03783839. doi: 10.1016/j.coastaleng.2020.103834.

Van Gent, Marcel R.A. and van der Werf, Ivo M. (2014). Rock toe stability of rubble mound breakwaters. *Coastal Engineering*, 83. ISSN 03783839. doi: 10.1016/j.coastaleng.2013.10.012.

Van Gent, Marcel R.A. , Smale, Atfons J. , and Kuiper, Coen (2003), Stability of rock slopes with shallow foreshores. In *Coastal Structures 2003 - Proceedings of the Conference*. doi: 10.1061/40733(147)9.

Van Gent, M.R.A. . *Odiflocs: Computations for a berm breakwater*. PhD thesis, Deltares, Delft (1992).

van Kester, Dennis (2021). Detailed Design Report Designed Coastal Structures 223046-VO-EXE-ENG-REP-0008. Technical report, Van Oord, Rotterdam.

van Thiel de Vries, Jaap S. M. . *Dune Erosion During Storm Surges*. PhD thesis (2009).

Verhagen, Henk Jan and Mertens, Marcel (2010), Riprap stability for deep water, shallow water and steep foreshores. In *Coasts, Marine Structures and Breakwaters: Adapting to Change - Proceedings of the 9th International Conference*, volume 2. doi: 10.1680/cmsb.41318.0046.

Verhagen, Henk Jan , Reedijk, Bas , and Muttray, Marcus (2006), THE EFFECT OF FORESHORE SLOPE ON BREAKWATER STABILITY. doi: 10.1142/9789812709554{_}0404.

Verhagen, Henk Jan , van Vledder, Gerbrant , and Arab, Sepehr Eslami (2008), A PRACTICAL METHOD FOR DESIGN OF COASTAL STRUCTURES IN SHALLOW WATER. doi: 10.1142/9789814277426{_}0241.

Vidal, C. , Medina, R. , and Lomónaco, P. (2006). Wave height parameter for damage description of rubble-mound breakwaters. *Coastal Engineering*, 53(9). ISSN 03783839. doi: 10.1016/j.coastaleng.2006.02.007.

Wang, Baoxing , Van Der Meer, Jentsje W. , Otta, Ashwini K. , Chadwick, Andrew J. , and Horrillo-Caraballo, Jose (2006), Reflection of obliquely incident waves at low-crested structures. In *Coastal Dynamics 2005 - Proceedings of the Fifth Coastal Dynamics International Conference*. doi: 10.1061/40855(214)117.

Wolters, Guido and Van Gent, Marcel (2011). OBLIQUE WAVE ATTACK ON CUBE AND ROCK ARMOURED RUBBLE MOUND BREAKWATERS. *Coastal Engineering Proceedings*, 1(32). ISSN 0589-087X. doi: 10.9753/icce.v32.structures.34.

Yu, Yu Xiu , Liu, Shu Xue , and Zhu, Chuan Hua (2002). Stability of armour units on rubble mound breakwater under multi-directional waves. *Coastal Engineering Journal*, 44(2). ISSN 17936292. doi: 10.1142/S0578563402000482.

Zaalberg, Piet , Ockeloen, Wouter , Hofland, Bas , Antonini, Alessandro , and Smith, Greg (2020). THE RELATION BETWEEN SAND AND OVERTOPPING FOR COBBLE REVETMENTS: A NUMERICAL APPROACH WITH OPENFOAM. *Coastal Engineering Proceedings*, (36v). ISSN 0589-087X. doi: 10.9753/icce.v36v.structures.14.

Zijlema, M. and Stelling, G. S. (2008). Efficient computation of surf zone waves using the nonlinear shallow water equations with non-hydrostatic pressure. *Coastal Engineering*, 55(10). ISSN 03783839. doi: 10.1016/j.coastaleng.2008.02.020.

Zijlema, Marcel , Stelling, Guus , and Smit, Pieter (2011). SWASH: An operational public domain code for simulating wave fields and rapidly varied flows in coastal waters. *Coastal Engineering*, 58(10). ISSN 03783839. doi: 10.1016/j.coastaleng.2011.05.015.